MR IMAGING OF THE BRACHIAL PLEXUS

H.W. van Es

From the Department of Radiology, University Hospital Utrecht, The Netherlands.

The production of this thesis was made possible by kind financial support of Baxter BV, Byk Nederland BV, Guerbet Nederland BV, Schering Nederland BV, Serono Benelux BV, Stichting het Remmert Adriaan Laan Fonds en het Van Leersumfonds.

MR IMAGING OF THE BRACHIAL PLEXUS

MRI VAN DE PLEXUS BRACHIALIS

(met een samenvatting in het Nederlands)

Proefschrift

ter verkrijging van de graad van doctor aan de Universiteit Utrecht
op gezag van de Rector Magnificus, Prof. Dr J.A. van Ginkel
ingevolge het besluit van het College van Decanen
in het openbaar te verdedigen op
vrijdag 23 mei 1997 des namiddags te 4.15 uur

door

Hendrik Wouter van Es
geboren op 19 december 1963 te Utrecht

Promotor : Prof. Dr M.A.M. Feldberg

Cover : Wax model of the brachial plexus (approximately 210 years old), used with kind permission from the Josephinum Museum, Vienna, Austria

Lay-out : Cees Haaring, Department of Radiology, University Hospital Utrecht, The Netherlands

ISBN : 90-393-1429-2

Contents

Chapter 1

General Introduction

INTRODUCTION

Until the introduction of cross-sectional imaging techniques it was not possible to directly visualize the brachial plexus, except for the roots using myelography. With computed tomography (CT) it became possible to depict some parts of the nerves of the brachial plexus in the axial plane. With the introduction of magnetic resonance (MR) imaging it became possible to visualize all parts of the brachial plexus in any plane. Soon MR imaging became the imaging modality of choice in patients with suspected brachial plexus pathology. In this study we describe a large group of patients who have had MR imaging of the brachial plexus for all sorts of indications. Besides a pictorial review of all pathology we found with imaging, we also describe the patients with normal imaging findings, so trying to find the useful indications for MR imaging of the brachial plexus.

Objectives

During the last five years we studied 230 patients who were suspected of having brachial plexus pathology. The aim of this retrospective study is to evaluate the value of MR imaging of the brachial plexus for the various indications such as neurogenic and non-neurogenic tumors, changes due to trauma, radiation injury and peripheral nerve disease, specifically multifocal motor neuropathy (MMN) and chronic inflammatory demyelinating polyradiculoneuropathy (CIDP).
Specific questions are:
- what is the optimal scan protocol at this moment?
- what details of the complex anatomy can be seen?
- what are the useful indications for requesting MR imaging of the brachial plexus?

Outlines

Chapter 1 includes, after a short introduction, the objectives of the study.
Chapter 2 describes the anatomy of the brachial plexus, the imaging techniques (conventional radiography, CT and MR imaging), and the scan protocol we use for the various indications. The anatomy as seen with MR imaging is shown and correlated with cryomicrotome sections.
Chapter 3 describes the MR imaging features of primary neurogenic tumors and of primary or secondary tumors in or near the brachial plexus. This chapter contains an extensive atlas of all the sorts of tumors we encountered. Of all patients who did not show any abnormalities with MR imaging the relevant history and symptoms are tabulated.
Chapter 4 contains two parts. The first part presents our experience with MR imaging of the brachial plexus in patients with a history of trauma, including some experience with the MR imaging features of nerve root avulsions.
The second part discusses the MR imaging findings in patients with thoracic outlet syndromes.
Chapter 5 describes three different MR imaging abnormalities we found in three patients with radiation-induced brachial plexopathy.
Chapter 6 reports the value of MR imaging in patients with MMN, CIDP and lower motor neuron disease (LMND).
Chapter 7 contains a summary and conclusions.

Chapter 2

Anatomy and Imaging Techniques

ANATOMY

The brachial plexus extends from the neck to the axilla and is a transpatial structure,[91] because it traverses multiple contiguous spaces. The brachial plexus begins in the prevertebral portion of the perivertebral space, it leaves this space and enters the posterior cervical space just lateral to the anterior and middle scalene muscles. It then travels inferolaterally into the axilla, the entrance of which is bordered by the clavicle anteriorly, the scapula posteriorly, the first rib medially and the medial side of the coracoid process laterally. The brachial plexus consists of four portions: five ventral rami of the roots, three trunks, six divisions (three anterior and three posterior) and three cords (Figs. 1 and 2).[50,78,86,109,111,132,151,158,238]

Ventral rami of the roots

The brachial plexus originates from the lower four cervical roots (C5, C6, C7 and C8) and the first thoracic root (Th1). The ventral and dorsal nerve roots unite at the inner aperture of the intervertebral foramen to form the spinal nerve (Fig. 3). The spinal nerve is situated in the intervertebral foramen and divides at the outer aperture into a dorsal and ventral ramus. The dorsal ramus innervates the musculature and the skin of the posterior region of the neck. The ventral rami of C5, C6, C7, C8 and Th1 form the proximal extent of the brachial plexus. Hovelacque[102] measured the roots as they exit the intervertebral foramen: C5 (3 - 4 mm), C6 (4 - 6 mm), C7 (4 - 4.5 mm), C8 (3 - 4.5 mm) and Th1 (3 - 4 mm). Just distal to their origin the ventral rami receive one or more grey rami communicantes from their corresponding ganglion (Fig. 3): C5 and C6 from the middle cervical ganglion, C7 and C8 from the inferior cervical ganglion, and Th1 from the first thoracic ganglion (Fig. 4). The first thoracic ventral ramus also contributes a white ramus communicans to the first thoracic ganglion. The inferior cervical ganglion and the first thoracic ganglion are usually fused and form the large and irregular cervicothoracic (stellate) ganglion (Fig. 4); its

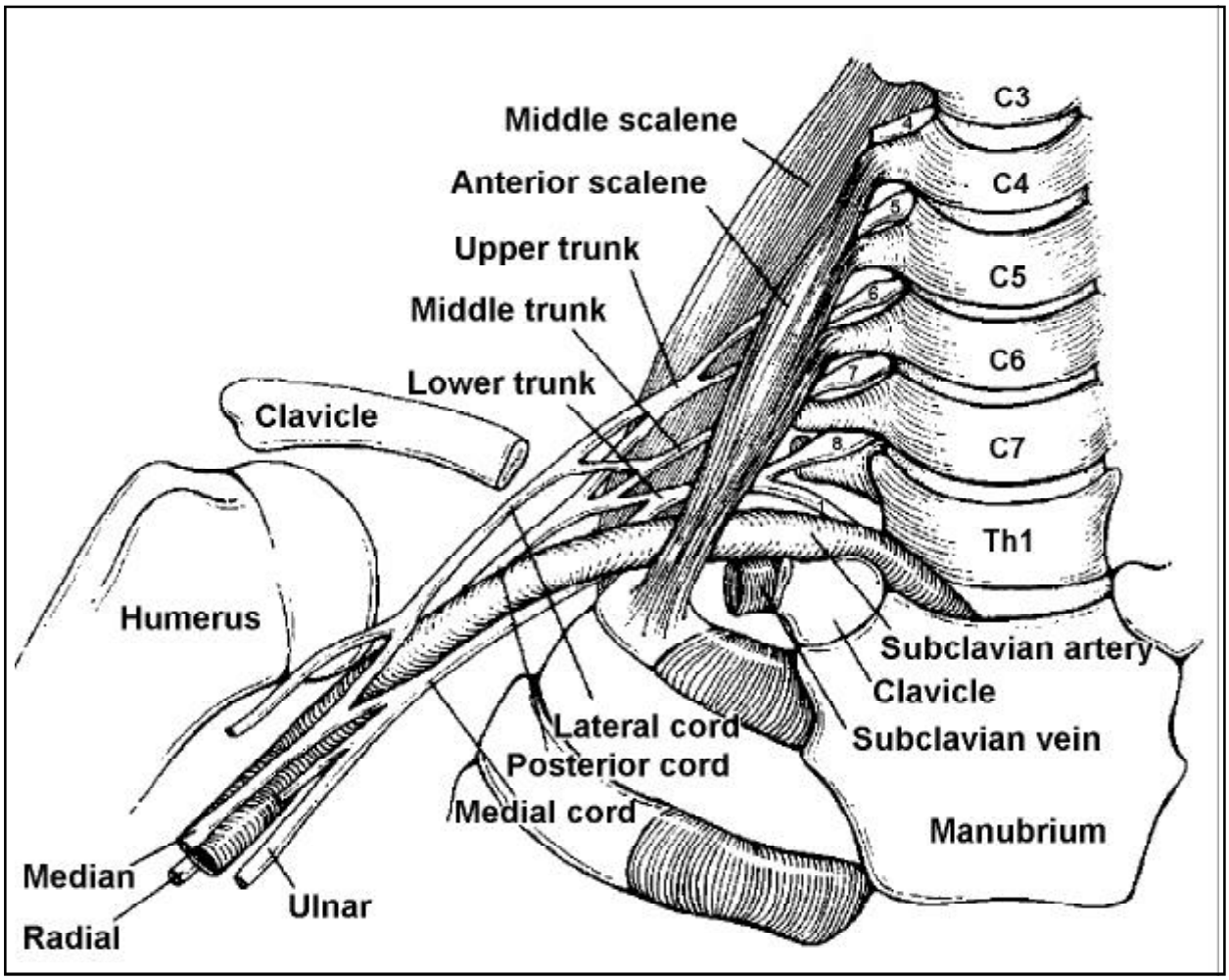

Fig. 1. Anatomy of the brachial plexus showing the relationship to muscles, subclavian artery and bones. Adapted from Posniak,[194] with permission.

length varies from 1 to 3 cm and its width from 3 to 10 mm.[187] The stellate ganglion lies anterior to the transverse process of the seventh cervical vertebra, just lateral to the lateral border of the longus colli muscle, posterior to the vertebral artery and vein, and cranial to the pleural dome.[101,187] The grey ramus communicans contributes postganglionic unmyelinated fibers from the sympathetic ganglion to the ventral ramus of the spinal nerve regulating sweat gland secretion, vasoconstriction and piloerection. The white ramus communicans from the ventral ramus of root Th1 contributes preganglionic fibers to the stellate ganglion. Damage to these preganglionic fibers causes Horner's syndrome, consisting of miosis, ptosis, enophthalmos and facial anhidrosis.

The ventral rami of the roots C5, 6, 7, 8 and Th1 run inferolaterally and enter the interscalene triangle, which is formed by the anterior and middle scalene muscles (Fig. 1). The anterior scalene muscle is located anterior and the middle scalene muscle posterior to the ventral rami. The subclavian artery also lies within the interscalene triangle, anterior to the lower two rami and inferior to the upper three rami (Figs. 1

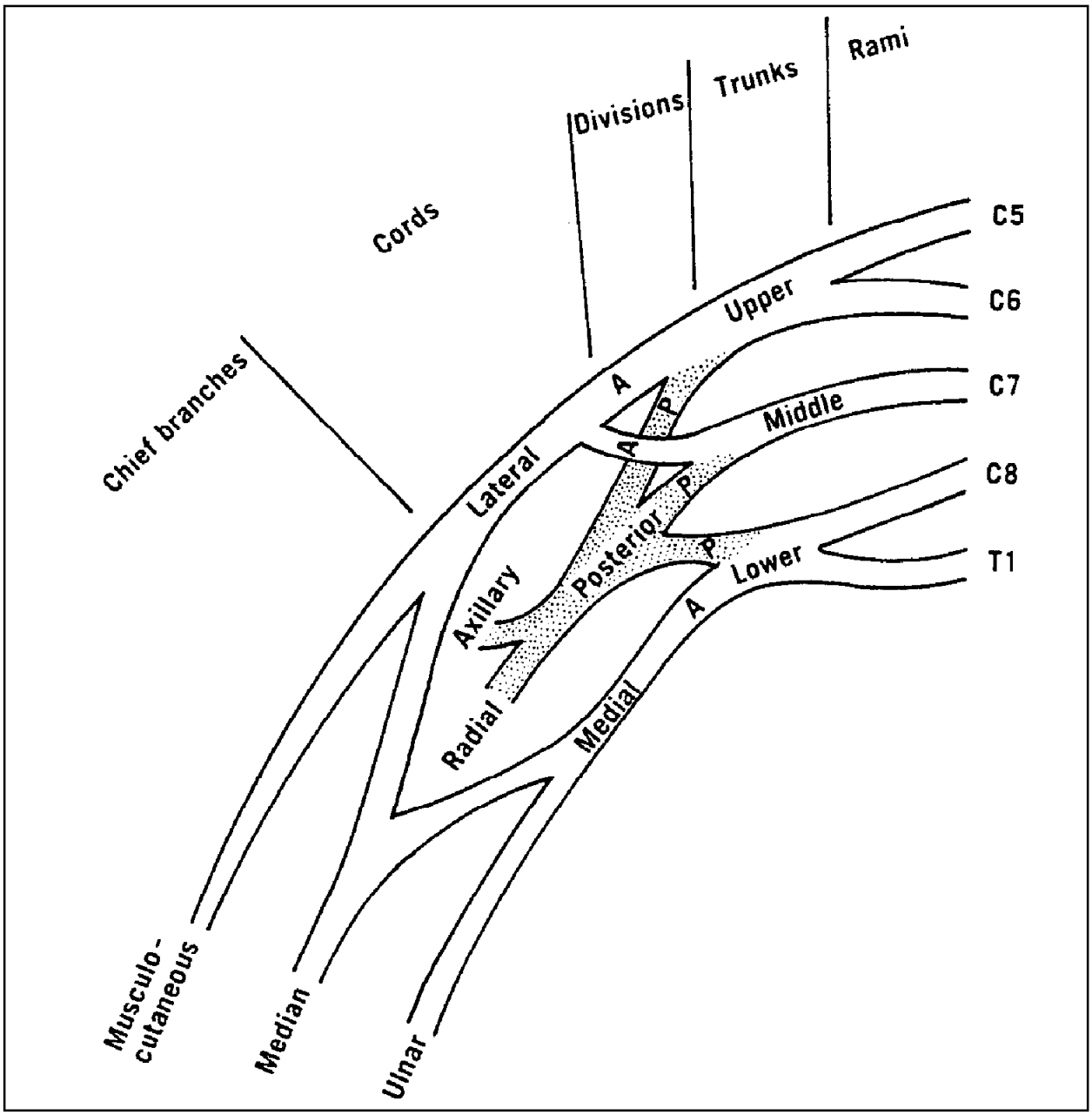

Fig. 2. Schematic drawing of the architecture of the brachial plexus. Adapted from O'Rahilly,[78] with permission.

and 5A). The subclavian vein is located between the anterior scalene muscle and the clavicle. The anterior scalene muscle arises from the transverse processes of the third to the sixth cervical vertebrae and inserts on the first rib by a narrow tendon. The middle scalene muscle, which is the largest, arises from the transverse processes of the second to the seventh cervical vertebrae and has a broad insertion on the first rib, posterior to the insertion of the anterior scalene muscle (Fig. 1). The smallest is the posterior scalene muscle which arises from the fifth to seventh cervical vertebrae and inserts on the second rib. The upper ventral rami of the roots (C5 and C6) can pass through the anterior scalene muscle itself as found in 30% of dissections.[77]

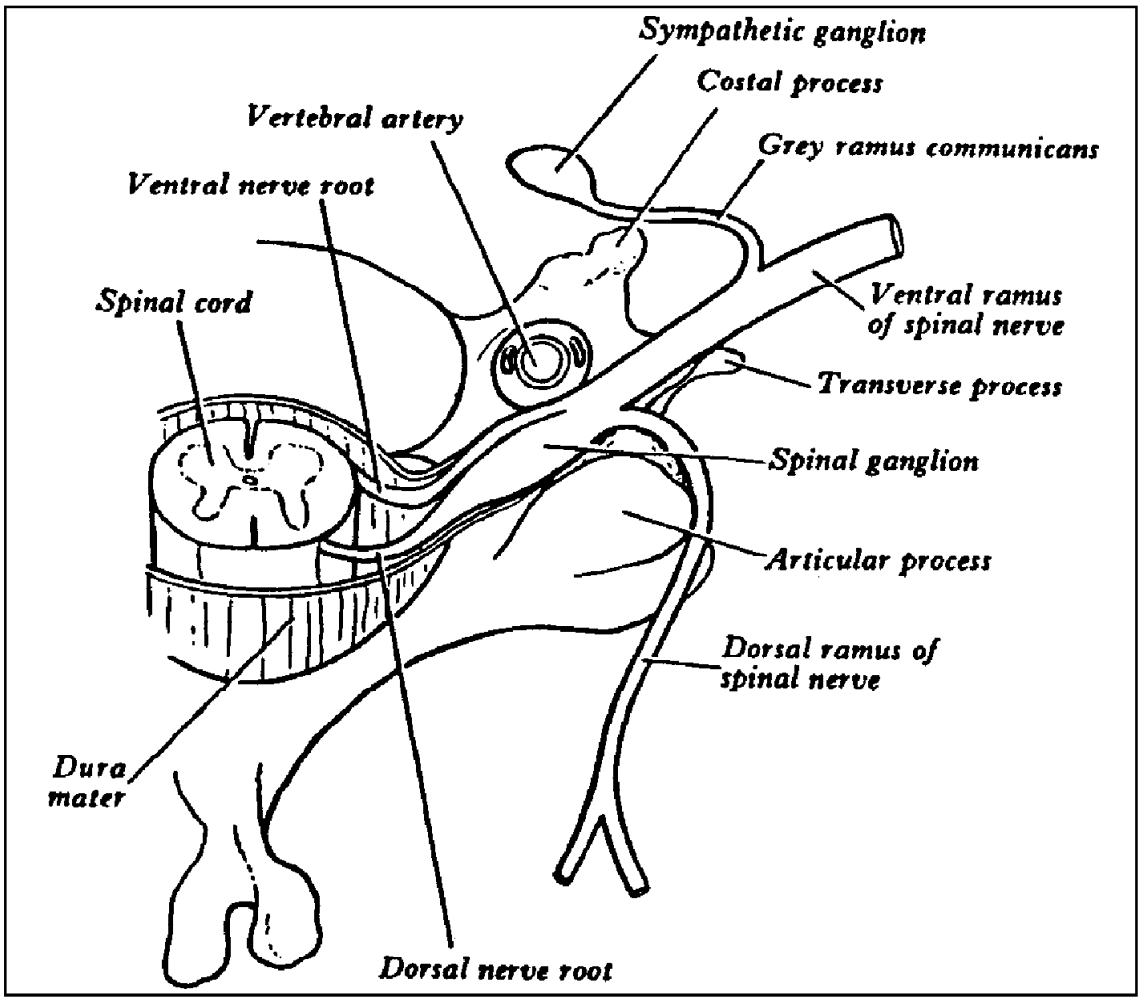

Fig. 3. Anatomy of a cervical root. Reproduced from "Gray's Anatomy" (1989, 37th edition). By kind permission of Churchill Livingstone.

Trunks

The three trunks are formed at the lateral border of the interscalene triangle. The ventral rami of roots C5 and C6 join to become the upper trunk, the ventral ramus of root C7 continues as the middle trunk, and the ventral rami of roots C8 and Th1 unite to become the lower trunk (Fig. 2). The lower trunk lies on the first rib dorsal to the subclavian artery. The middle and upper trunks are located cranial to the subclavian artery (Fig. 5A). The diameters of the upper and lower trunks are found to be between 5 and 7 mm.[102]

Divisions

Just before or at the point where the brachial plexus passes posterior to the clavicle the divisions are formed (Fig. 5B). Each of the trunks divides into an anterior and posterior division (Fig. 2). This is also a functional division: the anterior division supplies the flexor muscles, and the posterior division the extensor muscles of the upper limb.

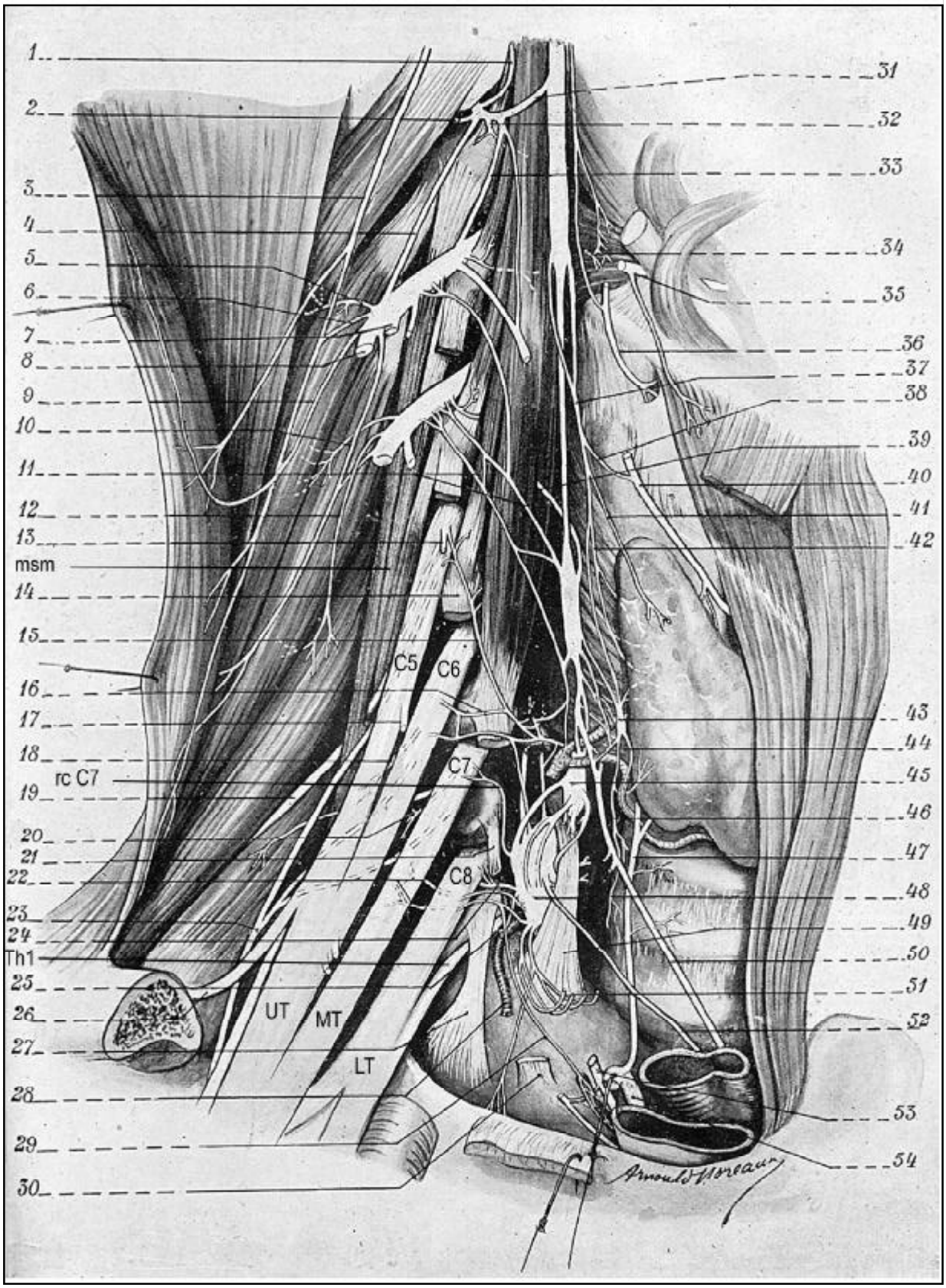

Fig. 4. The relationship between the stellate ganglion and the brachial plexus. The anterior scalene muscle is cut away, only the cut proximal tendons which insert to the transverse processes of the cervical vertebral bodies are shown (14 = the insertion to the transverse process of C5), msm = middle scalene muscle. The rami communicantes are shown between the middle cervical ganglion (45) and the ventral rami of C5 (15) and C6 (16), and between the stellate ganglion (48) and the ventral rami of C7 (rc C7), C8 (24) and Th1 (25). UT = upper trunk, MT = middle trunk, LT = lower trunk. Adapted from Hovelacque.[102]

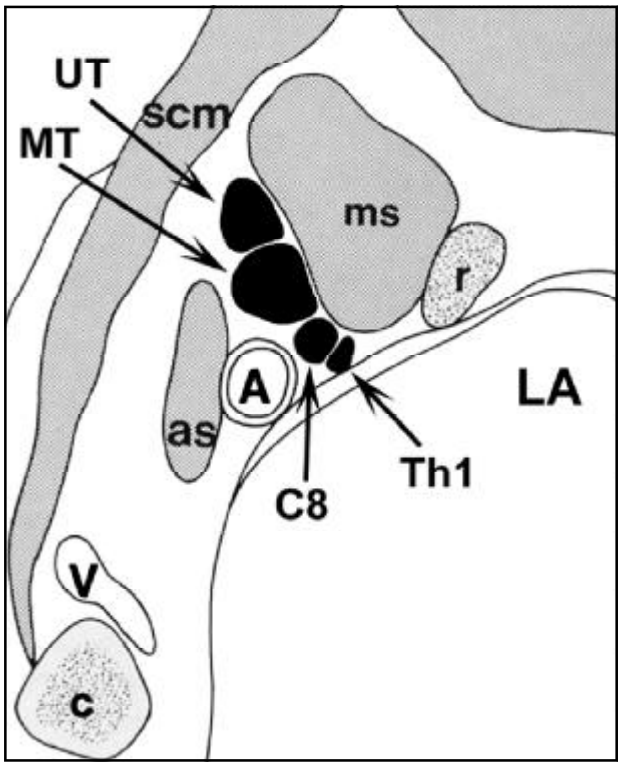

Fig. 5A

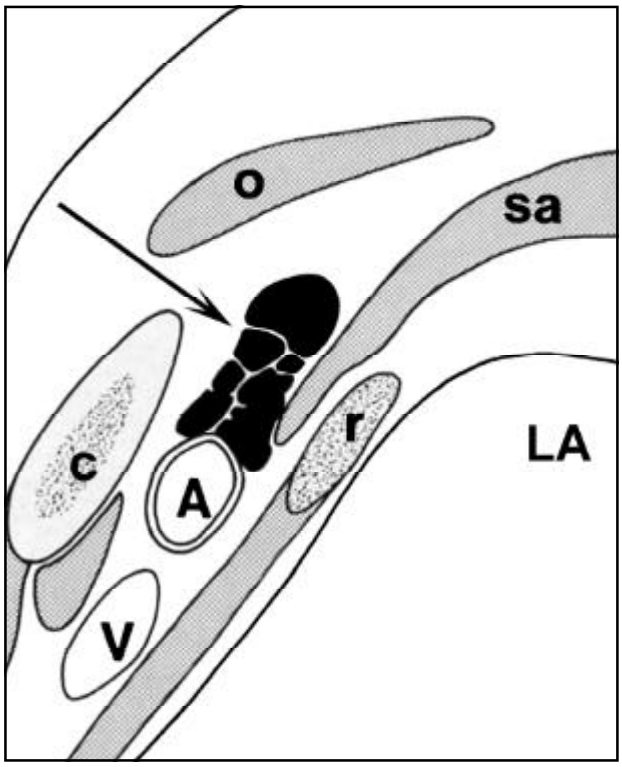

Fig. 5B

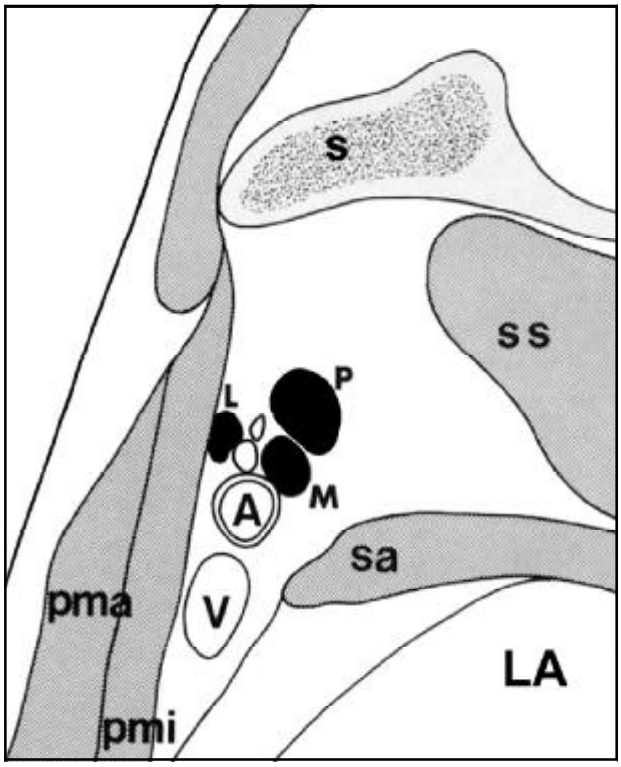

Fig. 5C

Fig. 5. Diagrams showing the sagittal anatomy, left side is ventral aspect. Adapted from Blair,[24] with permission.

A. Diagram at the level of the interscalene triangle showing the upper trunk (UT), the middle trunk (MT) and the ventral rami of roots C8 and Th1. The upper and middle trunks are located above the subclavian artery (A), while the ventral rami of roots C8 and Th1, which join to become the lower trunk, are positioned behind the subclavian artery. V = subclavian vein, as = anterior scalene muscle, ms = middle scalene muscle, scm = sternocleidomastoid muscle, r = first rib, c = clavicle, LA = lung apex.

B. Diagram at the level of the divisions. The divisions (arrow) lie superior to the subclavian artery (A). V = subclavian vein, r = first rib, c = clavicle, sa = serratus anterior muscle, o = omohyoid muscle, LA = lung apex.

C. Diagram at the level of the cords. At this level the cords can be seen separately. L = lateral cord, P = posterior cord, M = medial cord, A = axillary artery, V = axillary vein, s = scapula, ss = subscapularis muscle, sa = serratus anterior muscle, pma = pectoralis major muscle, pmi = pectoralis minor muscle, LA = lung apex.

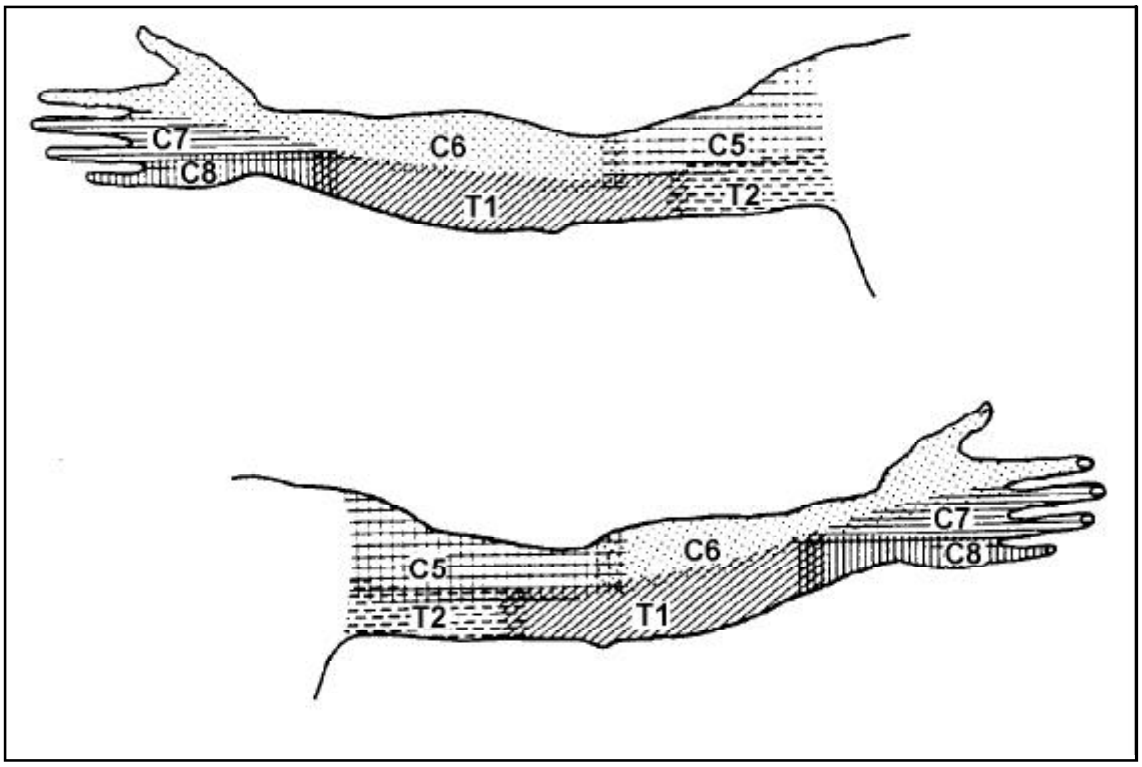

Fig. 6. The sensory distribution of the upper limb. Reproduced from Sunderland.[238] By kind permission of Churchill Livingstone.

Cords

Lateral to the first rib's outer border, where the subclavian artery and vein become the axillary artery and vein, the three cords are formed (Fig. 1). The cords, which form the distal extent of the brachial plexus, are the largest components of the brachial plexus. The lateral cord is formed by the anterior divisions from the upper and middle trunks, the medial cord by the anterior division from the lower trunk, and the posterior cord by the posterior divisions from all trunks (Fig. 2). This means that the lateral cord contains fibers from C5, C6 and C7, the medial cord from C8 and Th1, and the posterior cord from C5, C6, C7, C8 and Th1. Just lateral to the pectoralis minor muscle the cords divide into the five chief or terminal branches. In the sagittal plane the lateral cord is located most anteriorly, the posterior cord most superiorly, and the medial cord most posteriorly in relation to the axillary artery (Fig. 5C).

Terminal branches of the brachial plexus

The five terminal branches arise at the inferolateral border of the pectoralis minor muscle. The median nerve arises from the medial and lateral cords, the ulnar nerve arises from the medial cord, the musculocutaneous nerve arises from the lateral cord, and the axillary nerve and radial nerve arise from the posterior cord (Fig. 2). Each terminal branch contains fibers from several spinal nerves, due to the complex

formation in the brachial plexus. Consequently every muscle is innervated by several spinal nerves. Sunderland[238] described a practical formula to relate movements to spinal nerves:

C5: Abductors, external rotators and extensors of the shoulder, pectoralis major (clavicular fibers). Flexors and supinators of the forearm.

C6: Adductors, internal rotators and forward flexors of the shoulder, pectoralis major (clavicular fibers). Pronators of the forearm.

C7: Internal rotators of the shoulder, pectoralis major (sternal fibers). Extensors of the forearm, wrist and long extensors of the digits.

C8: Pectoralis major (sternal fibers). Flexors of the wrist and long flexors of the digits.

Th1: Intrinsic muscles of the hand.

The sensory distribution of the upper limb is shown in Fig. 6.

Variations

There are variable contributions to the brachial plexus from C4 and Th2,[93,94,98] so shifting the brachial plexus cranially (prefixed, which is more common) or caudally (postfixed). A large contribution of C4 coincides with no branch from Th2 and a small branch from Th1, so forming the prefixed type of the brachial plexus. The postfixed type consists of an absent branch from C4, a reduced contribution from C5, a large branch from Th1 and one from Th2. When the first rib is rudimentary the postfixed type is prominent.[57] Many variations exist in the complex intermingling of the nerves in the brachial plexus and in the formation of the many branches.[109,113,240,268]

IMAGING TECHNIQUES

Conventional radiography

With conventional radiography it is not possible to visualize the brachial plexus at all. The value of conventional radiography is limited to the depiction of the bony anatomy in the environment of the brachial plexus, its anatomic variations, such as cervical ribs, and the evaluation of the lung apex.

Myelography with positive contrast has been used since 1947[159] for diagnosing traumatic nerve root avulsions.

Computed Tomography

With the introduction of CT it became possible to image important landmarks of the brachial plexus and some parts of the nerves in the axial plane.[8,30,44,45,72,79,255,265] The

individual components of the brachial plexus are difficult to distinguish on CT, but its course can be identified by its anatomic relationships. These important landmarks are from medially to laterally: the neural foramina, the anterior and middle scalene muscles and the subclavian and axillary artery. The axial plane is not the optimal image direction for the brachial plexus, because it courses in an oblique coronal plane. Direct parasagittal CT scanning has been described,[208] as well as axial CT supplemented by multiplanar reconstructions.[71] The use of these multiplanar reconstructions has become easier with the introduction of spiral CT. However, despite these technical improvements, it is still not possible to acquire detailed peripheral nerve imaging with CT, and the image quality is disturbed by beam-hardening artifacts due to the presence of the shoulders in the region of interest. However, for the diagnosis of traumatic nerve root avulsions CT myelography is very useful.[95,142,207,266,267]

Magnetic Resonance Imaging

In comparison with CT, MR imaging of the brachial plexus has three major advantages: (1) the multiplanar capabilities, (2) the inherent differences in contrast between the nerves, the related vessels and the surrounding fat, and (3) lack of artifacts. In 1987 Blair[24] first described the anatomic details of the brachial plexus seen with MR imaging. Other studies followed and described optimistically the excellent capabilities of MR imaging in delineating the anatomy and pathology of the brachial plexus.[21,31,41,42,54,87,106,112,114,177,194,200,201,223,259-262]

The brachial plexus has the same signal intensity as muscle, that is low to intermediate on both T1- and T2-weighted images (Figs. 7 and 8).[24,31,194] The T1-weighted images (short echo time (TE), short repetition time (TR)) provide an excellent resolution for the anatomy, the T2-weighted images (long TE, long TR) have a poor signal to noise ratio but show a markedly increased lesion conspicuity. Proton-density sequences (short TE, long TR) have a better signal to noise ratio than T2-weighted sequences and an improved lesion conspicuity compared to T1-weighted sequences. Proton-density images can be very useful in delineating a tumor with a relatively increased signal intensity from surrounding muscle and brachial plexus with low signal intensities. There is some experience with newer techniques such as fast spin echo (FSE) imaging and fat suppression.[177,193,194] We have limited experience with a coronal "turbo spin echo short inversion time inversion recovery" (TSE STIR) sequence. With this sequence nerves can become slightly hyperintense; it has been demonstrated that in fat-suppressed heavily T2-weighted images nerve is hyperintense to muscle and that the nerve fascicles predominate within a fat-suppressed environment.[55,69,70,104] This so-called MR-neurography will be a very promising technique in the future for the evaluation of peripheral nerve disorders, especially with the use of improved surface coils and vessel suppression techniques.

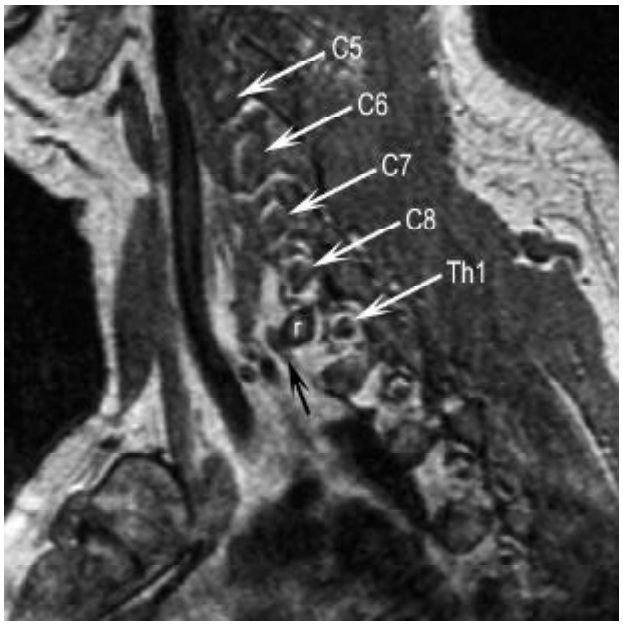

Fig. 7A

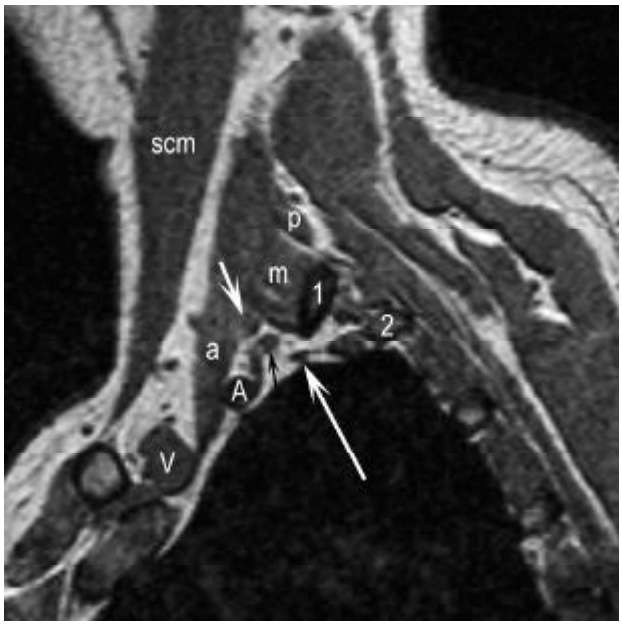

Fig. 7B

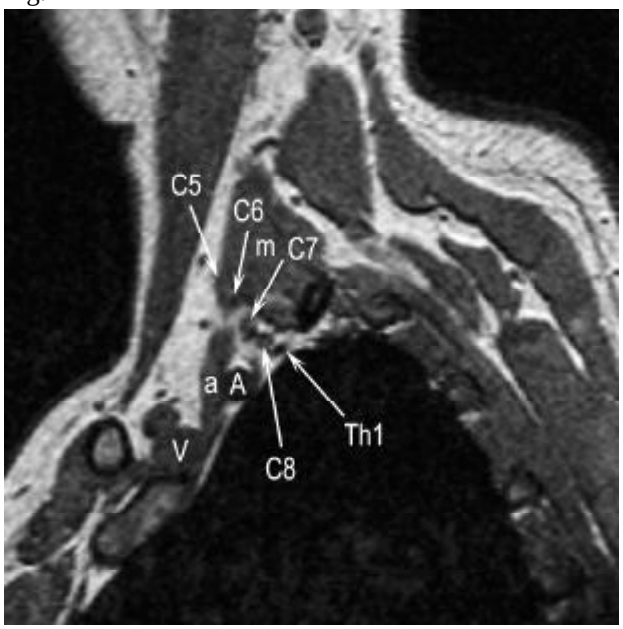

Fig. 7C

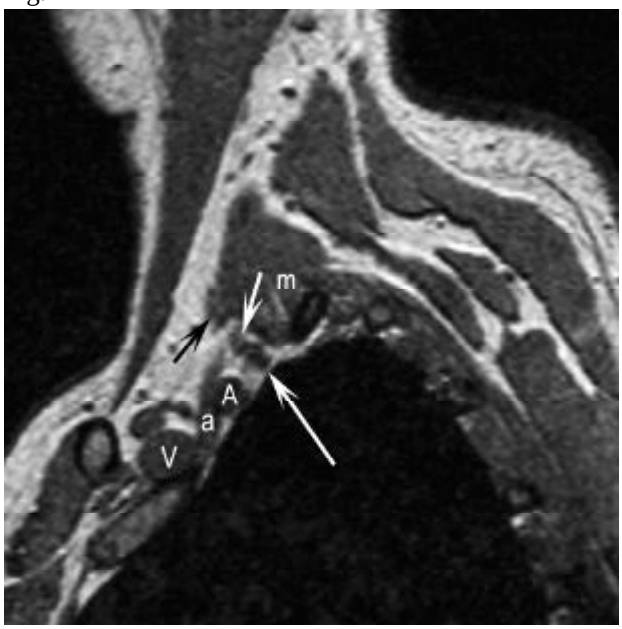

Fig. 7D

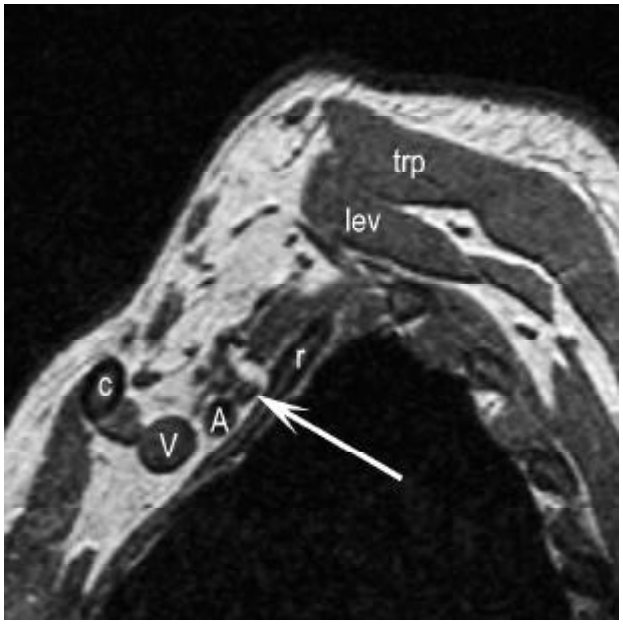

Fig. 7E

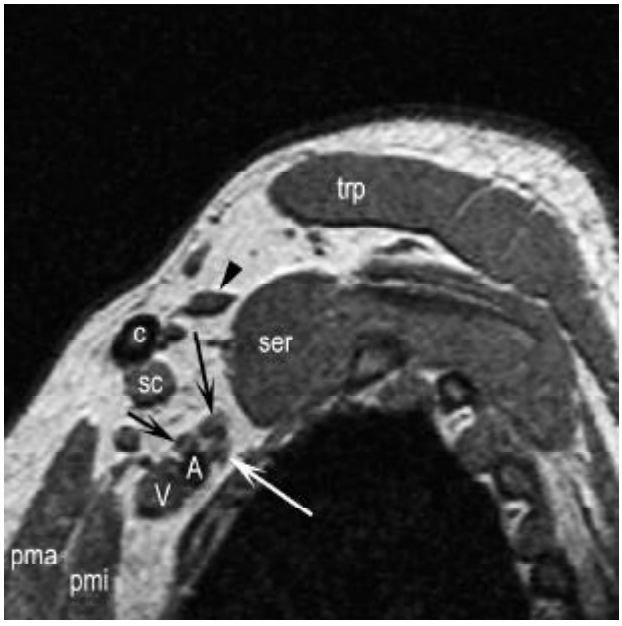

Fig. 7F

Fig. 7. Normal sagittal anatomy from a sagittal T1-weighted 3D volume acquisition.

A. The ventral rami of the roots C5, 6, 7, 8 and Th1 are shown (white arrows) just as they have left their foramina. The stellate ganglion (black arrow) is seen anterior to the first rib (r) as a flat density discernible from the surrounding fat.

B. Sagittal image 2.5 cm lateral from **A**. The ventral rami of the roots C7 (short white arrow), C8 (black arrow), and Th1 (long white arrow) can be seen entering the interscalene triangle, which is formed by the anterior (a) and middle (m) scalene muscles. The ventral rami of the roots C5 and C6 are not identifiable as separate structures from the anterior and middle scalene muscles. A = subclavian artery, V = subclavian vein, p = posterior scalene muscle, scm = sternocleidomastoid muscle, 1 = first rib, 2 = second rib.

C. Slightly lateral to **B**, the ventral rami of the roots C5, 6, 7, 8 and Th1 can be identified (arrows). A = subclavian artery, V = subclavian vein, a = anterior scalene muscle, m = middle scalene muscle.

D. Slightly lateral to **C**, just lateral to the interscalene triangle the three trunks are seen: the upper trunk (black arrow), the middle trunk (short white arrow), and the lower trunk (long white arrow). A = subclavian artery, V = subclavian vein, a = anterior scalene muscle, m = middle scalene muscle.

E. Sagittal image 2.5 cm lateral from **B**. Superior to the subclavian artery (A) the divisions (arrow) are formed just before or when the brachial plexus crosses the clavicle (c). V = subclavian vein, r = first rib, trp = trapezius muscle, lev = levator scapulae muscle.

F. Sagittal image 2.5 cm lateral from **E**. Lateral to the lateral side of the first rib the three cords have formed. At this level the lateral cord (short black arrow) is positioned anterior, the posterior cord (long black arrow) superior and the medial cord (white arrow) posterior to the axillary artery (A). V = axillary vein, pma = pectoralis major muscle, pmi = pectoralis minor muscle, c = clavicle, sc = subclavius muscle, trp = trapezius muscle, ser = serratus anterior muscle, arrowhead points to omohyoid muscle.

Fig. 8. Proton-density (**A**) and T2-weighted (**B**) sagittal image of the cords in the same patient and at the same level as in **Fig. 7F**. Note that the brachial plexus (arrow) has a low signal intensity on both the proton-density and T2-weighted images. A = axillary artery, V = axillary vein.

Fig. 8A

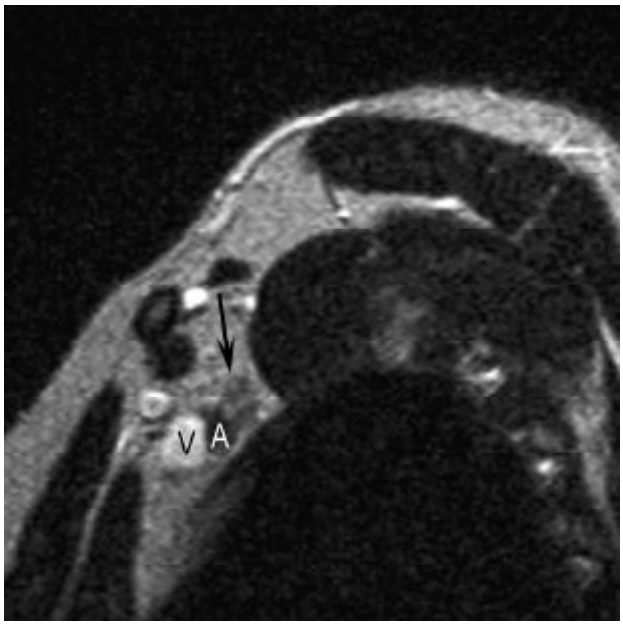

Fig. 8B

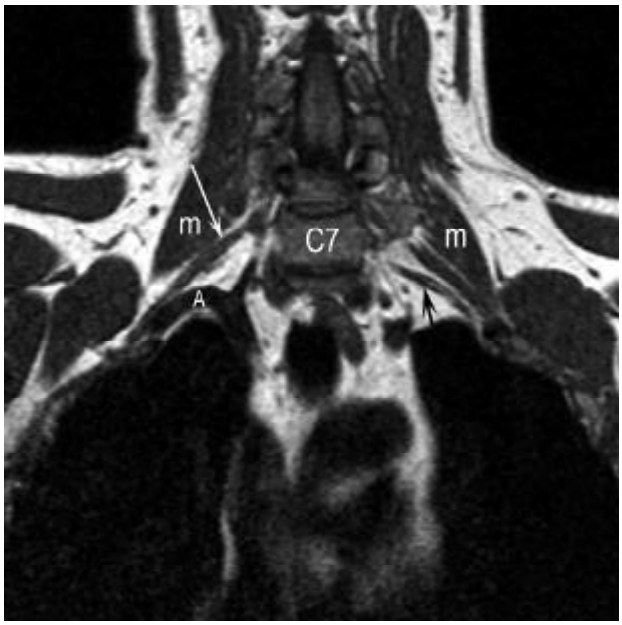

Fig. 9A

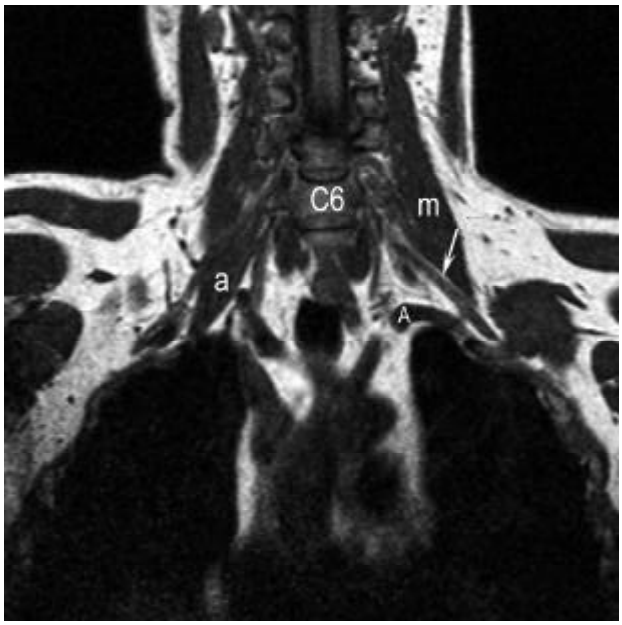

Fig. 9B

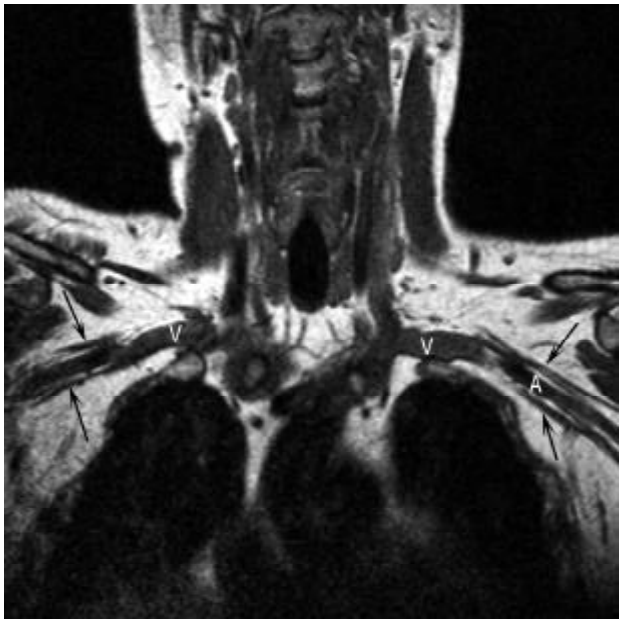

Fig. 9C

Fig. 9. Normal coronal anatomy of the same patient as in **Fig. 7** with T1-weighted images in a posterior (**A**), middle (**B**) and anterior (**C**) plane.

A. Right ventral ramus of root C7 (white arrow) and left ventral ramus of root C8 (black arrow). A = subclavian artery, m = middle scalene muscle, C7 = vertebral body C7.

B. Left ventral ramus of root C7 (arrow), left middle scalene muscle (m) and right anterior scalene muscle (a). A = subclavian artery, C6 = vertebral body C6.

C. Cords (arrows) surrounding the axillary artery (A). V = subclavian vein.

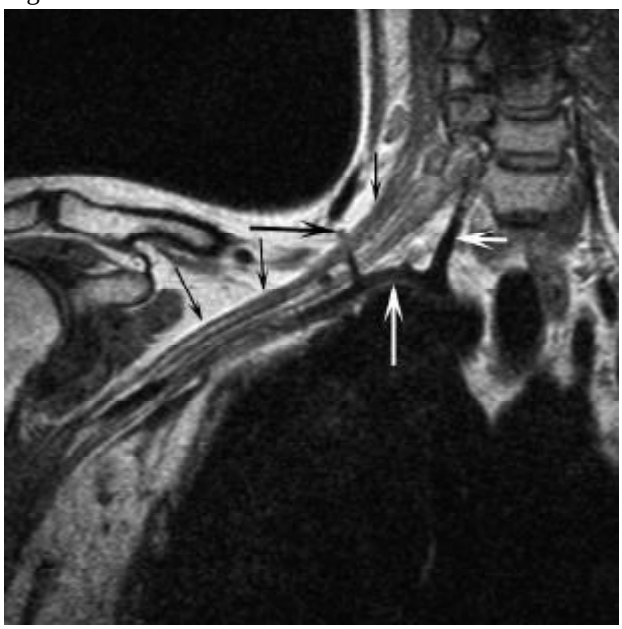

Fig. 10

Fig. 10. Normal coronal anatomy in a different patient. The ventral rami of the roots, trunks, divisions and cords (short black arrows) can be seen in one plane. Note the dorsal scapular artery originating from the subclavian artery which passes through the brachial plexus (long black arrow). Long white arrow points to the subclavian artery, short white arrow points to the vertebral artery.

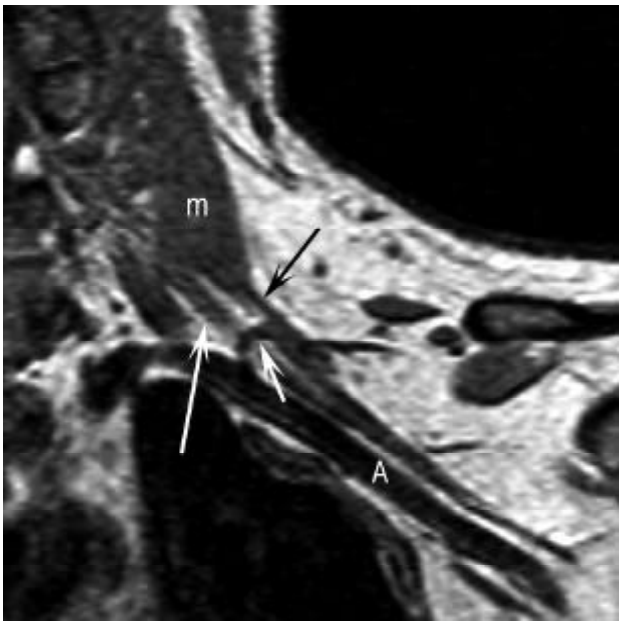

Fig. 11A

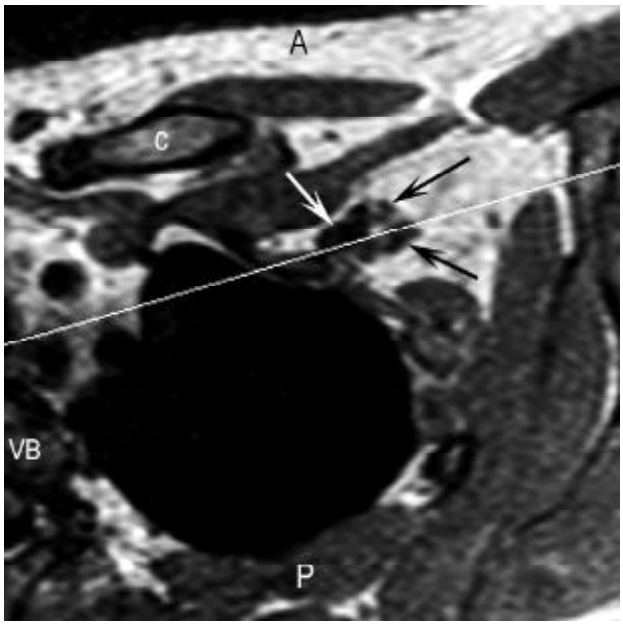

Fig. 11B

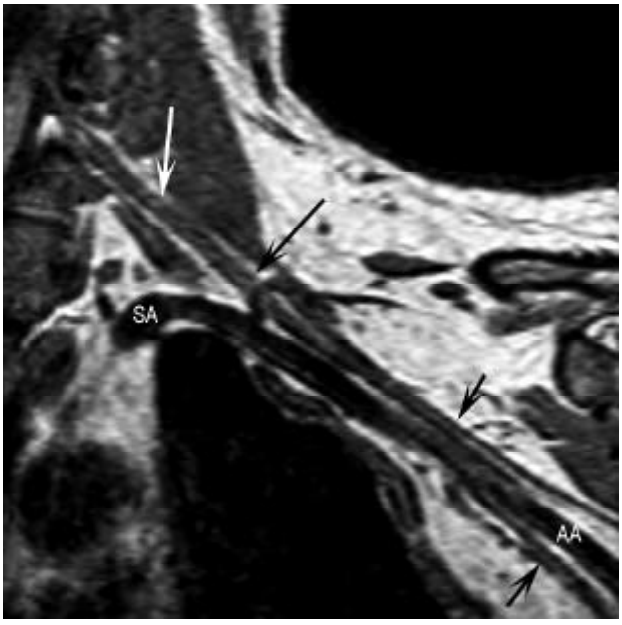

Fig. 11C

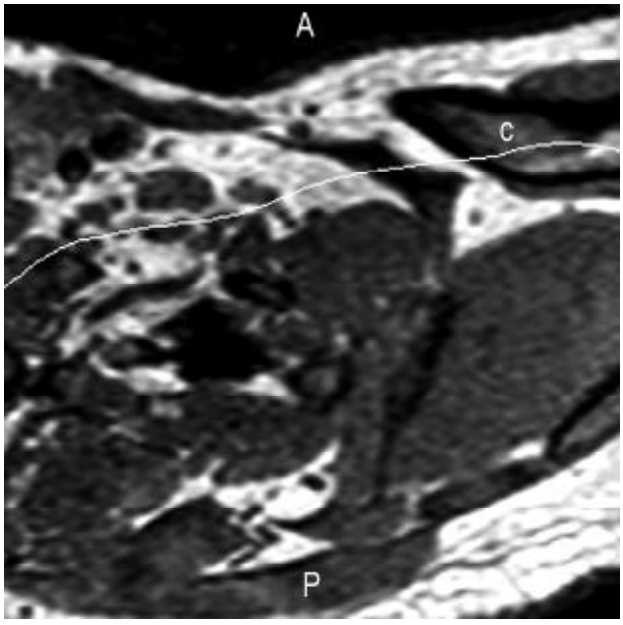

Fig. 11D

Fig. 11. Because the brachial plexus runs from medial-posterior to lateral-anterior in most cases, an oblique reconstruction can show the full courses of these structures, from the ventral rami of the roots through to the cords, in one plane. In this figure an oblique and a curved coronal reconstruction from the T1-weighted 3D volume acquisition of **Fig. 7** are shown.

A. and **B.** Oblique coronal reconstruction (**A**) with the axial scanogram (**B**; A = anterior, P = posterior, VB = vertebral body, c = clavicle, white arrow points to the subclavian artery, black arrows point to the brachial plexus). The dorsal scapular artery (short white arrow) passes between the upper (black arrow) and middle (long white arrow) trunks. A = axillary artery, m = middle scalene muscle.

C. and **D.** Curved coronal reconstruction (**C**) with the axial scanogram (**D**; A = anterior, P = posterior, c = clavicle). The brachial plexus is shown in one plane, from the ventral ramus of root C7 (white arrow), which continues as the middle trunk (long black arrow) through to the cords (short black arrows). SA = subclavian artery, AA = axillary artery.

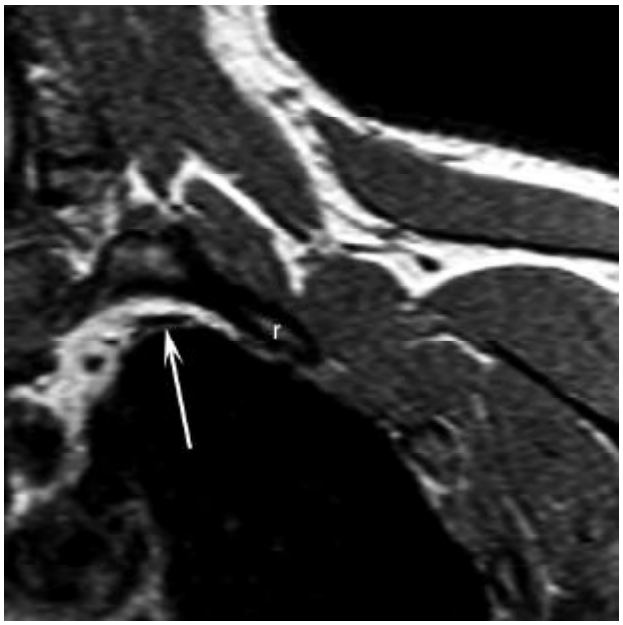

Fig. 12A

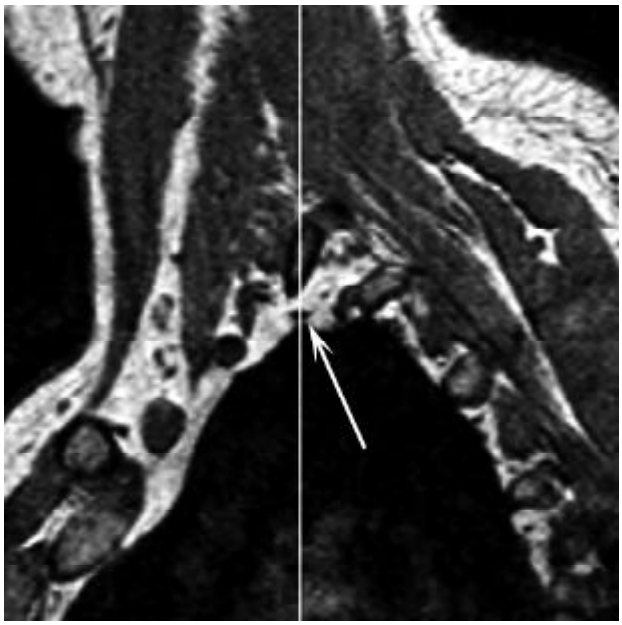

Fig. 12B

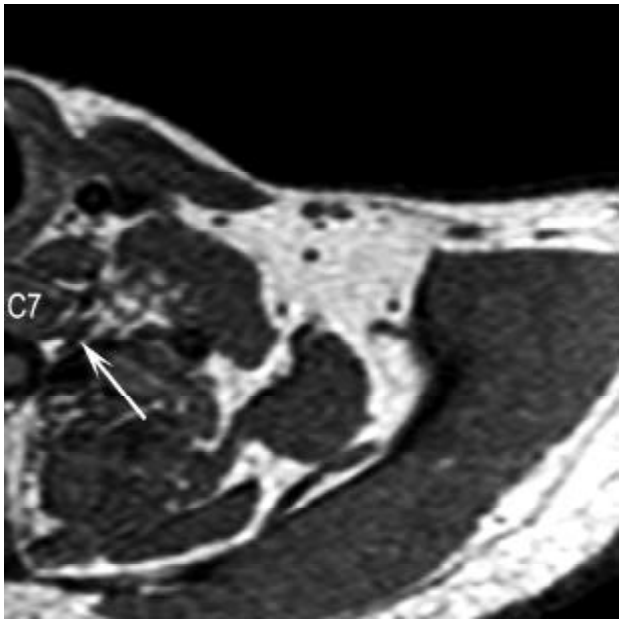

Fig. 13A

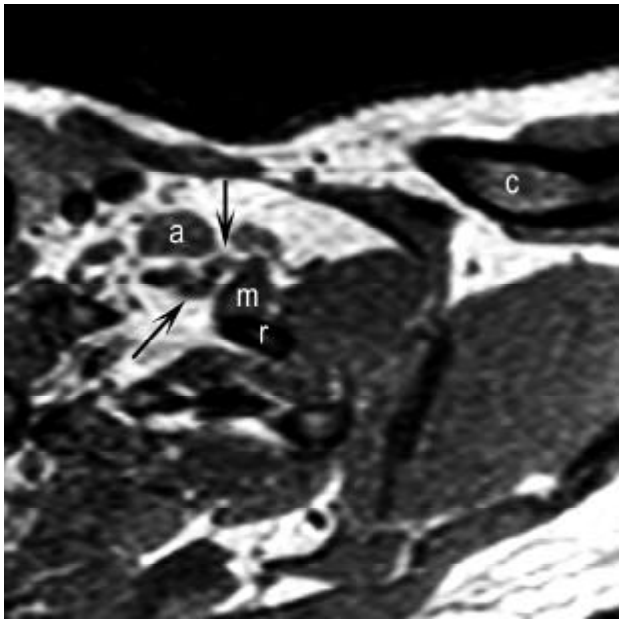

Fig. 13B

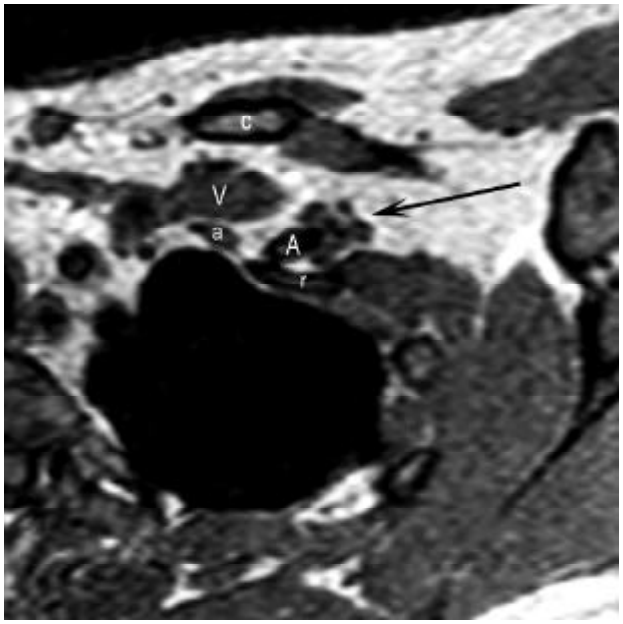

Fig. 13C

Fig. 13D

In the literature there is no consensus about the imaging strategy for evaluating the brachial plexus. The axial and coronal planes permit left-to-right comparisons. The sagittal plane demonstrates the brachial plexus most consistently because the nerves and the related vessels are seen in cross section. The axial plane is particularly useful for delineating the nerve roots as they exit the foramina, because the imaging plane is then parallel to the orientation of the nerve roots. The coronal plane can show parts of the ventral rami, trunks, divisions and cords in one plane. However it is usually impossible to visualize all five ventral rami in one single plane because the upper ventral rami are located anterior to the lower ventral rami due to the cervical lordosis. Several combinations have been recommended: axial and coronal views,[21,31] axial and sagittal views,[200] sagittal and coronal views with axial slices only scanned on an as needed basis,[114,260] coronal views with additional axial or sagittal planes[54,194] and all planes.[87,177,223] None of these protocols could optimally delineate the brachial plexus because the brachial plexus is oriented obliquely to each one of the three standard orthogonal planes. Oblique coronal images parallel to the subclavian and axillary arteries can be obtained.[177] Because scanning in three directions is time consuming and to prevent the problem of a choice of two out of the three imaging planes, we explored the use of a T1-weighted three-dimensional (3D) volume acquisition to depict the full course of the brachial plexus and the surrounding structures.[259,261,262] The advantages of a volume acquisition in this complex anatomic region are: (1) the availability of thin overlapping slices, (2) multiplanar reformatting (MPR) possibilities, and (3) cine-display viewing. Disadvantages are: (1) a longer reconstruction time, and (2) the use of a separate workstation for optimally evaluating the many images is mandatory. A T1-weighted 3D volume acquisition with a scan matrix of 256, a field of view (FOV) of 256 mm, and a slice thickness of 2 mm with a 1 mm overlap can generate reformatted images in any plane that have the same quality as the original sagittal images.

Fig. 12. One of the advantages of the MPR is the possibility of obtaining an image reconstruction in any direction at any desired point.

A. and **B.** Coronal image (**A**) with the sagittal scanogram (**B**) shows the ventral ramus of root Th1 (arrow in **A** and **B**) which lies inferior to the first rib (r). Note the close relationship with the apex of the lung.

Fig. 13. Normal axial anatomy. The images shown in this figure are reconstructions from the T1-weighted 3D volume acquisition of **Fig. 7**.

A. Axial image shows root C8 as it exits the intervertebral foramen (arrow). C7 = vertebral body C7.

B. Axial image at the level of the interscalene triangle shows the ventral rami of the roots (arrows) between the anterior (a) and middle (m) scalene muscles, r = first rib, c = clavicle.

C. Axial image at the level of the divisions (arrow). A = subclavian artery, the subclavian vein (V) runs between the clavicle (c) and the anterior scalene muscle (a), r = first rib.

D. Axial image at the level of the cords, the lateral cord (long black arrow) is located anterior, the posterior cord (short black arrow) lateral and the medial cord (white arrow) posterior to the axillary artery (A), c = clavicle.

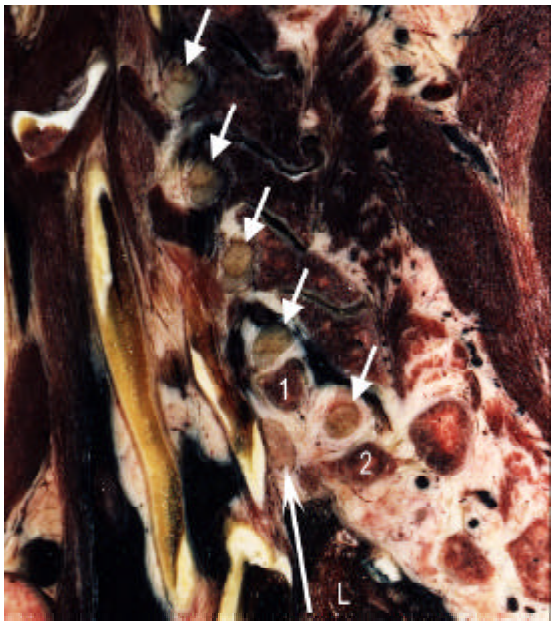

Fig. 14A

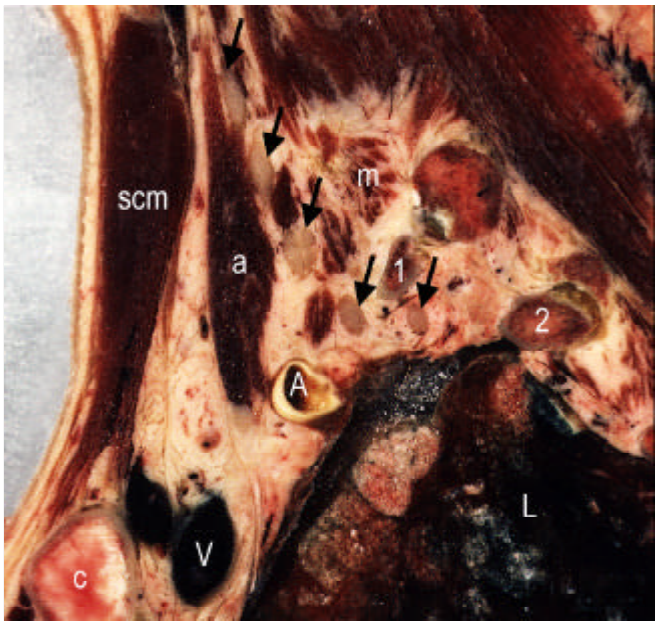

Fig. 14B

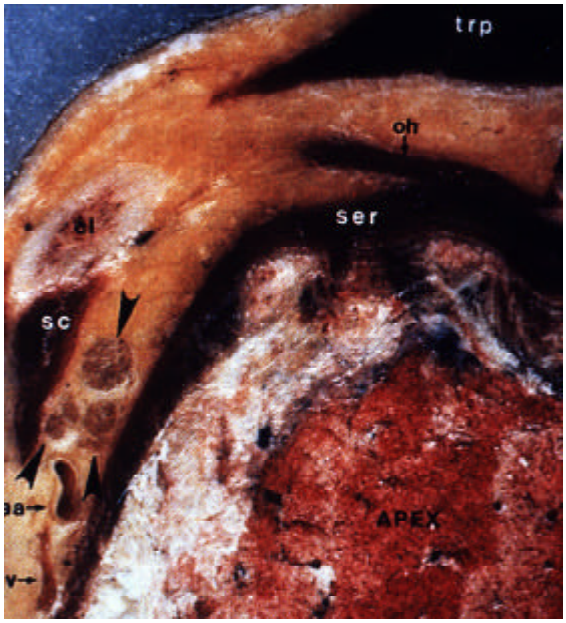

Fig. 14C

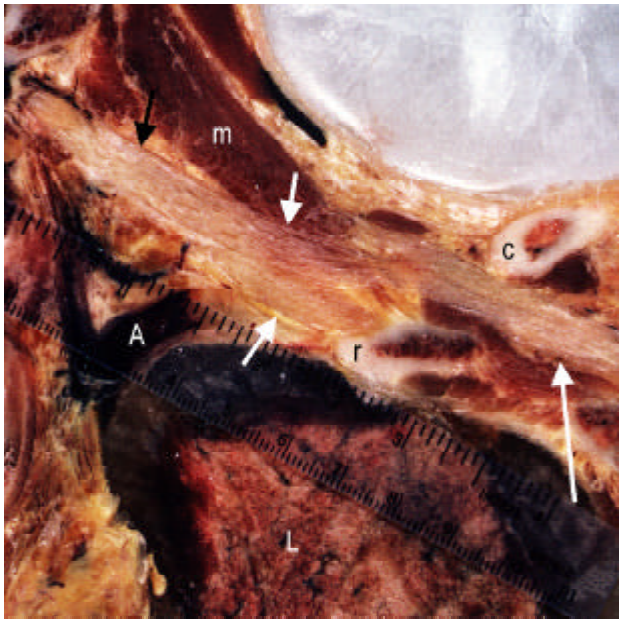

Fig. 14D

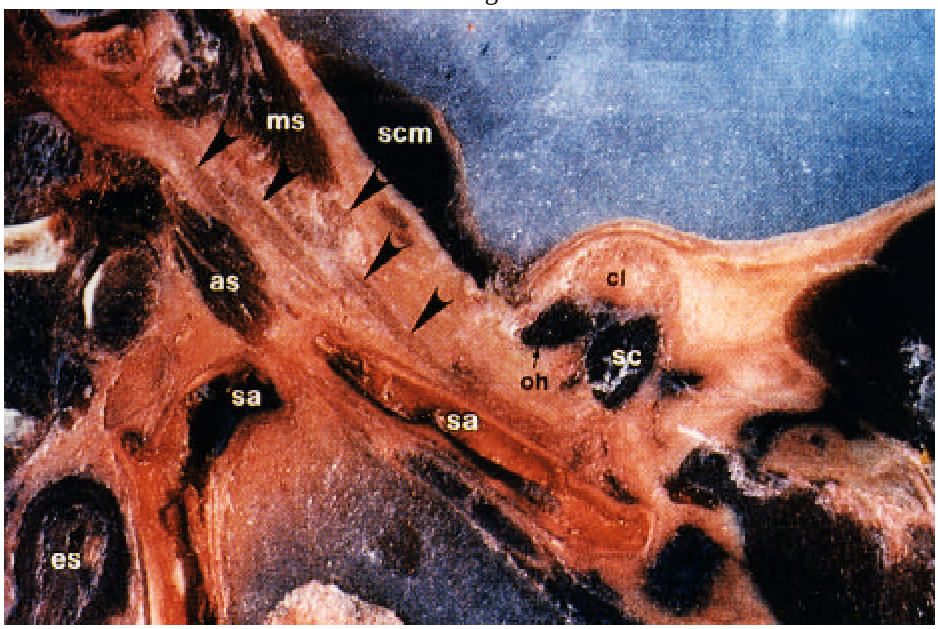

Fig. 14E

Own scan protocol

The protocol has changed during the course of the years. In our first protocol[260] we performed sagittal T1-weighted, proton-density and T2-weighted images and coronal T1-weighted images of one side. The whole brachial plexus of one side was imaged in the sagittal plane from the spinal cord to the medial side of the humeral head with a slice thickness of 6 mm and an interslice gap of 4 mm. In the coronal plane the slice thickness was 3 mm with an interslice gap of 0.3 mm. Because of the complex anatomy of the brachial plexus we preferred to use thinner contiguous slices. For this reason we devised an alternative protocol in which the standard sagittal T1-weighted spin echo sequence is replaced by a sagittal T1-weighted 3D volume acquisition.[259,261,262] These two protocols were mainly used on a 0.5 Tesla machine (Gyroscan T5 and T5-II, Philips, Philips Medical Systems, Best, The Netherlands) with the use of the body-wrap-around surface coil.[260] The post-processing is done on separate workstations (Gyroview or EasyVision, both from Philips, Philips Medical Systems, Best, The Netherlands). After obtaining a new 1.5 Tesla machine (Gyroscan ACS-NT, Philips, Philips Medical Systems, Best, The Netherlands) in our department, we prefer to image the brachial plexus on this scanner because of the improved signal to noise ratio. Although a body-wrap-around surface coil is not available for this scanner, the quadrate body coil generates a very good image quality. The T1-weighted 3D volume acquisition was replaced by a 3D turbo field echo (TFE) sequence, which has less flow and movement artifacts. An acronym for this acquisition is 3D magnetization-prepared rapid gradient echo imaging (3D MP RAGE).[11,27,157]

Fig. 14. Cryomicrotome sections: sagittal and coronal anatomy of the brachial plexus. Courtesy of Bruce H. Nowicki and Victor M. Haughton, Froedtert Memorial Lutheran Hospital, Medical College of Wisconsin, Milwaukee, Wisconsin, USA; reproduced with permission from van Es.[262]

A. Sagittal cryomicrotome section matching **Fig. 7A**. Short arrows: the ventral rami of the roots C5, 6, 7, 8 and Th1. Long arrow: stellate ganglion. L = lung, 1 = first rib, 2 = second rib.

B. Sagittal cryomicrotome section matching **Fig. 7B**. Arrows: the ventral rami of the roots C5, 6, 7, 8 and Th1. A = subclavian artery, V = subclavian vein, a = anterior scalene muscle, m = middle scalene muscle, c = clavicle, scm = sternocleidomastoid muscle, L = lung, 1 = first rib, 2 = second rib.

C. Sagittal cryomicrotome section in the proximity of **Fig. 7F**. Arrowheads: the three cords. The lateral cord is positioned anterior to, the posterior cord superior to, and the medial cord posterior to the axillary artery (aa). APEX = lung apex, v = axillary vein, cl = clavicle, sc = subclavius muscle, ser = serratus anterior muscle, oh = omohyoid muscle, trp = trapezius muscle.

D. Coronal cryomicrotome section. A part of the brachial plexus is seen extending laterally parallel to the ruler, with, from medial to lateral, in order, a root (black arrow), trunks (short white arrows) and cords (long white arrow). A = subclavian artery, m = middle scalene muscle, r = first rib, c = clavicle, L = lung.

E. Coronal cryomicrotome section. Black arrowheads point to the proximal part of the brachial plexus: the roots and trunks; scm = sternocleidomastoid muscle, ms = middle scalene muscle, as = anterior scalene muscle, sa = subclavian artery, oh = omohyoid muscle, sc = subclavius muscle, cl = clavicle, es = esophagus.

The protocols used on the 1.5 Tesla and 0.5 Tesla scanners, which are correlated to pathology, are shown in Tables 1-4. Gadolinium-DTPA (Magnevist®, Schering, Berlin, Germany) is administered in cases of any tumor for better delineation of the extent of the tumor.

Figs. 7-13 show the anatomy of the brachial plexus in all planes as seen with MR imaging, which is correlated with cryomicrotome sections in Fig. 14. The following anatomic details can be discerned: the individual ventral rami of the nerve roots, the three trunks, the three cords and the stellate ganglion. We were not able to discern the six divisions separately. The anatomy of the terminal branches is beyond the scope of this thesis. In our experience the many anatomic variations of the brachial plexus cannot be seen with MR imaging.

Table 1

Scan parameters Gyroscan ACS-NT (1.5 Tesla)

SCANNAME	SURVEY	SAG T2	3D-TFE	COR T1	TSE STIR	SAG T1	3D-TSE
coil	body	body	body	body	body	body	synergy spine
scan mode	SE	SE	TFE	SE	IR	SE	TSE
scan direction	cor	sag	sag	cor	cor	sag	trs
phase direction	RL	AP	AP	RL	RL	AP	AP
fold over	yes	yes	yes	yes	yes	yes	no
slice thickness (mm)	10	6	2	3	3	6	2
interslice gap (mm)	1	3	-1	0.3	0.3	3	0
number of slices	11	18	150/200	18	18	18	60
number of chunks							10
FOV (mm)	450	300	256	350	350	300	250
rectangular FOV %	100	80	90	100	100	80	50
matrix	256	256	256	256	256	256	256
scan %	75	70	70	70	80	80	70
NSA	2	2	2	3	4	2	1
TR (ms)	383	2221	13	563	3103	563	5000
TE (ms)	20	25/90	4.6	18	100	18	200
TI (ms)					150		
flip angle (degrees)	90	90	15	90	180/90	90	90
TFE prepulse			saturate				
prepulse delay (ms)			350				
3D order			YZ				
shots			4				
shot interval			shortest				
turbo factor					11		27
profile order					linear		linear
echoes	1	2	1	1	1	1	1
flow compensation	yes	yes	no	yes	yes	yes	no
water fat shift (pixels)	max	2	2	2	max	2	max
scantime (min)	2:28	6:39	7:49/10:31	5:04	7:45	3:05	8:00

Table 2

Scan protocol Gyroscan ACS-NT (1.5 Tesla)

standard protocol

1. SURVEY
2. SAG T2 of symptomatic side
3. 3D-TFE (150 slices) of symptomatic side
4. COR T1 of both sides

tumors

1. SURVEY
2. SAG T2 of symptomatic side
3. 3D-TFE (150 slices) of symptomatic side
4. COR T1 + GADOLINIUM-DTPA of both sides
5. SAG T1 + GADOLINIUM-DTPA of symptomatic side

superior sulcus tumors or tumors which have a close relationship with the vertebral column

1. SURVEY
2. SAG T2 of symptomatic side
3. 3D-TFE (200 slices) with 150 slices of symptomatic side and 50 slices of other side
4. COR T1 + GADOLINIUM-DTPA of both sides
5. SAG T1 + GADOLINIUM-DTPA of symptomatic side

thoracic outlet syndrome or cervical ribs

1. SURVEY
2. SAG T2 of symptomatic side
3. 3D-TFE (200 slices) with 150 slices of symptomatic side and 50 slices of other side
4. COR T1 of both sides

multifocal motor neuropathy (MMN) or chronic inflammatory demyelinating polyradiculoneuropathy (CIDP)

1. SURVEY
2. SAG T2 of both sides
3. COR T1 of both sides
4. TSE STIR of both sides
5. if pathologically increased signal intensity of the brachial plexus:
   COR T1 + GADOLINIUM-DTPA of both sides

trauma

1. SURVEY
2. SAG T2 of symptomatic side
3. COR T1 of both sides
4. TSE STIR of both sides
5. 3D-TSE of C-spine from C3-4 through Th2-3

Table 3

Scan parameters Gyroscan T5-II (0.5 Tesla)

SCANNAME	SURVEY	SAG T2	3D-T1	COR T1	SAG T1
coil	bwa	bwa	bwa	bwa	bwa
scan mode	SE	SE	FFE	SE	SE
scan direction	cor	sag	sag	cor	sag
phase direction	RL	AP	AP	RL	AP
fold over	yes	yes	yes	yes	yes
slice thickness (mm)	10	6	2	3	6
interslice gap (mm)	1	3	-1	0.3	3
number of slices	11	18	150/200	15	18
FOV (mm)	450	300	256	330	300
rectangular FOV %	100	80	80	80	80
matrix	256	256	256	256	256
scan %	70	70	80	80	80
NSA	2	2	2	4	2
TR (ms)	405	2336	30	536	662
TE (ms)	20	25/90	13	20	20
flip angle (degrees)	90	90	30	90	90
contrast enhancement			T1W		
echoes	1	2	1	1	1
flow compensation	yes	yes	no	yes	yes
water fat shift	max	max	max	max	max
scantime (min)	2:30	7:05	7:49/10:26	5:54	3:41

Table 4

Scan protocol Gyroscan T5-II (0.5 Tesla)

standard protocol

1. SURVEY
2. SAG T2 of symptomatic side
3. 3D-T1 (150 slices) of symptomatic side
4. COR T1 of both sides

tumors

1. SURVEY
2. SAG T2 of symptomatic side
3. 3D-T1 (150 slices) of symptomatic side
4. COR T1 + GADOLINIUM-DTPA of both sides
5. SAG T1 + GADOLINIUM-DTPA of symptomatic side

superior sulcus tumors or tumors which have a close relationship with the vertebral column

1. SURVEY
2. SAG T2 of symptomatic side
3. 3D-T1 (200 slices) with 150 slices of symptomatic side and 50 slices of other side
4. COR T1 + GADOLINIUM-DTPA of both sides
5. SAG T1 + GADOLINIUM-DTPA of symptomatic side

thoracic outlet syndrome or cervical ribs

1. SURVEY
2. SAG T2 of symptomatic side
3. 3D-T1 (200 slices) with 150 slices of symptomatic side and 50 slices of other side
4. COR T1 of both sides

List of abbreviations used in Tables 1-4

AP	anterior posterior
bwa	body-wrap-around surface coil
cor	coronal
FFE	fast field echo
FOV	field of view
IR	inversion recovery
max	maximal
NSA	number of signals averaged
RL	right left
sag	sagittal
SE	spin echo
TE	echo time
TFE	turbo field echo
TI	inversion time
TR	repetition time
trs	transverse
TSE	turbo spin echo
STIR	short inversion time inversion recovery

Chapter 3
Tumors

MR imaging of the brachial plexus is frequently requested to rule out a tumor in or near the brachial plexus, or to evaluate the extension of a known tumor in the region of the brachial plexus. In this chapter two groups of patients are described. The first group (Tables 1-4) consists of patients where a tumor was found with MR imaging. The second group (Tables 5-7) consists of patients where no tumor was detected with MR imaging. In this group the follow-up and diagnosis, if known, are described. Tumors are an important cause of brachial plexopathies. Tumors which affect the brachial plexus can be divided into primary neurogenic tumors and secondary tumors, which can be of primary or metastatic origin. Primary neurogenic tumors are rare, while secondary tumors are much more common.

Primary neurogenic tumors

Primary neurogenic tumors of the brachial plexus are an uncommon but usually well treatable cause of brachial plexopathies.[52,137,204,217] In a large study performed by Lusk,[137] who had seen approximately 600 lesions of the brachial plexus, 40 neural sheath tumors in 39 patients were found among 386 patients who had surgery. The main primary neurogenic tumors are neurofibromas, schwannomas, malignant schwannomas and post-traumatic neuromas. The post-traumatic neuromas will be discussed in Chapter 4. The cell of Schwann is the origin of the neurofibromas, schwannomas and malignant schwannomas.[64,65,212] Two large studies, respectively over a 20-year period with 28 tumors[52] and over a 17-year period with 40 tumors,[137] found that a neurofibroma is the most common neurogenic tumor of the brachial plexus (respectively 50% and 65%), and that the schwannoma is the second most common neurogenic tumor (respectively 18% and 20%). In both studies 14% of the neural sheath tumors were malignant. A minority (respectively 43% and 35%) of the neurofibromas was associated with von Recklinghausen's disease (neurofibromatosis type I). Other reported very rare primary neurogenic tumors of the brachial plexus include a meningioma[137] and a fibrolipomatous hamartoma.[196]

Neurofibromas can develop in patients with and without von Recklinghausen's disease. A solitary neurofibroma occurs by definition in patients who do not have von Recklinghausen's disease. In patients with von Recklinghausen's disease localized neurofibromas, which are histologically identical to the solitary neurofibromas, and plexiform neurofibromas occur.[64] The peak age is 20 to 40 years with an equal sex distribution. Neurofibromas have no capsule and infiltrate the nerve fascicles. Because of the diffuse penetration of tumor into the nerve, it is difficult to resect the tumor without permanent damage to the nerve.[137,217,234]
The schwannoma (synonyms: neurilemoma, neurinoma) is a benign encapsulated eccentric nerve sheath tumor which arises from Schwann cells and displaces the nerve fascicles instead of infiltrating them. Schwannomas have an unusual relationship with von Recklinghausen's disease and malignant transformation is extremely rare.[64,212] If schwannomas show degenerative changes, such as calcification, cyst formation and hemorrhage, they are called ancient schwannomas. The peak age is 20 to 50 years with an equal sex distribution. It is usually possible to resect them without sacrificing the nerve or without neurologic damage.[137,217,234]
The malignant schwannoma (synonyms: neurogenic sarcoma, neurofibrosarcoma, malignant peripheral nerve sheath tumor) can arise de novo, in association with von Recklinghausen's disease and post irradiation.[58,59,65,73] Fifty percent occur in association with von Recklinghausen's disease.[212] The peak age is 20 to 50 years. In patients with von Recklinghausen's disease the mean age of incidence is considerably lower.

Clinical symptoms and signs of primary neurogenic tumors of the brachial plexus can consist of: paresthesias, numbness, sensory and motor deficits, pain, atrophy, and a palpable mass which, when manipulated, can cause radiating paresthesias or pain. Electromyography (EMG) might be abnormal.

Imaging

Conventional radiography is of limited value. Widening of the neural foramina can be seen on C-spine radiographs in patients with neurofibromatosis. Intrathoracic extension of a neurogenic tumor is possible and can be detected on a chest radiograph.[88]
CT features of primary neurogenic tumors are:[19,40,124] a well delineated mass with lower density than muscle, focal contrast enhancement, and inhomogeneities which can represent benign as well as malignant disease. There have been some reports about CT of primary neurogenic tumors of the brachial plexus.[8,36,195,255,265]
With MR imaging the detection of primary neurogenic tumors of the brachial plexus has increased and many case reports of those tumors have been described.[21,23,31,54,100,194,200-202,223,229,231,259-262,279]

The MR imaging characteristics of a neurogenic tumor are: (1) low signal intensity on T1-weighted images, an increased signal intensity on proton-density images, a high signal intensity on T2-weighted images, which can be inhomogeneous, and enhancement after administration of gadolinium-DTPA, (2) fusiform growth, (3) sharply defined edge, and (4) in many cases the involved nerve can be found entering and leaving the tumor.

With MR imaging it is not possible to reliably differentiate between a neurofibroma, a schwannoma, and a malignant schwannoma.[136,194,231,234] However, some signs might suggest the correct diagnosis. The so-called "target" appearance, which is a low signal intensity central zone with a peripheral zone of higher signal intensity on T2-weighted images, is only found in neurofibromas, whereas schwannomas and malignant schwannomas show an inhomogeneous signal intensity on T2-weighted images.[234] This target appearance represents the geographic difference between two different histological zones, namely a central zone of dense fibrous and collagenous tissue and abundant myxoid material with a high fluid content in the periphery. Malignancy can be suggested if one of the following signs is present: an increased heterogeneity, a large tumor with areas of hemorrhage and necrosis, infiltration into the soft tissues or indistinct margins.

Secondary tumors

Secondary tumors can be divided into primary tumors in the region of the brachial plexus and metastatic disease. The main primary tumors are: lung tumors, skeletal tumors, soft tissue tumors,[118,119] head and neck tumors, and lymphoma. The most common metastases in the region of the brachial plexus are those from breast, lung, and head and neck tumors. True isolated metastatic invasion of the brachial plexus is rare, but has been described.[145] It is important to make a distinction between tumors that are only adjacent to the brachial plexus, and those that invade or compress the nerves. As MR imaging can clearly demonstrate the course of the brachial plexus and can show the relationship in any plane between the tumor and the brachial plexus, MR imaging is very capable of making this distinction. Most tumors have a low signal intensity on T1-weighted images, a high signal intensity on T2-weighted images, and enhance after gadolinium-DTPA.

The following tumors will be discussed below: superior sulcus tumor, metastatic breast cancer, aggressive fibromatosis and lipoma.

Superior sulcus tumor (Pancoast's tumor)

Pancoast[178,179] reported a clinical syndrome associated with a tumor at the apex of the lung. Pancoast's syndrome consists of pain around the shoulder and in the arm in the eighth cervical and first and second thoracic root distribution, Horner's syndrome,

muscle atrophy of the hand and radiologic evidence of a shadow at the lung apex always with rib destruction and often with vertebral body involvement. In his first report[178] he called it an ”apical chest tumor”, which became “superior pulmonary sulcus tumor” in his second article.[179] He changed the name because superior pulmonary sulcus tumor implies its appropriate location and a lack of origin from the lung, pleura, ribs or mediastinum. With the superior pulmonary sulcus he presumably meant the anatomical sulcus made by the passage of the subclavian artery in the cupula of the pleura (subclavian artery groove).[97,185] As Hepper[97] did not find the anatomic term “superior pulmonary sulcus” in any anatomy book, he suggested the name “thoracic inlet tumor”. However, until now the term superior (pulmonary) sulcus tumor or Pancoast’s tumor is still widely used. Pancoast suggested that the tumor originates from an embryonal rest. The true site of origin, namely the lung, was recognized by Tobias.[249] Hepper[97] demonstrated that these tumors are pathologically identical to other primary tumors of the lung. The histology of superior sulcus tumors can be adenocarcinoma, squamous cell, large cell and small cell carcinoma.[138,185] A commonly used definition of superior sulcus tumor is: radiographic evidence of a shadow in the apex of the lung, associated with a characteristic history of pain along the first and second thoracic and eighth cervical nerve pathways.[138,147,185] Horner’s syndrome and bone involvement are not necessary for the diagnosis. MR imaging can also be requested for the evaluation of other apical lung tumors, which are located more posteriorly in the lung apex. These tumors should not be called superior sulcus tumors, but apical lung tumors. The clinical syndrome of a superior sulcus tumor is quite characteristic.[185] The first sign is local pain in the shoulder and at the medial side of the scapula, caused by referred pain mediated through afferent pain fibers of the sympathetic trunk and ganglia. Involvement of Th1 is characterized by pain at the medial side of the upper arm. If the pain extends to the ulnar surface of the forearm and small and ring fingers, the C8 nerve root is also involved. Involvement of the white ramus communicans of Th1 or the stellate ganglion itself causes Horner’s syndrome. Other commonly involved anatomic structures include the subclavian artery, the ribs (usually the first and second) and the vertebral bodies with possible invasion of the spinal canal which can cause spinal cord compression. Pulmonary symptoms are usually absent.

According to the TNM classification[155,156] superior sulcus tumors are by definition at least T3. If there is invasion of the mediastinum or involvement of the heart, great vessels, trachea, esophagus, vertebral body or carina, or presence of malignant pleural effusion the tumor becomes T4 and is considered inoperable. Any lymph node involvement or distant metastases also usually preclude surgery. There are several therapeutic options for the T3N0M0 superior sulcus tumor. Preoperative low-dose radiation therapy followed by surgery, initially reported by Shaw,[220] has shown good results.[138,147,173,185,228,276] Paulson[185] reported a five years survival rate of 34% and a 10

years survival rate of 29%. The purpose of the preoperative radiation therapy is to decrease the extent of disease and to create a pseudocapsule, which increases the resectability.[185] Other therapeutic options are high-dose curative radiation therapy,[115,263] pre- and postoperative radiation therapy,[219] and operation with or without postoperative irradiation.[9] At our institution the therapeutic strategy is as follows. If MR imaging or CT shows that the tumor is unresectable, that is if the tumor is staged as T4, or metastases have been found, then curative or palliative radiation therapy will be given. If the tumor is staged as T3 and there are no signs of metastases, then a mediastinoscopy will be performed to determine the N status. When there are any positive lymph nodes, curative radiation therapy will be given. Preoperative low-dose radiation therapy followed by surgery will be performed if the mediastinoscopy is negative. Postoperative radiation therapy is applied in certain cases, when radical surgery has not been successful. So imaging plays an important role in defining the therapy. CT is capable of detecting invasion of the mediastinum, encasement of the subclavian artery, involvement of ribs and vertebral bodies.[168,270] Cortical bone destruction is better detected with CT than with MR imaging.[123] The use of MR imaging has markedly improved the visualization of the superior sulcus tumors.[96,123,141,143,197,201,269] The coronal and sagittal planes are especially useful in determining the inferior, superior, posterior and anterior extent of the tumors. In both planes the relation between the brachial plexus and the tumor can be very well shown. Vertebral body destruction is best visualized in the axial plane. There is excellent tissue contrast between the tumor and muscles on T2-weighted images. With proton-density images there is less tissue contrast, but the anatomical details are clearer. Rib invasion is more difficult to detect with MR imaging than with CT, but is not decisive for determining the therapy. Rib invasion can be recognized by the replacement of the high signal bone marrow fat by low signal tumor on T1-weighted images. Vertebral body invasion, which in contradiction is important for the choice of therapy, is easier to detect, because of the large amount of fat within the vertebral bodies.[143] Chest wall invasion, which is by definition always present in superior sulcus tumors, can be reliably detected with MR imaging.[89,176] Interruption of the extrapleural fat plane on T1-weighted images is a good sign of pleural invasion. It can be difficult to differentiate a tumor originating in the lung from extrapleural lesions. A helpful sign is the aspect of the interface between the tumor and the lung parenchyma: an irregular border suggests a lesion originating from the lung parenchyma, whereas a smooth edge is usually seen with pleural and extrapleural lesions.[201]

Metastatic breast cancer

Brachial plexopathy in patients with breast cancer can be caused by metastatic tumor or by radiation therapy. Differentiation between these two can be difficult and will be discussed in Chapter 5. Typical sites for metastases of breast cancer are the skin,

subcutaneous tissues, axilla, pectoralis muscles, the parasternal zone and the region of the brachial plexus.[123,221,222] Metastatic tumor in the axilla, the pectoralis muscles and the region of the brachial plexus can cause brachial plexopathy by direct tumor invasion or compression. If surgery is considered, it is important to make a distinction between tumors that are only adjacent to the brachial plexus, and those that invade or compress the nerves. It has been shown that this distinction can be achieved with MR imaging.[21,31,54,194,200,260]

Aggressive fibromatosis

Aggressive fibromatosis (synonyms: fibromatosis, desmoid and non-metastasizing fibrosarcoma) is a benign soft tissue tumor with an infiltrative growth pattern. The axilla and neck are not uncommon sites for aggressive fibromatosis. Enzinger[63] looked at 367 cases, from which 22.1% occurred in the shoulder region and 7.6% in the neck. The tumor primarily arises from the connective tissue of muscle or the aponeurosis. The peak incidence is between 25 and 35 years. Because of its infiltrative character, which can cause brachial plexus involvement, complete resection is difficult and local recurrence common. On CT the tumor enhances and appears usually well marginated.[72,105] The MR imaging appearance is variable, most tumors show a high signal intensity on the T2-weighted images with scattered foci of low signal intensities, presumably representing hypocellular areas with a high collagen content.[68,121,198,253] Despite the invasion into adjacent structures microscopically, the tumor might appear well demarcated, limiting the value of imaging.[121,198]

Lipoma

Lipomas are benign fatty tumors that in most instances occur in the extremities, but can occur in the axilla. At MR imaging lipomas show signal intensities characteristic of fat with all pulse sequences.[56,123,250,253] Liposarcomas can contain more soft tissue elements, but MR imaging is not always capable of distinguishing between benign and malignant tumors.[29,120] The relationship between a lipoma and the brachial plexus can be well depicted.

Own material

Patients with primary neurogenic tumors

Eight patients had proven primary tumors of the brachial plexus. This was surgically proven in six and diagnosed by biopsy in two. In two other patients the diagnosis was suggested by imaging characteristics alone without further procedures to prove this diagnosis. The characteristics of the group of primary tumors are shown in Table 1, examples are shown in Figs. 1-7. Patient No. 3 (Fig. 6) with a neurofibroma was

the only patient in this group with von Recklinghausen's disease. The MR imaging findings of patient No. 8 were not typical for a primary neurogenic tumor, the tumor appeared to originate outside the nerves, although it was related to a thickened ventral ramus of root C7 (Fig. 7) and pathologically it appeared to be a malignant schwannoma, probably a radiation-induced tumor 17 years after radiation therapy for breast carcinoma.

Patients with secondary tumors

A. LUNG TUMORS

The largest group of secondary tumors closely related to the brachial plexus are the primary lung tumors (24 patients). The characteristics are shown in Table 2 and examples in Figs. 8-13. Brachial plexus involvement was suggested clinically in 14 patients (patients Nos. 12-14, 16-18, 21, 22, 24-26, 30-32). In these patients brachial plexus involvement was found with MR imaging in 12 patients. The pain in patients Nos. 17 (Fig. 10) and 32, where no brachial plexus involvement was found, could be explained by involvement of the ventral ramus of root Th2. The findings found with MR imaging were confirmed at surgery in two patients (patients Nos. 16 and 25). Clinically there was no suspicion of brachial plexus involvement in 10 patients (patients Nos. 11, 15, 19, 20, 23, 27-29, 33 and 34), which was confirmed with MR imaging in eight patients and also at surgery in four patients (patients Nos. 19, 28, 33 and 34). In two patients (patients Nos. 11 and 27) MR imaging showed brachial plexus involvement, which was confirmed at surgery in one patient (patient No. 27). In this patient the tumor was found to be adjacent to the brachial plexus but could be separated from it.

In patients Nos. 15, 22 and 32 surgery was precluded because vertebral body invasion was found with MR imaging. Mediastinal invasion with tumor surrounding the aorta was a contra-indication for surgery in patient No. 13 (Fig. 12). In patients Nos. 14 and 27, MR imaging was performed before and after radiation therapy; tumor shrinkage was considered enough to perform surgery in patient No. 27, while no surgery was performed in patient No. 14 because of no reaction of the tumor to radiation therapy. In patient No. 25 (Fig. 9) the tumor was found to surround the ventral rami of roots C8 and Th1, and to displace the ventral ramus of root C7. These findings were confirmed at surgery and the ventral ramus of root C7 was not sacrificed.

B. BREAST CARCINOMA

The most common metastasis near or in the brachial plexus we found was that of breast carcinoma (nine patients). Characteristics are described in Table 3 and examples are shown in Figs. 14 and 15. The imaging findings were confirmed at surgery in patient No. 43 (Fig. 14). In patient No. 39, MR imaging showed a metastasis without brachial plexus involvement. However, three months later metastatic disease around

the brachial plexus was found at surgery next to the metastasis described with MR imaging. In patient No. 42 (Fig. 15) thickening of the brachial plexus was seen and interpreted as either metastatic tumor or radiation fibrosis. Biopsy revealed metastatic tumor. In all other patients the metastases presented as a mass adjacent to the brachial plexus.

C. MISCELLANEOUS TUMORS

The characteristics of the 23 other tumors are described in Table 4, examples are shown in Figs. 16-26. Primary malignant tumors include B-cell non-Hodgkin's lymphoma (patients Nos. 51 and 57, Figs. 16 and 17), leiomyosarcoma (patient No. 65, Fig. 22), liposarcoma (patient No. 58, Fig. 23), chondrosarcoma (patients Nos. 52 and 60, Fig. 25), and synoviosarcoma (patient No. 45, Fig. 26). Metastatic malignant tumors were from unknown origin (patients Nos. 49, 55, 63 and 64, Fig. 18), from head and neck tumors (patients Nos. 47 and 50), from chondrosarcoma (patient No. 53, Fig. 24), and renal cell carcinoma (patient No. 66). In patient No. 62 the tumor is of unknown origin. The liposarcoma in patient No. 58 (Fig. 23) appeared 24 years after radiation therapy for Hodgkin's disease, and is probably radiation-induced. Benign tumors include aggressive fibromatosis (patients Nos. 44 and 61, Fig. 19), meningocele in a patient with von Recklinghausen's disease (patient No. 59, Fig. 20), lipoma (patients Nos. 46, 54 and 56, Fig. 21), and a hematoma in a neck cyst (patient No. 48).

Patients without detected tumors

A. INFECTION

Table 5 shows the characteristics of three patients who were initially suspected of having a tumor in the region of the brachial plexus, but who turned out to have an infection.

B. RADIATION THERAPY

Patients who have had radiation therapy can develop complaints which could be due to radiation brachial plexopathy or tumor. Table 6 describes 17 patients with symptoms of the shoulder, arm and hand without signs of tumor recurrence or metastatic tumor. There were no abnormalities detected in seven patients (patients Nos. 71, 72, 77, 78, 80, 81 and 85). Five of these patients were presumed to have radiation-induced brachial plexopathy. In one patient spontaneous improvement was seen, and in one patient the symptoms were probably due to reflex sympathetic dystrophy. Five patients showed aspecific signs after radiation therapy,[248] namely an increased signal intensity in or near the brachial plexus (patients Nos. 74 and 79), signal abnormalities in the lung apex (patients Nos. 75 and 84) and loss of fat planes

(patient No. 73). Three of these patients were clinically diagnosed to have radiation-induced brachial plexopathy, one patient showed spontaneous improvement and in one patient a carpal tunnel syndrome was diagnosed. In one patient (patient No. 83) focal thickening of the brachial plexus was seen; no clinical progression was seen in one year and the thickening might have been due to prior surgery for a malignant schwannoma. In four patients more diffuse thickening of the brachial plexus was found, thought to be due to perineural fibrosis, which was confirmed at surgery in one (patient No. 76). In two patients a low signal intensity on the T2-weighted images was seen (patients Nos. 70 and 86), and in two patients a high signal was found (patients Nos. 76 and 82). Patients Nos. 70, 76 and 86 were clinically diagnosed as having radiation-induced brachial plexopathy, patient No. 82 showed improvement of the symptoms. Patients Nos. 70, 76 and 82 will be described in Chapter 5.

C. NO ABNORMALITIES ON MR IMAGING

In Table 7 the symptoms and the diagnoses, if known, are mentioned in 50 patients without abnormalities on MR imaging. In this group patients are included without a history of trauma. In many cases the request of the clinician was to exclude a tumor. In only one patient could the findings of the normal MR imaging scan be correlated with surgery. Patient No. 115 felt a tumor in the supraclavicular region, which, at palpation, caused severe pain irradiating into the arm. With MR imaging no tumor was detected, which was confirmed at surgery. The brachial plexus was located very superficially in this patient, so it is conceivable that the palpable “tumor” was the brachial plexus itself. The most common diagnosis found in these patients with normal imaging findings was neuralgic amyotrophy. Neuralgic amyotrophy is a syndrome characterized by an acute onset of pain, followed by weakness and atrophy of the shoulder girdle muscles.[184,233,251,252] The prognosis is good; in a series of 99 cases full recovery was seen in over 90% by four years.[251] Synonyms for neuralgic amyotrophy are acute brachial neuropathy, brachial plexus neuropathy, brachial neuritis, Parsonage-Turner syndrome and shoulder girdle syndrome. The etiology of this disorder is not known, but some antecedent events, such as viral infections and immunizations, often herald the onset of neuralgic amyotrophy. An inflammatory-immune pathogenesis has been suggested.[232] This syndrome can be hereditary.[275] With imaging an increased signal intensity on T2-weighted images has been described,[194,223,229] however in another study no abnormalities were detected and MR imaging served to exclude other structural abnormalities.[21] Two studies found swelling of the brachial plexus with MR imaging or CT which were biopsied and showed mononuclear cell infiltrates.[51,232] We found no abnormalities at all in six patients with neuralgic amyotrophy and in four patients with hereditary neuralgic amyotrophy. In six patients the symptoms were probably due to cervical radiculopathy and two patients were diagnosed with carpal tunnel syndrome.

The MR imaging findings of nine patients diagnosed with multifocal motor neuropathy (MMN), five patients with chronic inflammatory demyelinating polyradiculoneuropathy (CIDP) and eight patients with lower motor neuron disease (LMND) will be discussed in Chapter 6.

Conclusions

Primary neurogenic tumors usually have typical imaging characteristics. Of the eight proven primary tumors, only one (patient No. 8, Fig. 7) had atypical findings. Of the non-neurogenic tumors only one had the imaging characteristics which could be compatible with a neurogenic tumor, this was a metastasis of a chondrosarcoma (patient No. 53, Fig. 24). Our series of primary tumors is too small to evaluate whether MR imaging can differentiate between schwannomas, neurofibromas and malignant schwannomas.

MR imaging appears to be useful in the evaluation of superior sulcus tumors. In 14 patients with Pancoast's syndrome, involvement of the brachial plexus on MR imaging was found in 12. In the two other patients the pain could be explained by involvement of Th2. In 10 patients with an apical lung tumor without Pancoast's syndrome brachial plexus involvement was found in two patients. In one of these patients the tumor appeared to be contiguous with the brachial plexus, but could be released. The MR imaging findings correlated well with surgery in six patients. Some superior sulcus tumors present with only a small part in the lung and the largest part in the supraclavicular space. In these cases it might be difficult to determine the origin of the tumor: in- or outside the lung. In our experience looking at the aspect of the interface between the tumor and the lung parenchyma, as described by Reede[201], is a very reliable sign. Examples of smooth borders in tumors originating outside the lung are shown in Figs. 3, 7 and 24, whereas examples of irregular borders of lung tumors are shown in Figs. 8, 9, 10, 11 and 12.

Other primary malignant non-neurogenic tumors we have seen include: B-cell non-Hodgkin's lymphoma, leiomyosarcoma, liposarcoma, chondrosarcoma, and synoviosarcoma. In our experience MR imaging could very well delineate the extension of these tumors, however the imaging characteristics of these tumors were not specific enough to make a diagnosis.
The origin of the metastatic malignant tumors was from breast carcinoma, head and neck tumors, chondrosarcoma, renal cell carcinoma, or from unknown origin.
The benign non-neurogenic tumors include: aggressive fibromatosis, meningocele,

lipoma, and a hematoma in a neck cyst. Of these benign tumors the meningocele, lipoma, and the hematoma show specific imaging characteristics. Aggressive fibromatosis (Fig. 19) presents as a large tumor and has the same imaging characteristics as the leiomyosarcoma (Fig. 22), the liposarcoma (Fig. 23) and the chondrosarcoma (Fig. 25).

Fig. 1A

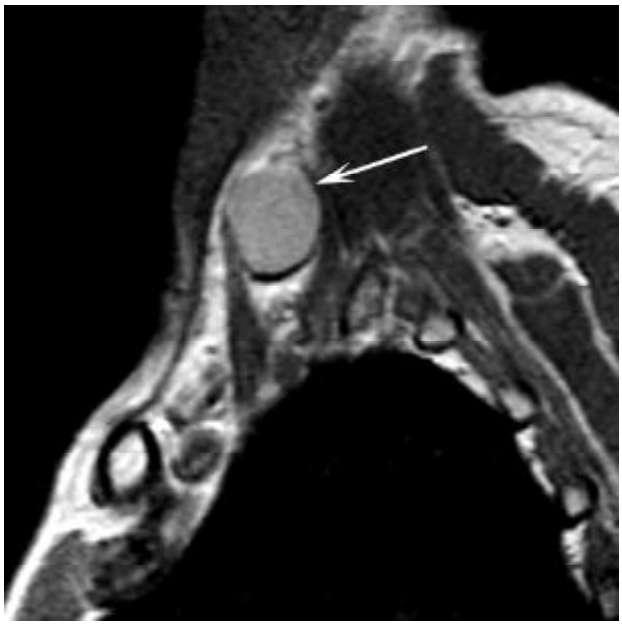
Fig. 1B

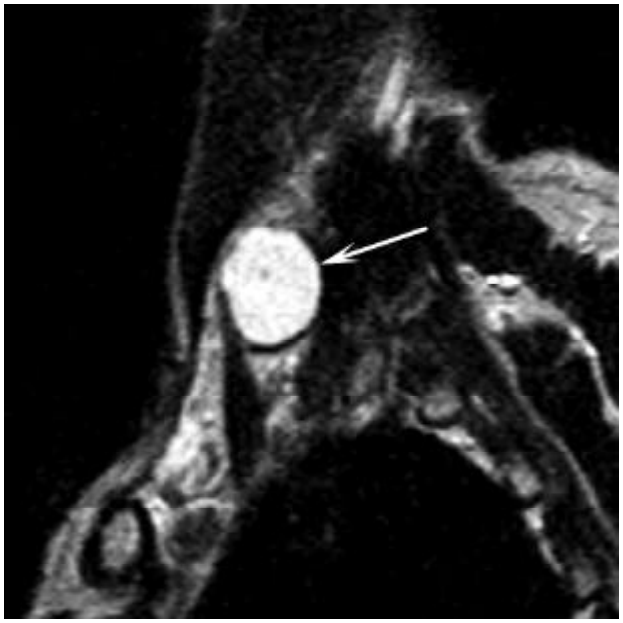
Fig. 1C

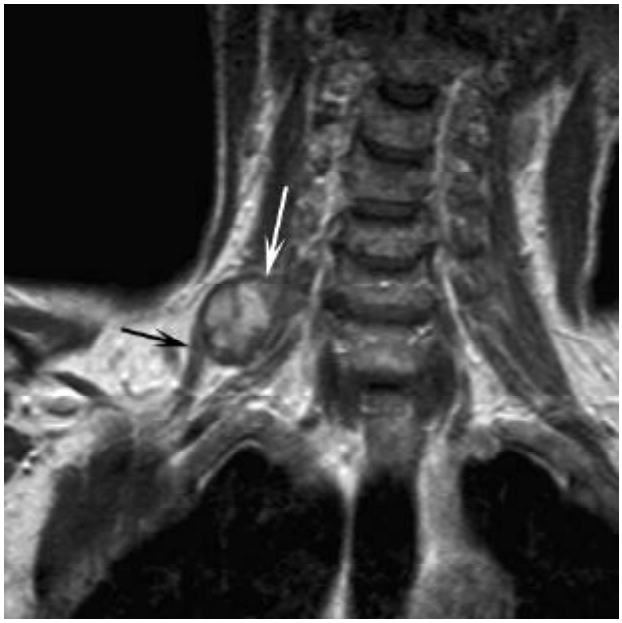
Fig. 1D

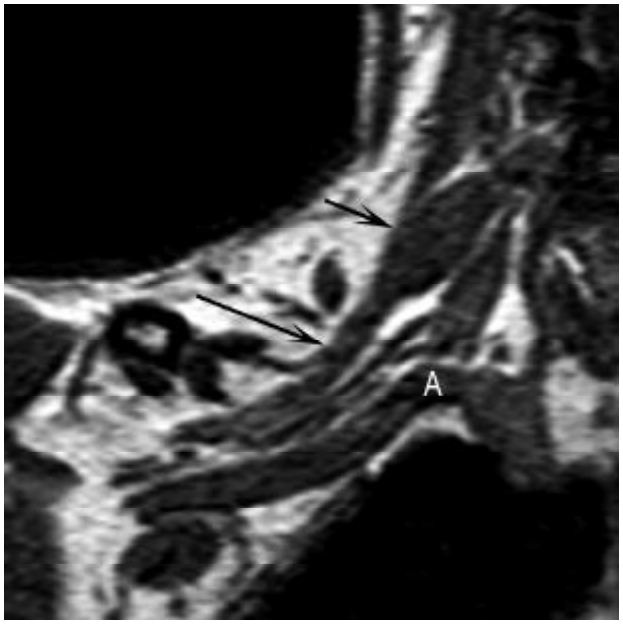

Fig. 1E

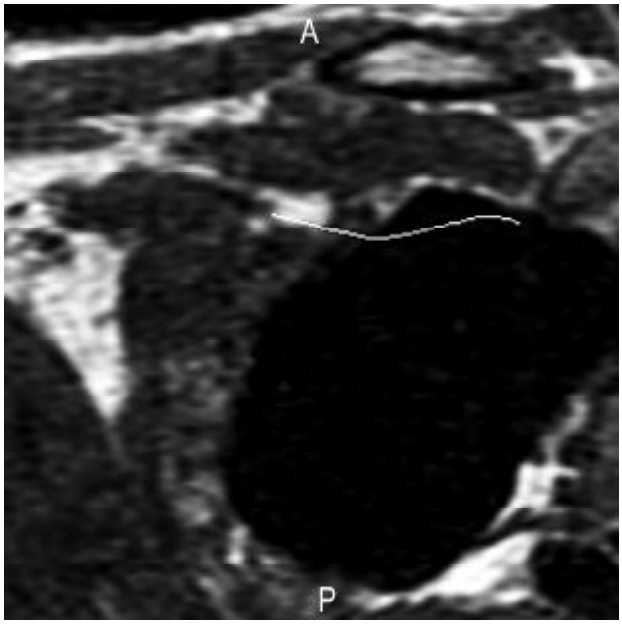

Fig. 1F

Fig. 1. Patient No. 9: schwannoma of the ventral ramus of root C6. This tumor shows the typical MR imaging characteristics of a neurogenic tumor, i.e. a low signal intensity on the T1-weighted image, an increased signal intensity on the proton-density image, a high signal intensity on the T2-weighted image, enhancement after administration of gadolinium-DTPA, a fusiform growth, a sharply defined edge, and the involved nerve can be discerned after leaving the tumor.

A. Sagittal T1-weighted image at the level of the interscalene triangle shows a tumor (arrow) with the same signal intensity of muscle. Note the splaying of the anterior (a) and middle (m) scalene muscles. A = subclavian artery, V = subclavian vein.

B. Sagittal proton-density image at the same level as in **A**. The tumor (arrow) shows a slightly increased signal intensity compared to that of muscle.

C. Sagittal T2-weighted image at the same level as in **A**. The tumor (arrow) shows a homogeneously increased signal intensity compared to that of muscle.

D. Coronal T1-weighted image with gadolinium-DTPA shows the enhancing tumor (white arrow). Laterally the brachial plexus can be seen (black arrow) after leaving the tumor.

E and **F.** Unenhanced coronal curved reconstruction of a 3D-TFE sequence one year postoperatively (**E**) with the axial scanogram (**F**; A = anterior, P = posterior). There is a clear fusiform swelling of the ventral ramus of root C6 (short arrow) compared to the normal caliber of the nerve more laterally (long arrow), A = subclavian artery. Two years postoperatively the MR imaging findings were unchanged, so that this swelling is probably due to fibrosis.

Fig. 2. Patient No. 10: schwannoma of the ventral ramus of root C7.

A. Sagittal image from a T1-weighted 3D volume acquisition with gadolinium-DTPA. In the interscalene triangle an enhancing tumor with a hypointense center is seen (long white arrow) which displaces the anterior scalene muscle (a) anteriorly. The ventral rami of the roots C8 (short white arrow) and Th1 (black arrow) are normal. A = subclavian artery.

B. Coronal T1-weighted image with gadolinium-DTPA shows the fusiform enhancing tumor (long arrow), which tapers towards the intervertebral foramen (short arrow). C6, C7 = vertebral body of C6 and C7.

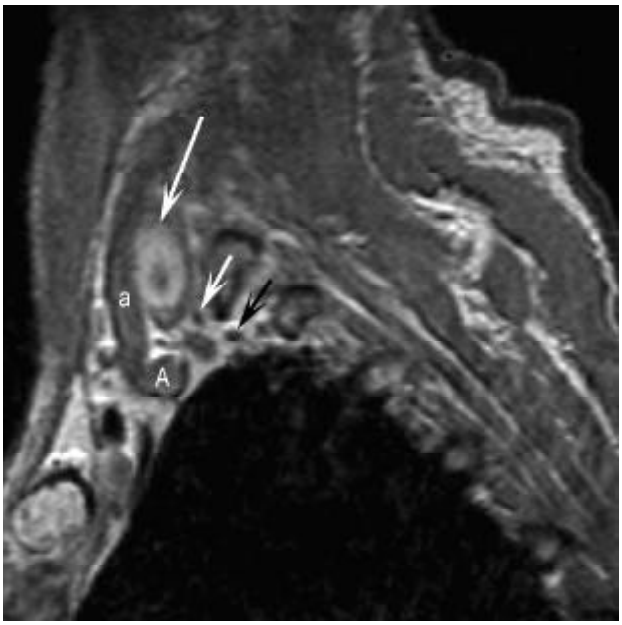

Fig. 2A

Fig. 2B

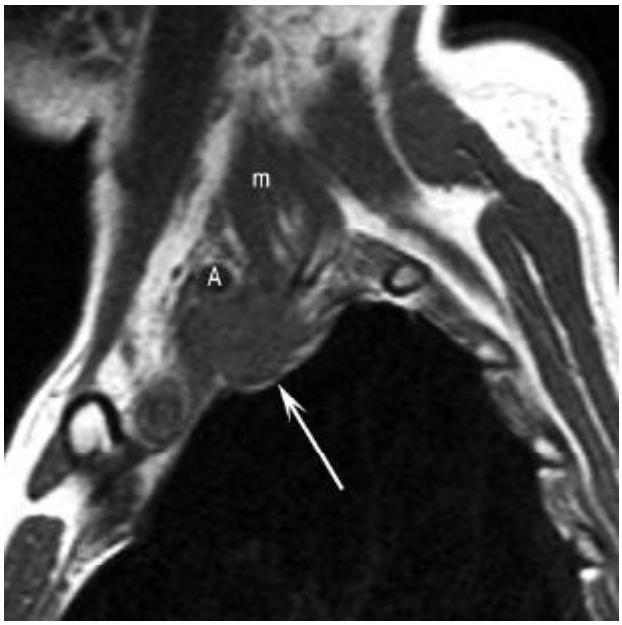

Fig. 3A

Fig. 3B

Fig. 3C

Fig. 3D

Fig. 3. Patient No. 5: ancient schwannoma of the ventral ramus of root C8 and lower trunk.

A. Sagittal T1-weighted image at the level of the interscalene triangle shows a tumor posterior to the subclavian artery (A). The tumor extends into the lung. Note the smooth interface between the lung and the tumor (arrow), consistent with an origin outside the lung; m = middle scalene muscle.

B. Sagittal T2-weighted image at the level of the interscalene triangle shows the high signal of the tumor (long arrow). The short arrow points to the subclavian artery, a = anterior scalene muscle, m = middle scalene muscle.

C. Coronal T1-weighted image with gadolinium-DTPA shows the fusiform, inhomogeneously enhancing tumor (short arrows). Note the normal ventral ramus of root C8 on the other side (long arrow). Th1 = vertebral body Th1.

D. Coronal T1-weighted image with gadolinium-DTPA more ventrally than **C** demonstrates a slight displacement of the ventral ramus of root C7 and the middle trunk (short arrows) by the tumor (long arrow). C7 = vertebral body C7.

Fig. 4

Fig. 4. Patient No. 4: schwannoma of the lower trunk. Coronal T1-weighted image with gadolinium-DTPA shows a small enhancing tumor in the brachial plexus (arrow). A = subclavian artery.

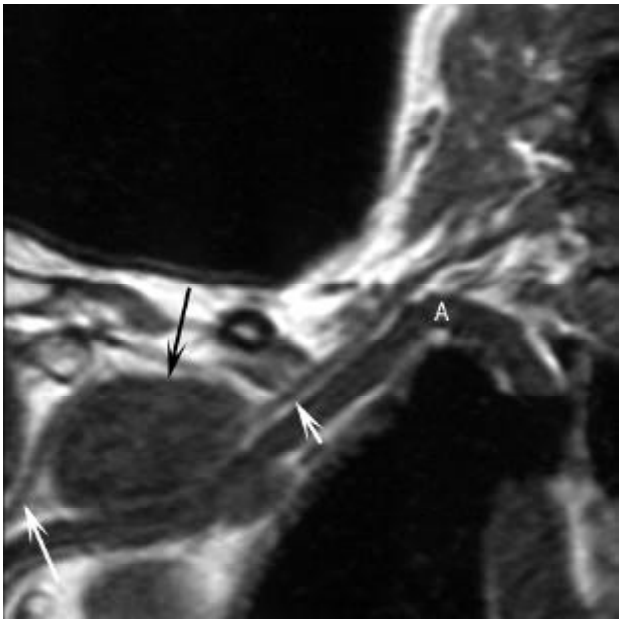

Fig. 5A

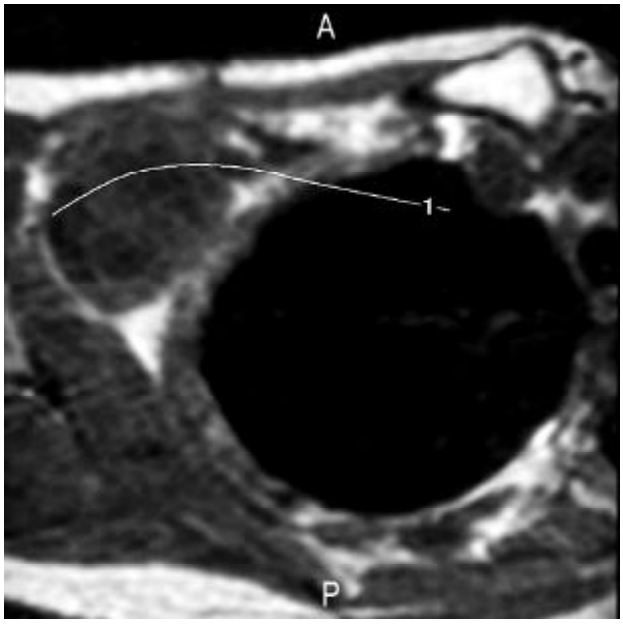

Fig. 5B

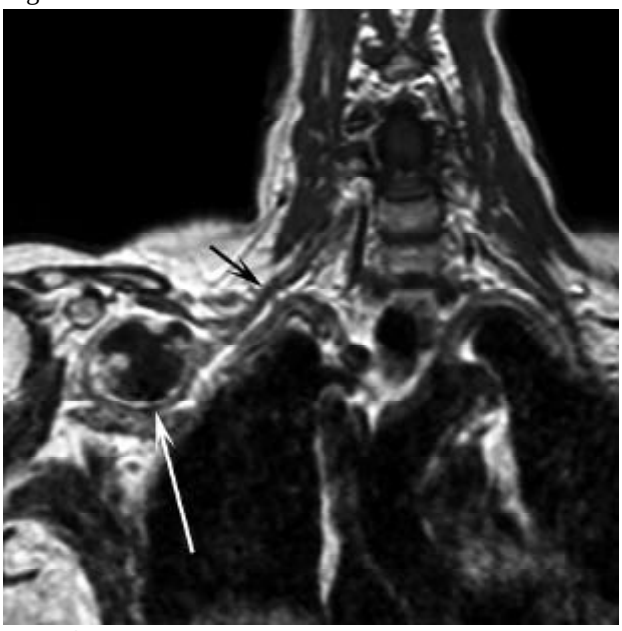

Fig. 5C

Fig. 5. Patient No. 2: schwannoma of the cords.

A and **B.** Coronal curved reconstruction from a 3D-TFE sequence (**A**) with the axial scanogram (**B**; A = anterior, P = posterior). The tumor (black arrow) is continuous with the brachial plexus proximally (short white arrow) and distally (long white arrow), A = subclavian artery.

C. Coronal T1-weighted image with gadolinium-DTPA shows enhancement in the periphery of the tumor (white arrow), black arrow points to the brachial plexus proximal to the tumor.

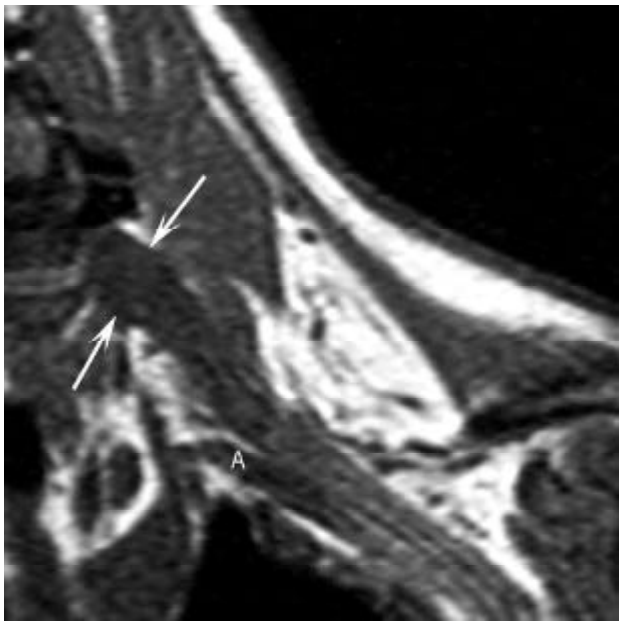

Fig. 6A

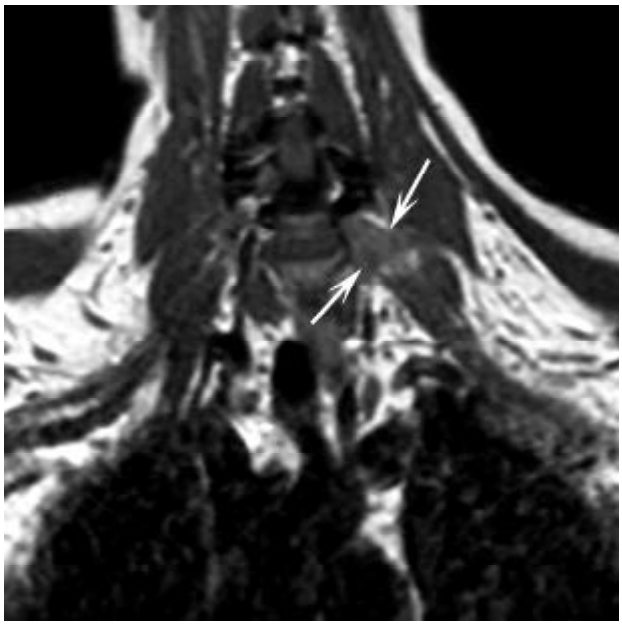

Fig. 6B

Fig. 6. Patient No. 3: neurofibroma of the ventral ramus of root C7 in a patient with von Recklinghausen's disease.

A. Coronal reconstruction from a 3D-TFE sequence shows a tumor in the ventral ramus of root C7 (arrows). A = subclavian artery.

B. Coronal T1-weighted image with gadolinium-DTPA demonstrates a slight enhancement of the fusiform tumor (arrows).

Fig. 7. Patient No. 8: malignant schwannoma of the ventral ramus of root C7. This patient had radiation therapy for breast carcinoma 17 years ago.

A. Sagittal proton-density image shows the hyperintense tumor (white arrows). Posterior to the tumor the ventral rami of roots Th1 (short black arrow) and C8 (long black arrow) are seen. Note the smooth interface between the tumor and lung parenchyma.

B. Coronal T1-weighted image shows the thickened ventral ramus of root C7 (short arrow) which is contiguous with a more caudally located mass (long arrow).

Fig. 7A

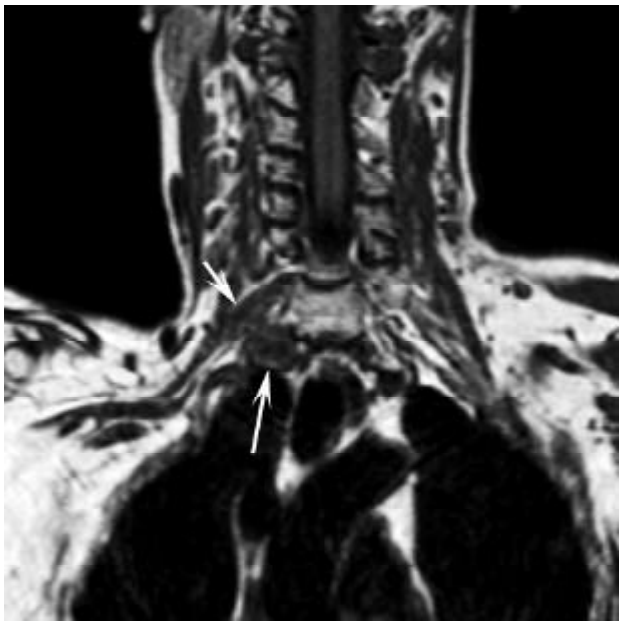

Fig. 7B

Fig. 8A

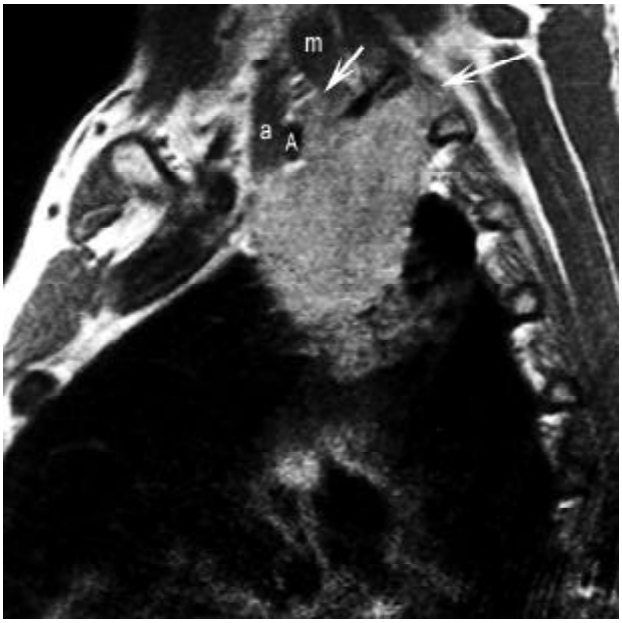

Fig. 8B

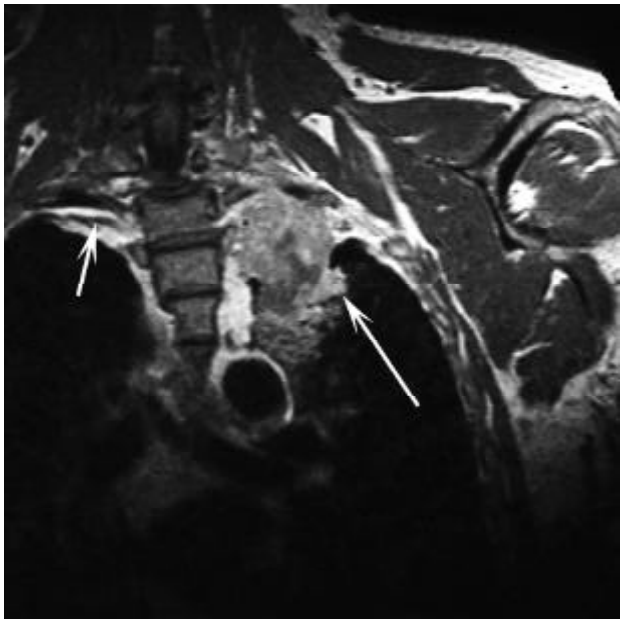

Fig. 8C

Fig. 8. Patient No. 21: superior sulcus tumor (squamous cell carcinoma). This patient presented with paresthesias in the fourth and fifth finger.

A. Chest radiograph shows a mass in the apex of the left lung (arrow).

B. Sagittal proton-density image shows the hyperintense tumor which infiltrates the interscalene triangle (short arrow), and the space between the first and second rib (long arrow). A = subclavian artery, a = anterior scalene muscle, m = middle scalene muscle.

C. Coronal T1-weighted image with gadolinium-DTPA demonstrates the involvement of the ventral ramus of root Th1 on the left side. The short arrow points to the ventral ramus of root Th1 on the right side. Note the irregular interface between the tumor and the lung parenchyma (long arrow), suggestive for an intraparenchymal origin of this tumor.

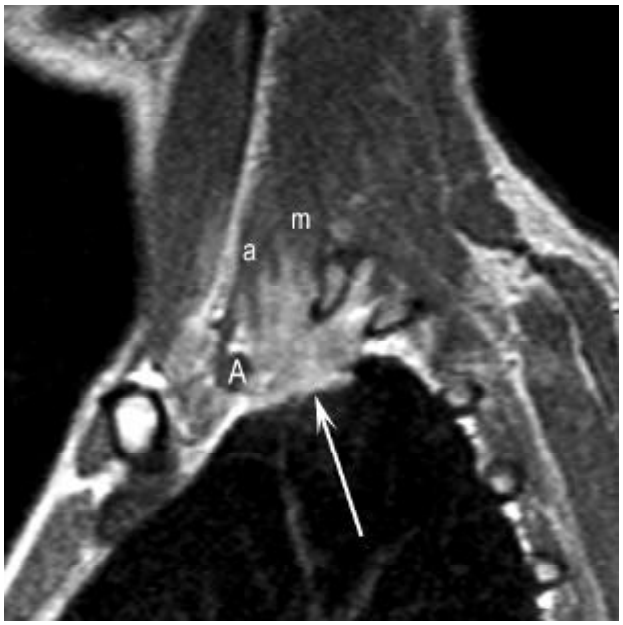

Fig. 9A

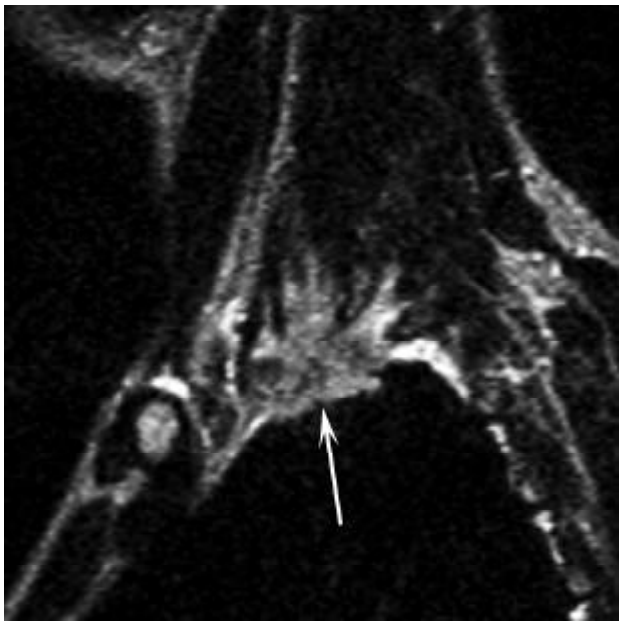

Fig. 9B

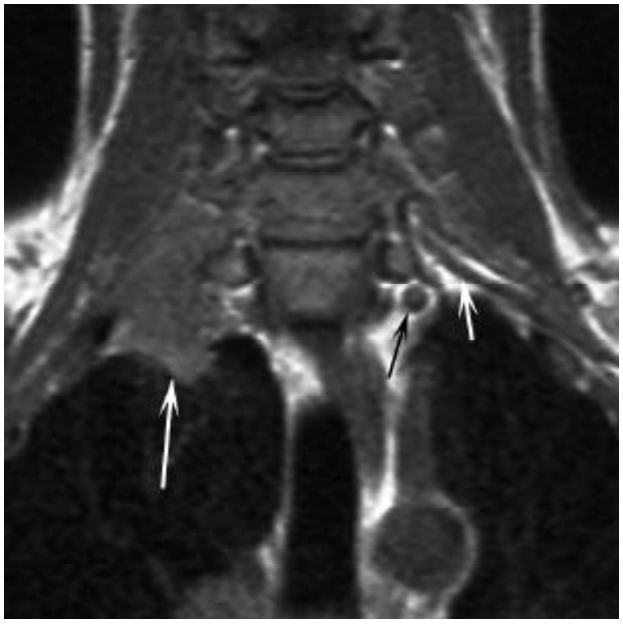

Fig. 9C

Fig. 9. Patient No. 25: superior sulcus tumor (adenocarcinoma). This patient presented with pain in the arm and Horner's syndrome.

A. Sagittal proton-density image shows that a minor part of this lung tumor is located inside the lung (arrow). A = subclavian artery, a = anterior scalene muscle, m = middle scalene muscle.

B. Sagittal T2-weighted image at the same level as in **A** shows the high signal intensity of the tumor (arrow).

C. Coronal T1-weighted image demonstrates the superior sulcus tumor (long white arrow) which obliterates the ventral ramus of root C8 and the stellate ganglion. On the other side, the normal stellate ganglion (black arrow) and ventral ramus of root C8 (short white arrow) can be discriminated.

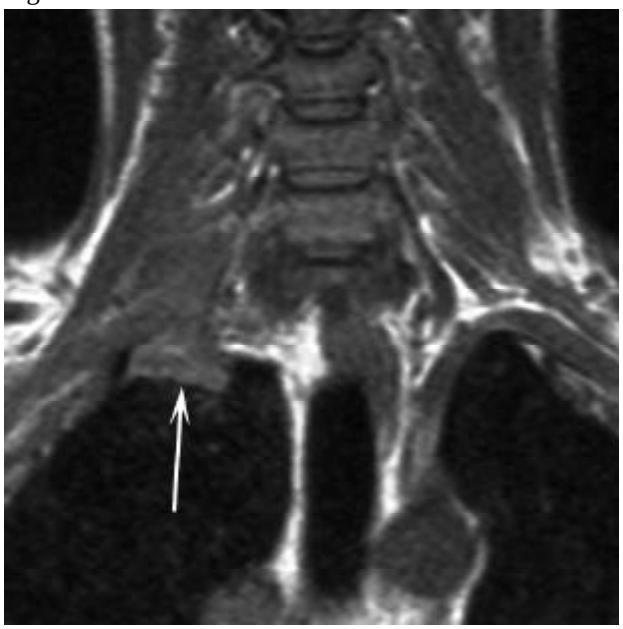

Fig. 9D

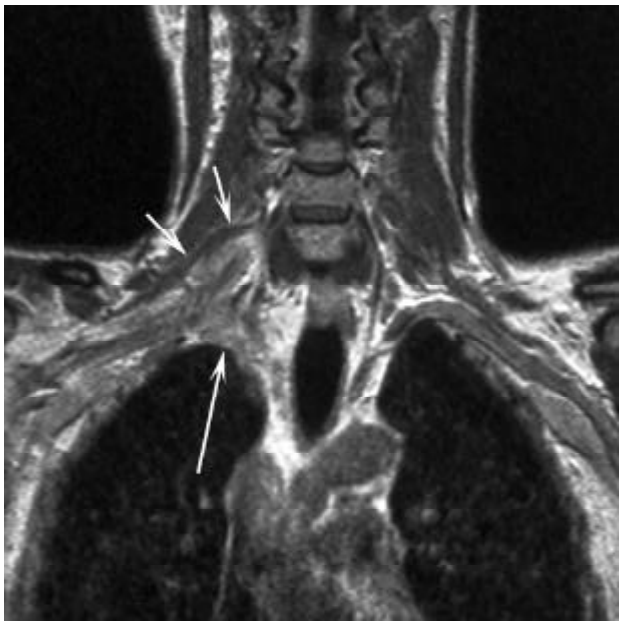

Fig. 9E

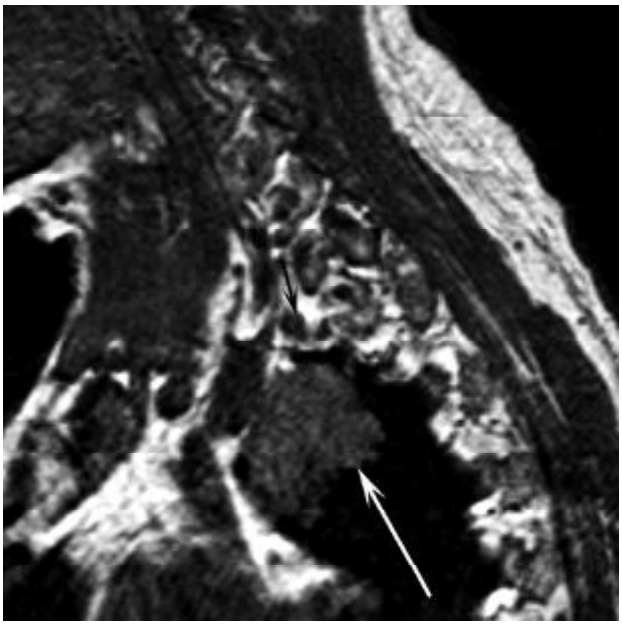

Fig. 10A

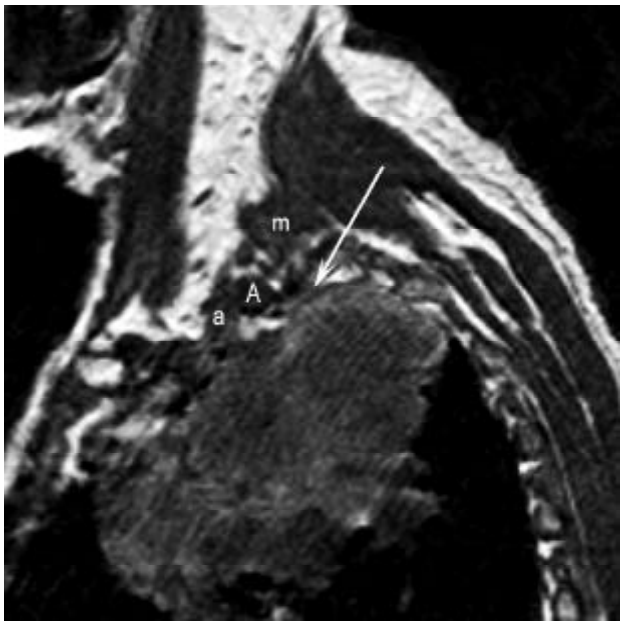

Fig. 10B

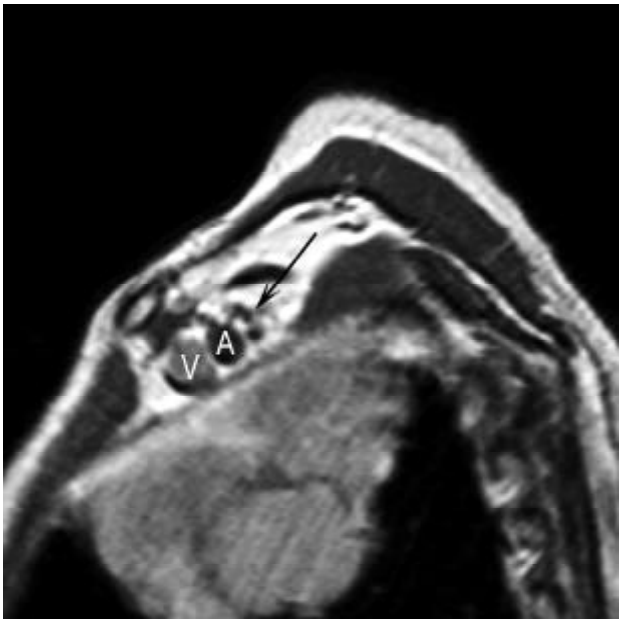

Fig. 10C

Fig. 10. Patient No. 17: superior sulcus tumor (adenocarcinoma). This patient presented with pain located at the scapula region.

A. Sagittal image from a 3D-TFE sequence demonstrates that the stellate ganglion (black arrow) is not involved by the tumor (white arrow).

B. Sagittal image from a 3D-TFE sequence slightly more lateral than **A** shows that the tumor does not infiltrate the interscalene triangle, arrow points to the cranial border of the tumor. A = subclavian artery, a = anterior scalene muscle, m = middle scalene muscle.

C. Sagittal proton-density image at the level of the divisions shows that the tumor is clearly separable from the brachial plexus (arrow). A = subclavian artery, V = subclavian vein.

Fig. 9. *Continued.*

D and **E.** Coronal T1-weighted image without (**D**) and with (**E**) gadolinium-DTPA. The tumor (long arrow) enhances and the post-contrast image shows better delineation of tumor extent cranially to the ventral ramus of root C7 (short arrows) that continues as the middle trunk. At surgery it was possible to release the tumor from the ventral ramus of root C7 and the middle trunk. The ventral rami of roots C8 and Th1 and the lower trunk had to be sacrificed.

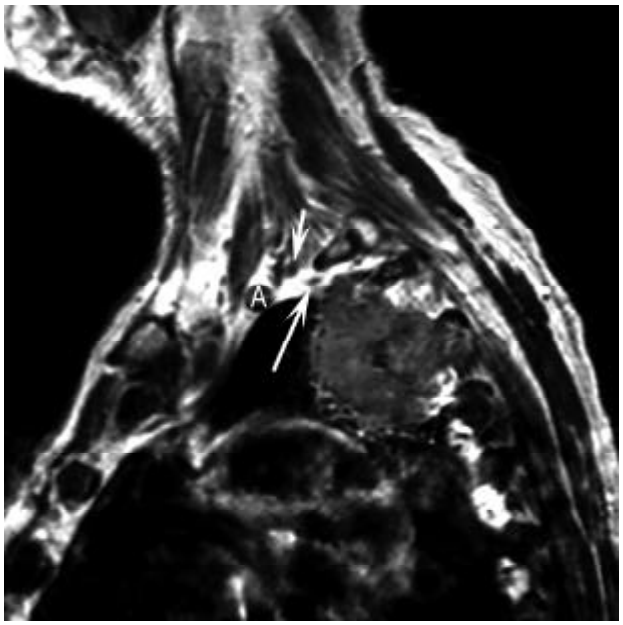

Fig. 11A

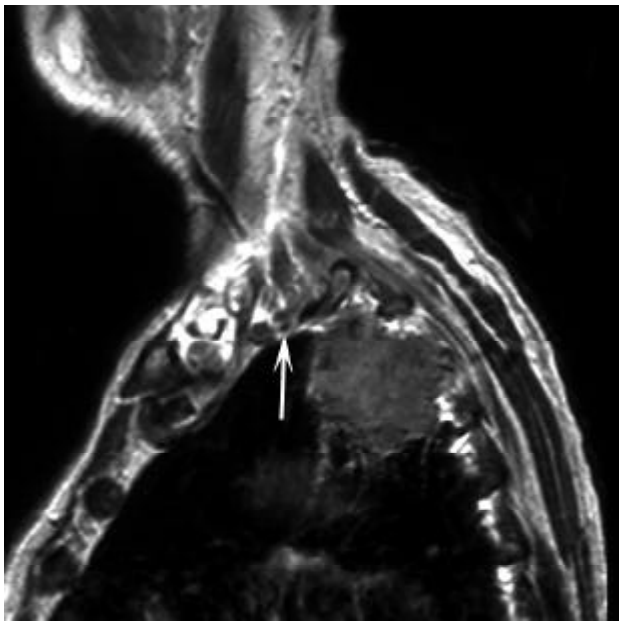

Fig. 11B

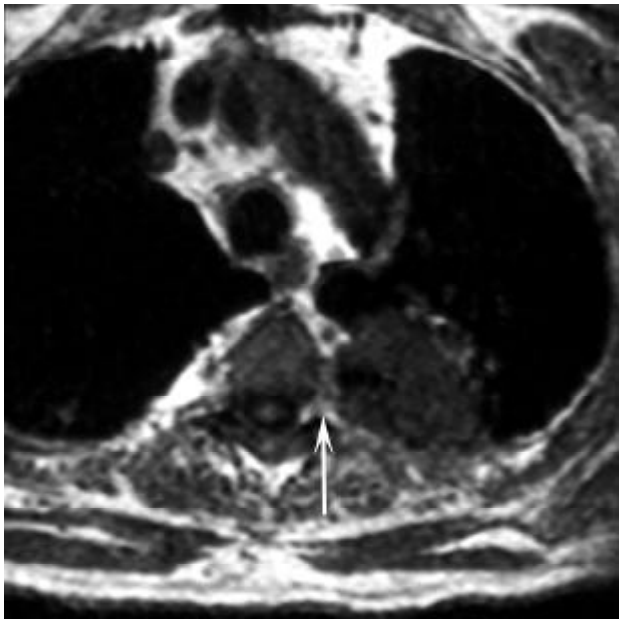

Fig. 11C

Fig. 11. Patient No. 29: apical lung tumor. This patient presented with hemoptysis without pain.

A. Sagittal T1-weighted image with gadolinium-DTPA shows that the ventral ramus of the roots C8 (short arrow) and Th1 (long arrow) are not involved by the lung tumor. A = subclavian artery.

B. Sagittal T1-weighted image with gadolinium-DTPA slightly more lateral than in **A** demonstrates that the tumor does not infiltrate the interscalene triangle (arrow).

C. Axial reconstruction from a 3D-TFE sequence shows that the vertebral body and the intervertebral foramen (arrow) are not infiltrated by the tumor.

Fig. 12

Fig. 13

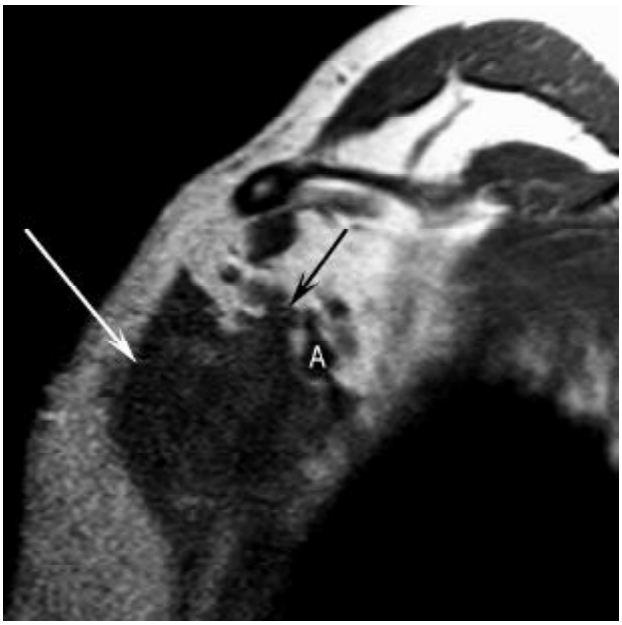

Fig. 14A

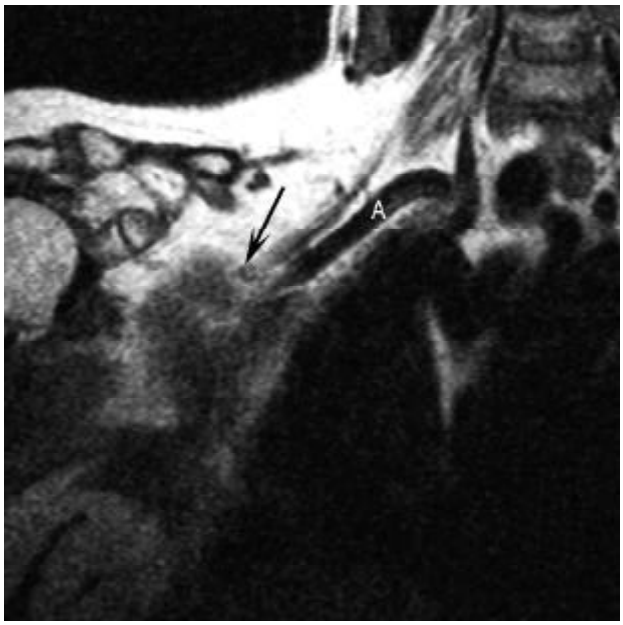

Fig. 14B

Fig. 12. Patient No. 13: superior sulcus tumor (squamous cell carcinoma). This patient presented with pain in the shoulder and arm.
Coronal T1-weighted image shows that the tumor extends into the mediastinum. The tumor is contiguous with the aorta and the brachiocephalic artery (arrows).

Fig. 13. Patient No. 34: bronchogenic cyst.
Sagittal T1-weighted image shows a tumor in the lung apex, which is slightly hyperintense compared to muscle. Note the intact extrapleural fat plane (arrow). A = subclavian artery, a = anterior scalene muscle, m = middle scalene muscle.

Fig. 14. Patient No. 43: metastasis of breast carcinoma.

A. Sagittal T1-weighted image shows a mass (white arrow) which infiltrates the pectoralis major and minor muscles. The tumor is contiguous with the lateral cord (black arrow). A = axillary artery. Findings were confirmed upon surgery, when it was possible to separate the axillary artery and lateral cord from the tumor.
B. Coronal T1-weighted image shows that the mass is continuous with the brachial plexus (arrow). A = subclavian artery.

Fig. 15. Patient No. 42: metastasis of breast carcinoma.

A. Sagittal proton-density image shows the thickened cords of the brachial plexus (arrows). A = axillary artery.
B. Coronal T1-weighted image demonstrates the thickening of the divisions and cords of the brachial plexus.

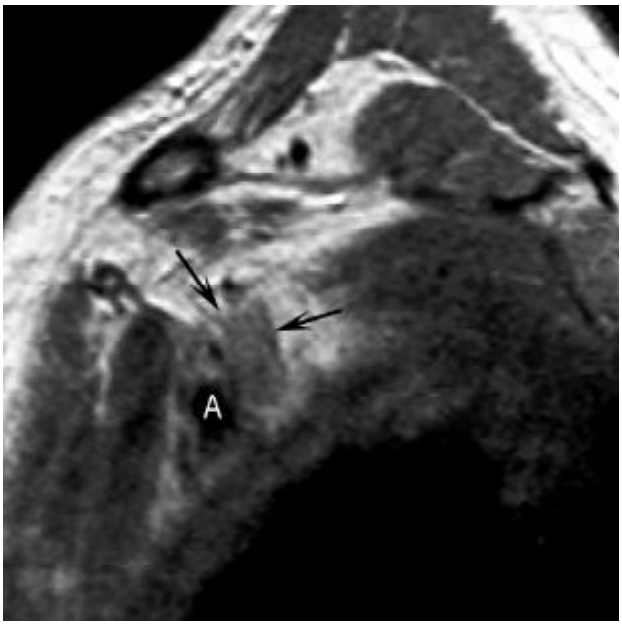

Fig. 15A

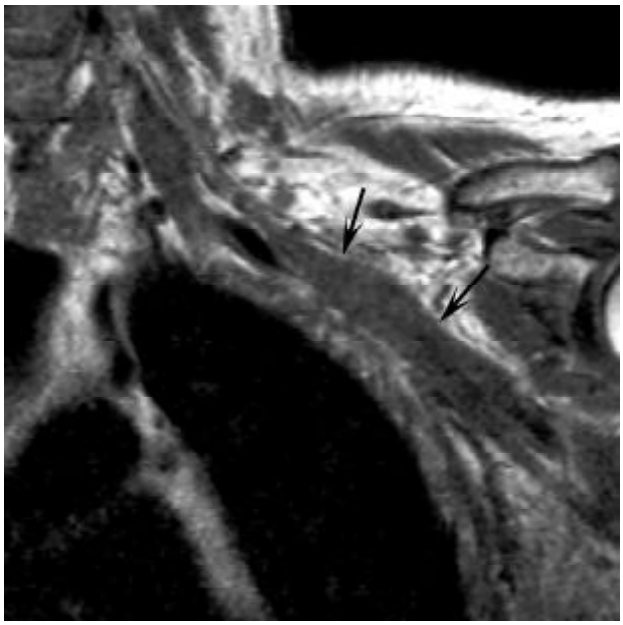

Fig. 15B

Fig. 16A

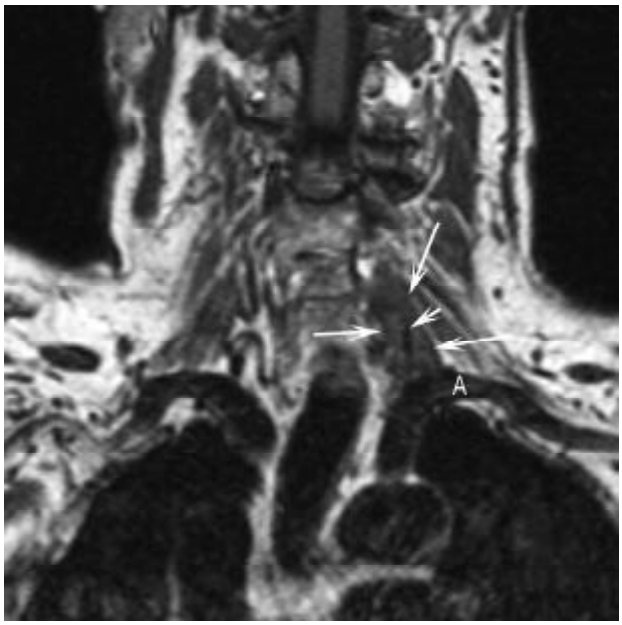

Fig. 16B

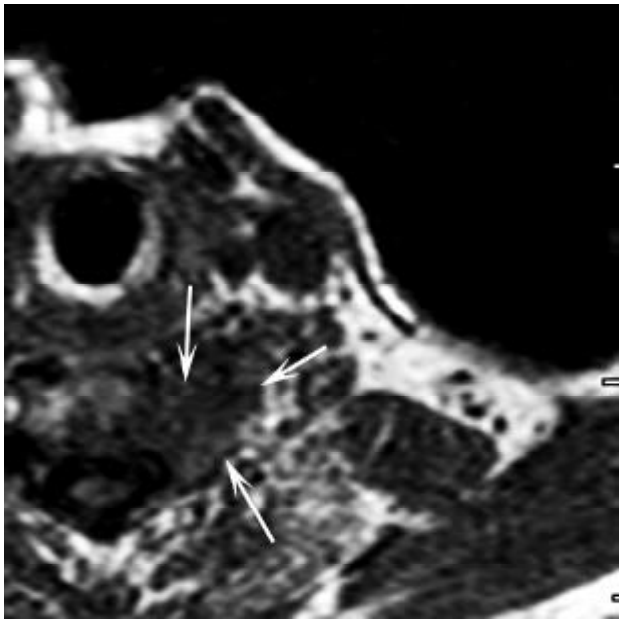

Fig. 16C

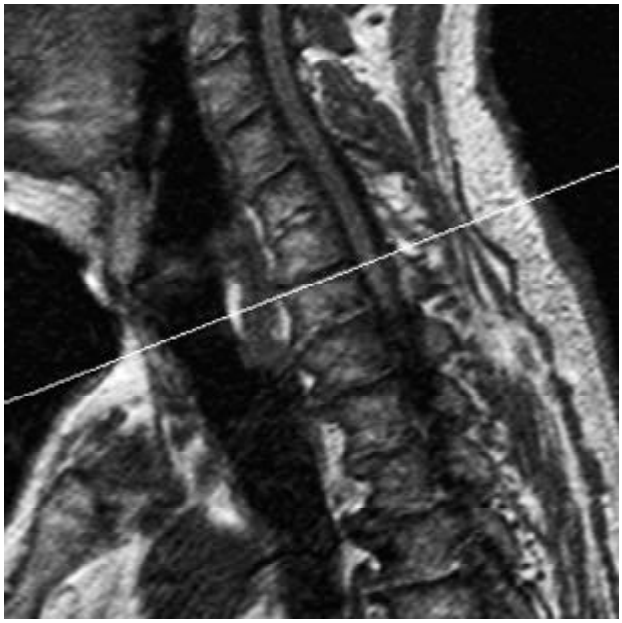

Fig. 16D

Fig. 16E

Fig. 16. Patient No. 51: paravertebral B-cell non-Hodgkin's lymphoma.

A. Sagittal proton-density image shows a hyperintense tumor (arrow) at the level of the vertebral body of C7.

B. Coronal T1-weighted image demonstrates that the tumor (long arrows) surrounds the vertebral artery (short arrow). A = subclavian artery.

C and **D.** Axial reconstruction from a 3D-TFE sequence (**C**) with the sagittal scanogram (**D**) shows the paravertebral location of the tumor (arrows).

E. In this case an axial CT slice after contrast enhancement shows better the tumor (white arrows) which surrounds the vertebral artery (black arrow).

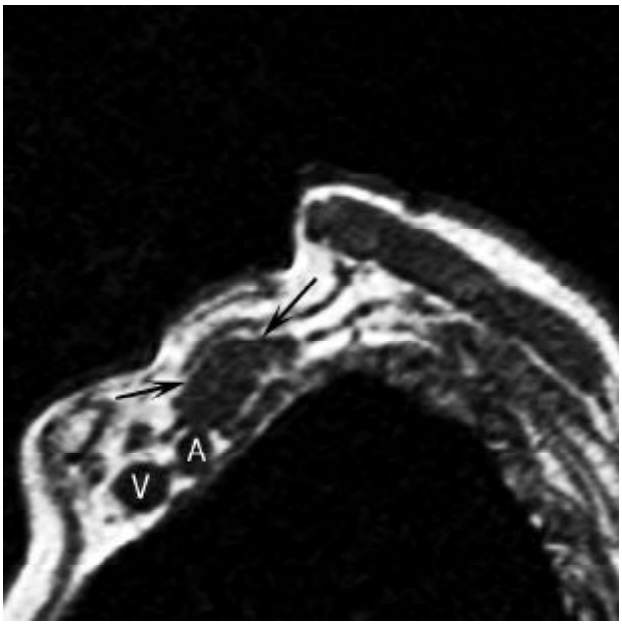

Fig. 17A

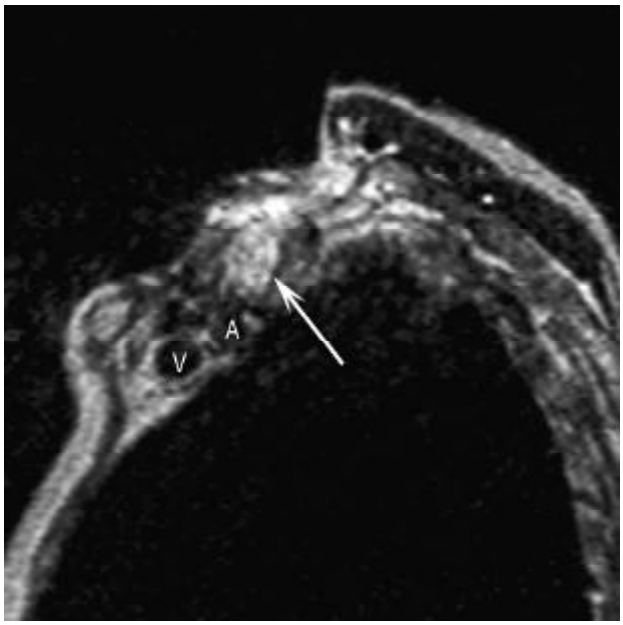

Fig. 17B

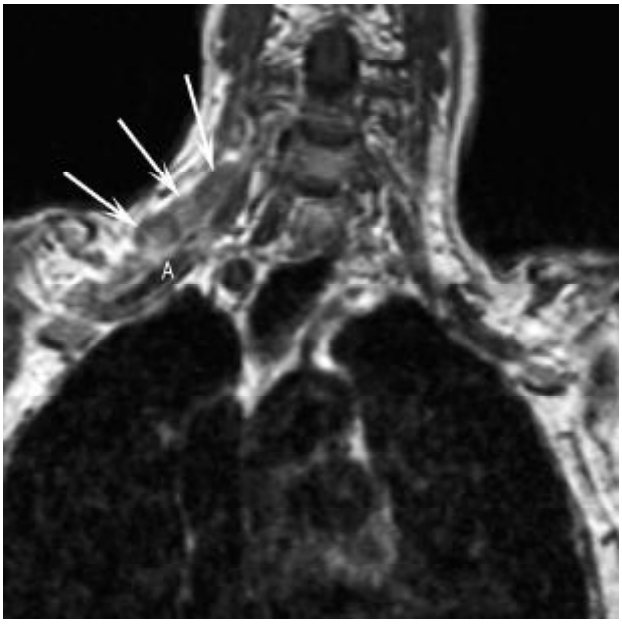

Fig. 17C

Fig. 17. Patient No. 57: B-cell non-Hodgkin's lymphoma with infiltration of the brachial plexus.
A. Sagittal image from a 3D-TFE sequence shows thickened trunks (arrows). A = subclavian artery, V = subclavian vein.
B. Sagittal T2-weighted image at the same level as in **A** demonstrates the hyperintensity of the thickened trunks (arrow). A = subclavian artery, V = subclavian vein.
C. Coronal T1-weighted image with gadolinium-DTPA shows a slight enhancement of the diffusely thickened brachial plexus (arrows). A = subclavian artery.
Fig. 18. Patient No. 64: metastasis (adenocarcinoma) of an unknown primary.
A. Sagittal T1-weighted image shows a large mass which is contiguous with the brachial plexus (arrow). A = subclavian artery, V = subclavian vein.
B. Coronal T1-weighted image confirms the involvement of the brachial plexus by the tumor (black arrow). Note another metastasis on the other side (white arrow).

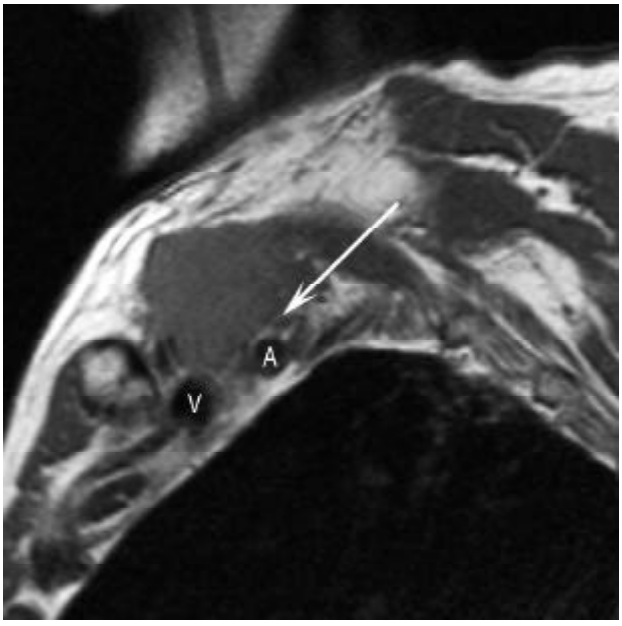

Fig. 18A

Fig. 18B

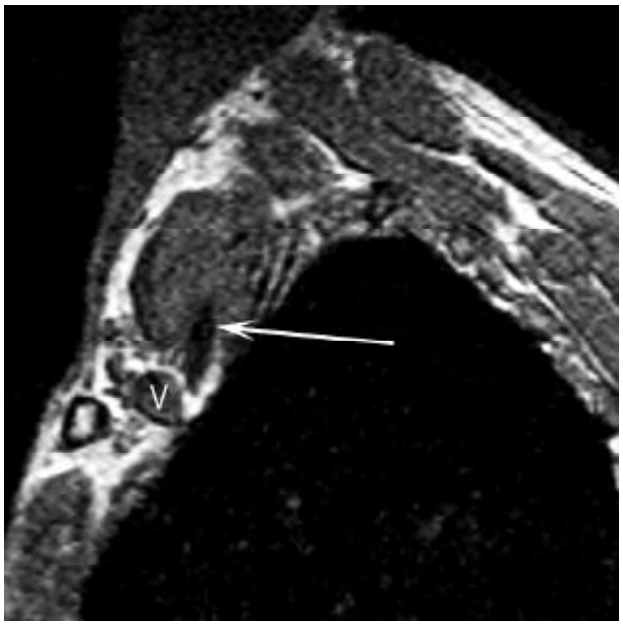

Fig. 19A

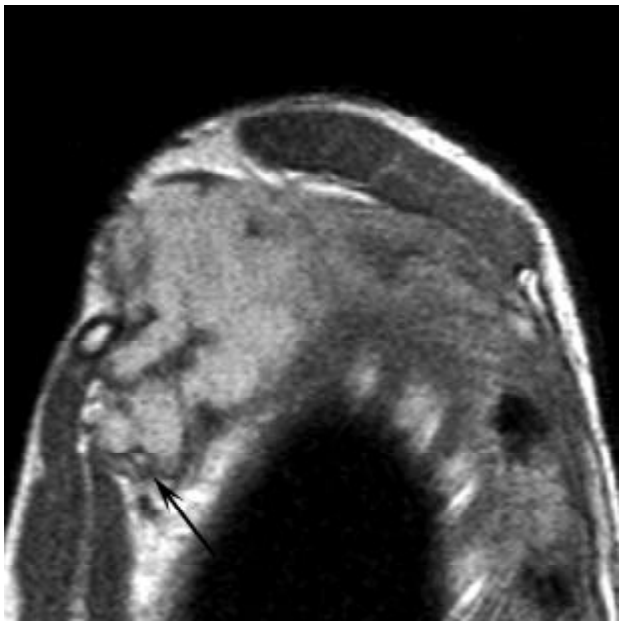

Fig. 19B

Fig. 19C

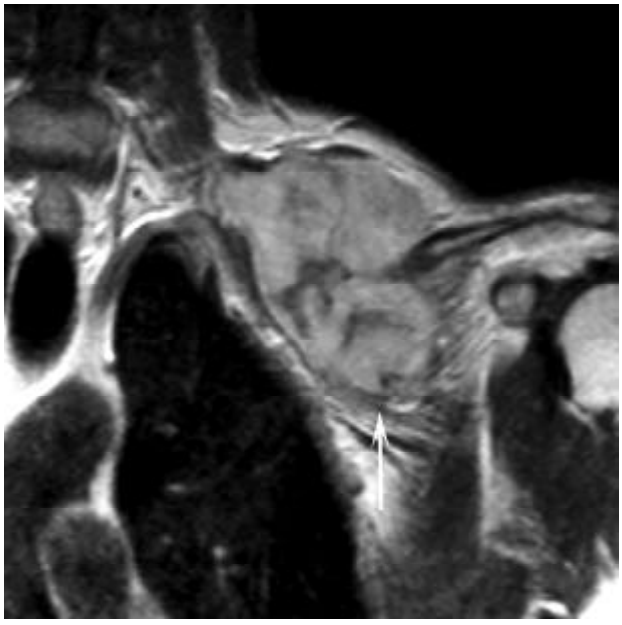

Fig. 19D

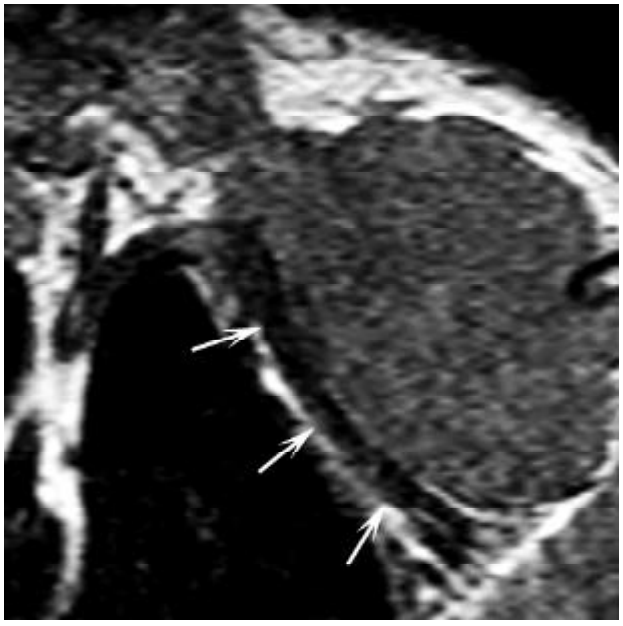

Fig. 19E

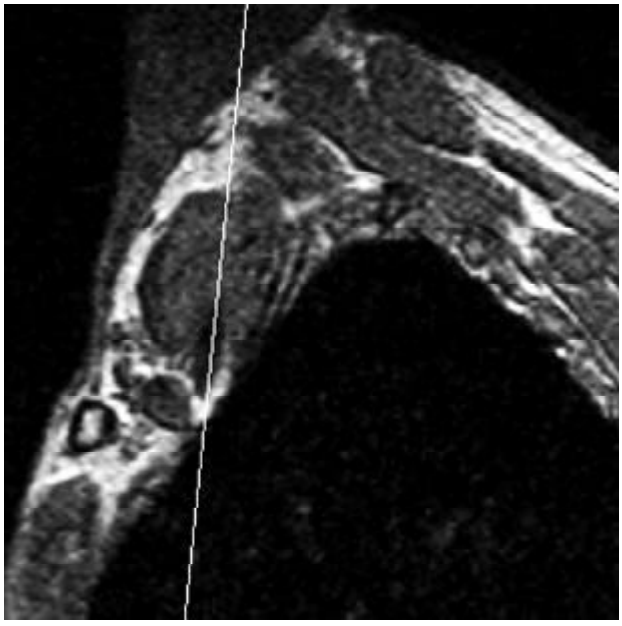

Fig. 19F

Fig. 19. Patient No. 44: aggressive fibromatosis.

A. Sagittal image from a T1-weighted 3D volume acquisition shows the tumor which is contiguous with the subclavian artery (arrow). V = subclavian vein.

B. Sagittal proton-density image shows a large hyperintense tumor. The axillary artery (arrow) is displaced caudally.

C. Sagittal T2-weighted image at the same level as in **B** shows the hyperintensity of the tumor.

D. Coronal T1-weighted image with gadolinium-DTPA demonstrates enhancement of the tumor. The brachial plexus cannot be distinguished from the tumor, but laterally the brachial plexus can be seen (arrow).

E and **F.** Oblique coronal reconstruction from a T1-weighted 3D volume acquisition (**E**) with the sagittal scanogram (**F**) better demonstrates the relationship between the subclavian and axillary artery (arrows) and the tumor; the artery is not encased by the tumor, but displaced caudally.

Fig. 20A

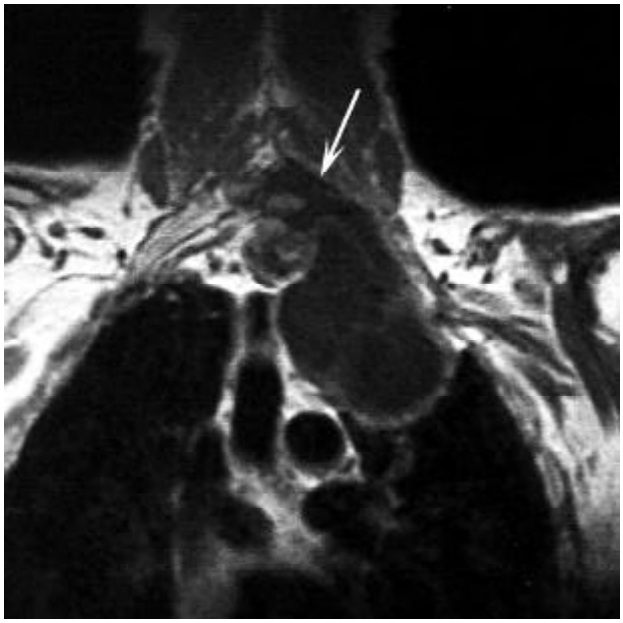

Fig. 20B

Fig. 20. Patient No. 59: meningocele in a patient with von Recklinghausen's disease.

A. Sagittal T1-weighted image shows a large fluid collection posterior to the subclavian artery (arrow).

B. Coronal T1-weighted image shows the connection of the meningocele with the spinal canal (arrow).

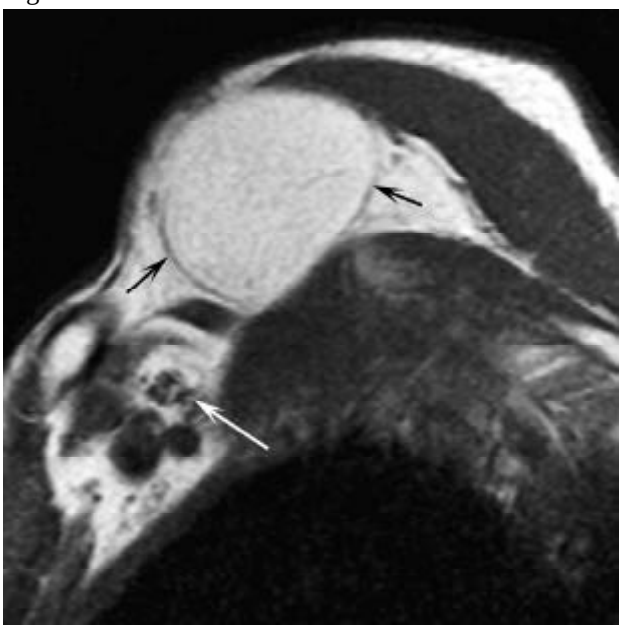

Fig. 21

Fig. 21. Patient No. 56: lipoma.
Sagittal T1-weighted image of a lipoma (black arrows), which is clearly separated from the brachial plexus (white arrow).

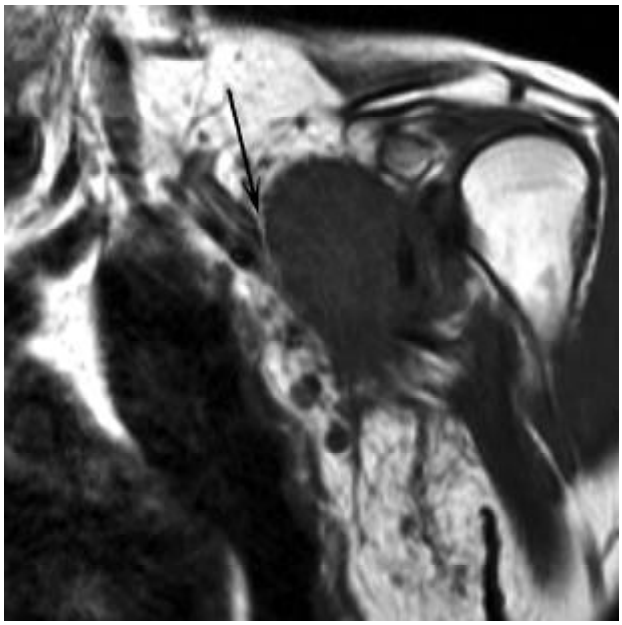

Fig. 22A

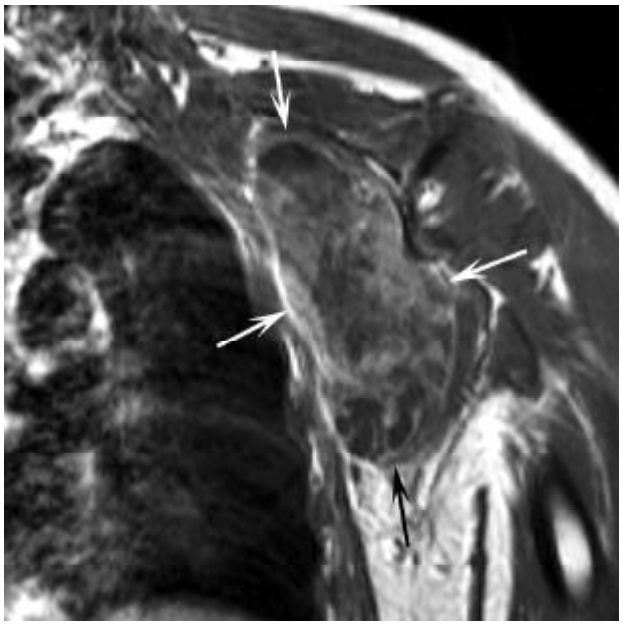

Fig. 22B

Fig. 22. Patient No. 65: leiomyosarcoma.

A. Coronal T1-weighted image of the leiomyosarcoma which involves the brachial plexus (arrow).

B. Coronal T1-weighted image with gadolinium-DTPA shows the inhomogeneous enhancement of the large tumor (arrows) in the axilla.

Fig. 23. Patient No. 58: liposarcoma.

A and **B.** Sagittal proton-density (**A**) and T2-weighted (**B**) image of the liposarcoma with an increased signal intensity. The brachial plexus cannot be recognized, but the vessels (short arrow points to the axillary artery and long arrow points to the axillary vein in **A**) are displaced anteriorly.

C. Coronal T1-weighted image shows the involvement of the ventral ramus of root C7 by the tumor (arrow).

D. Coronal T1-weighted image with gadolinium-DTPA shows the inhomogeneous enhancement of the tumor.

E and **F.** Oblique coronal reconstruction from a T1-weighted 3D volume acquisition (**E**) with the sagittal scanogram (**F**) shows better the relationship between the tumor and the subclavian and axillary artery (arrows), which is displaced caudally and anteriorly.

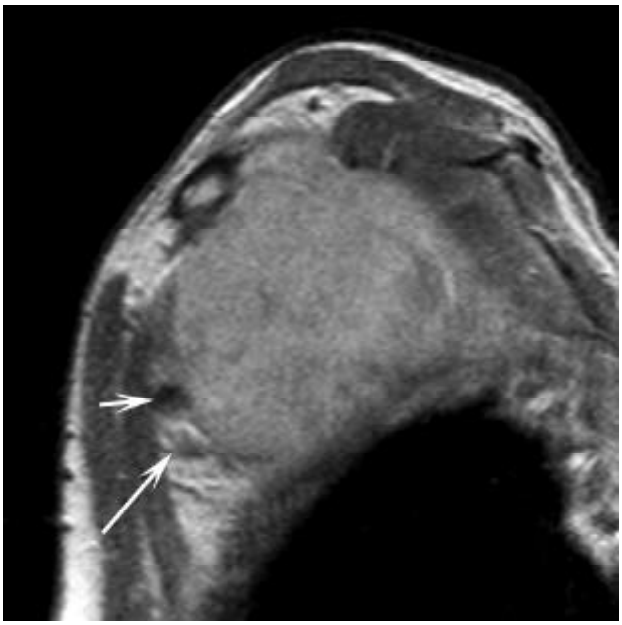

Fig. 23A

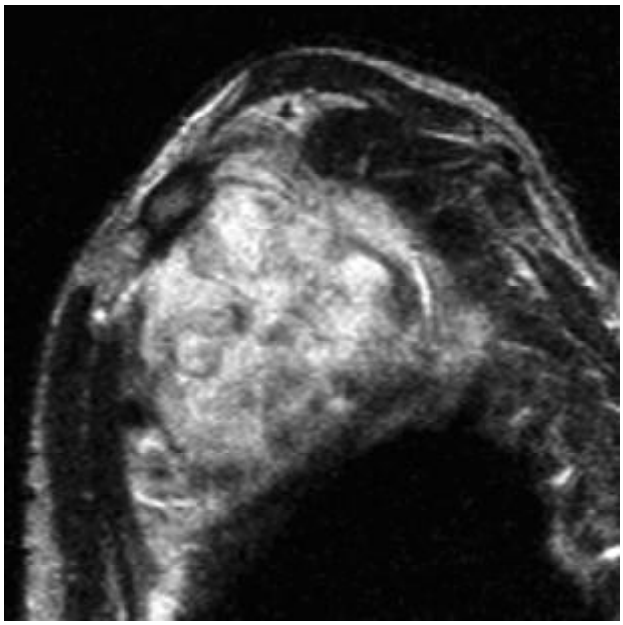

Fig. 23B

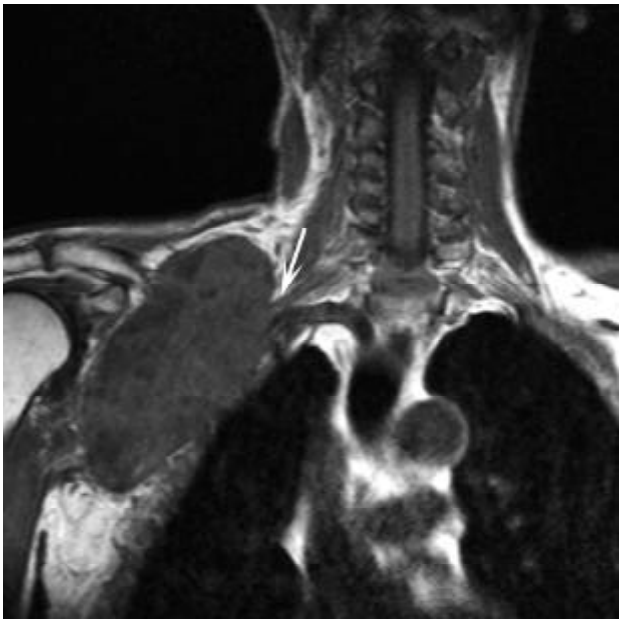

Fig. 23C

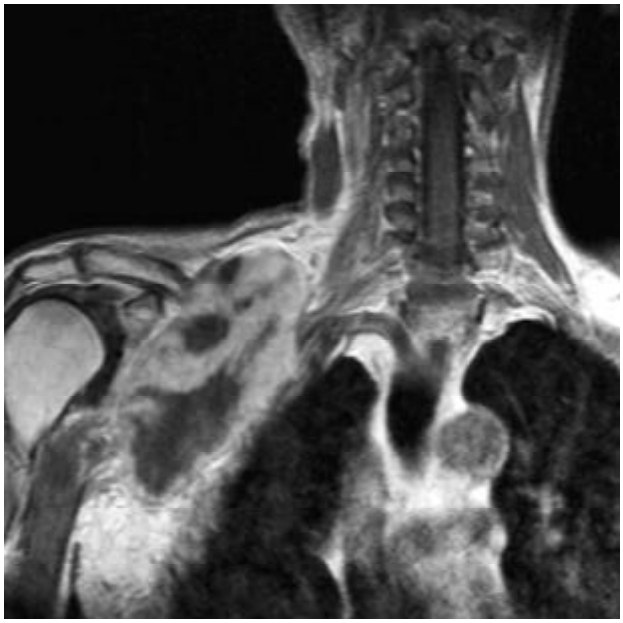

Fig. 23D

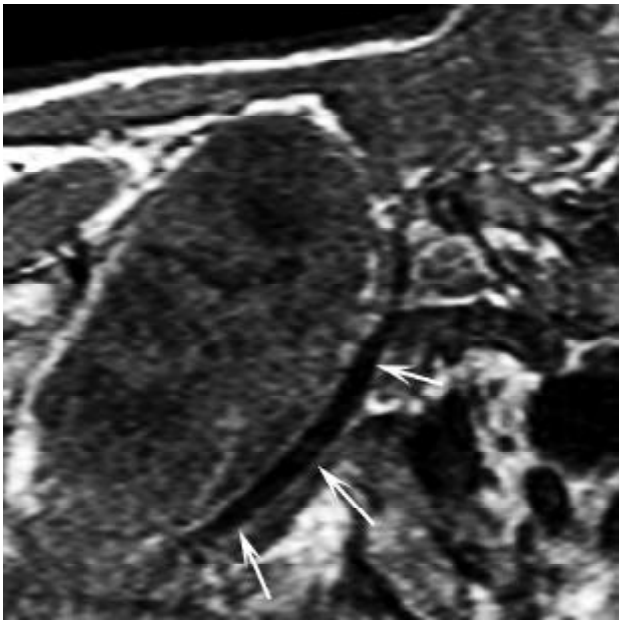

Fig. 23E

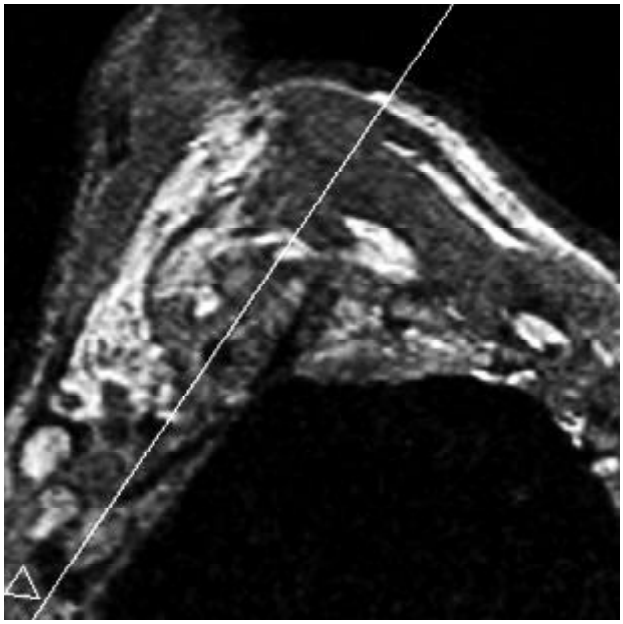

Fig. 23F

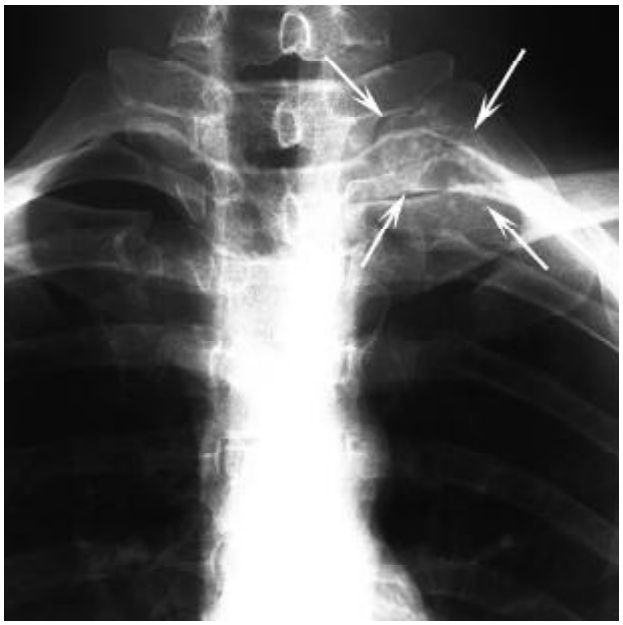

Fig. 24A

Fig. 24B

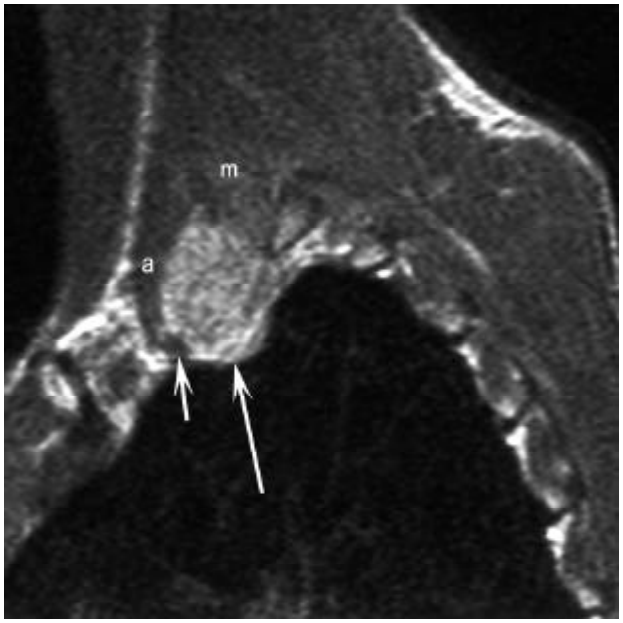

Fig. 24C

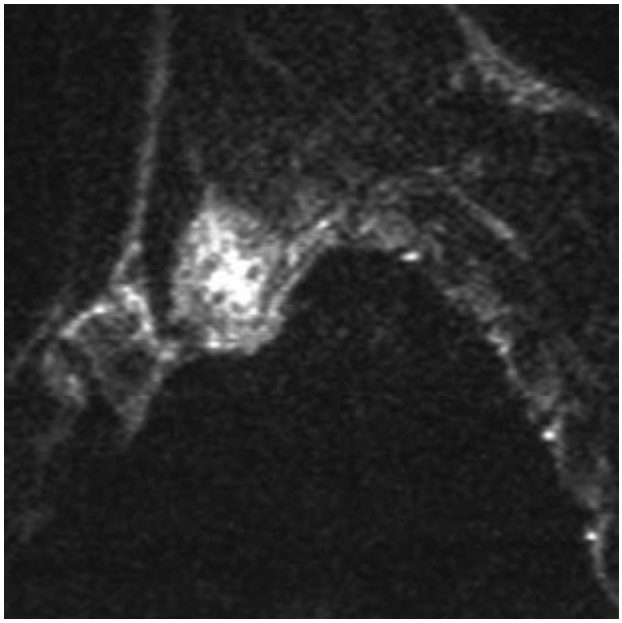

Fig. 24D

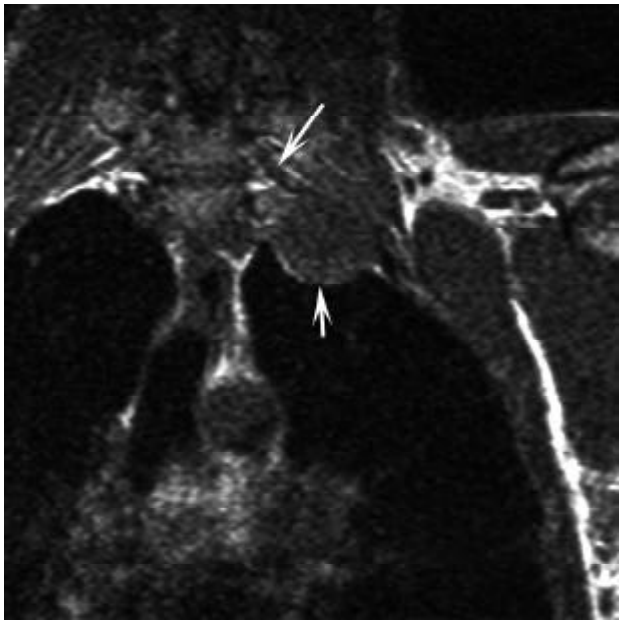

Fig. 24E

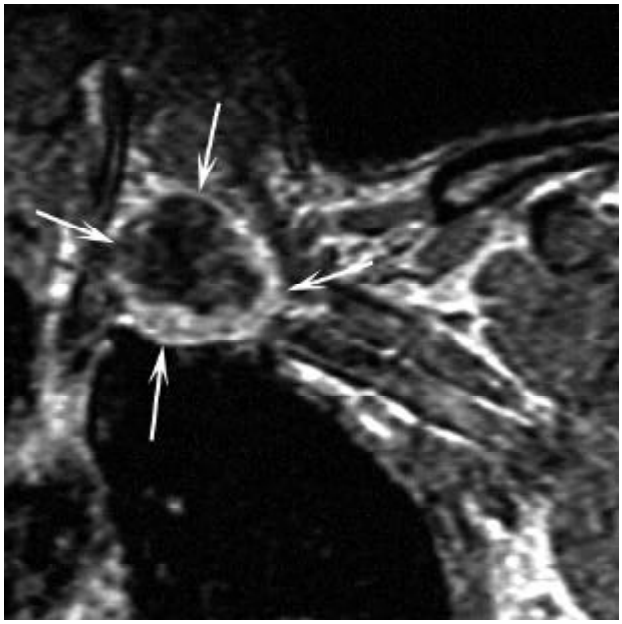

Fig. 24F

Fig. 24. Patient No. 53: metastasis of a chondrosarcoma.

A. Chest radiograph shows an opacity with calcifications in the apex of the left lung (arrows).

B. CT scan with intravenous contrast confirms the calcifications in the mass (arrow).

C and **D.** Sagittal proton-density (**C**) and T2-weighted (**D**) image of the tumor with an increased signal intensity. The tumor (long arrow) is located in the interscalene triangle and displaces the subclavian artery (short arrow) and anterior scalene muscle (a) anteriorly; m = middle scalene muscle.

E. Coronal T1-weighted image shows that the ventral ramus of root C8 (long arrow) is involved by the tumor (short arrow).

F. Coronal reconstruction from a T1-weighted 3D volume acquisition with gadolinium-DTPA demonstrates the peripheral enhancement of the tumor.

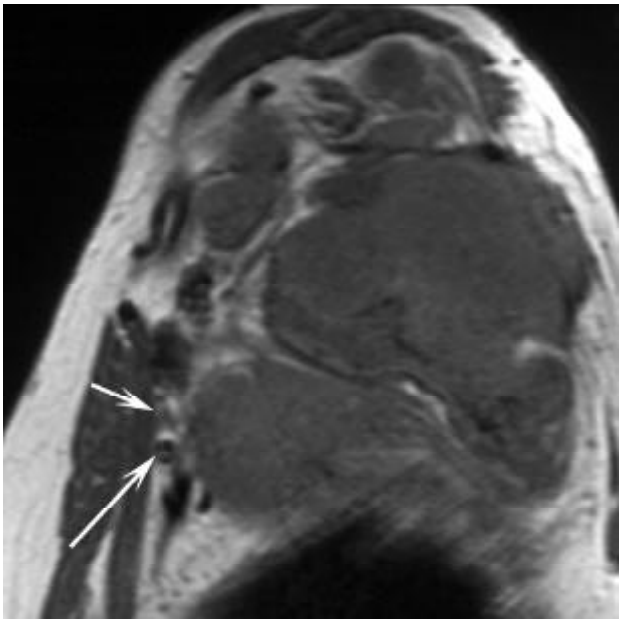

Fig. 25A

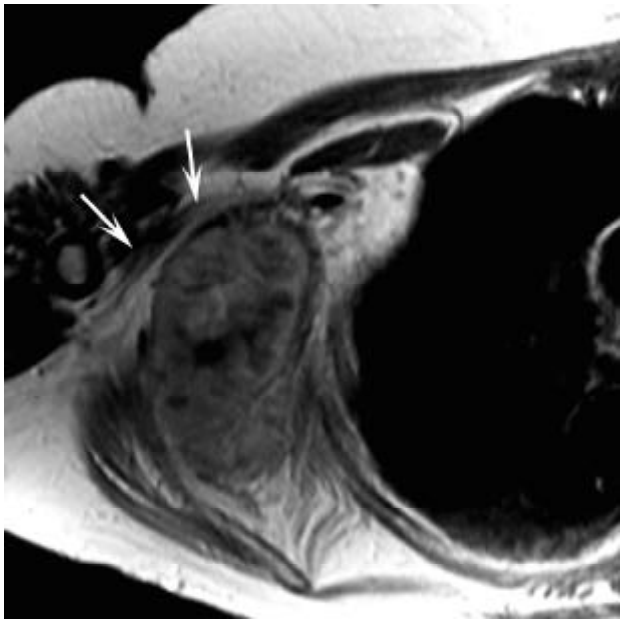

Fig. 25B

Fig. 25. Patient No. 60: chondrosarcoma of the scapula.

A. Sagittal T1-weighted image shows the large chondrosarcoma which displaces the axillary artery (long arrow) and the brachial plexus (short arrow) anteriorly.

B. Axial T1-weighted image with gadolinium-DTPA confirms the anterior displacement of the brachial plexus (arrows) by the tumor.

Fig. 26A

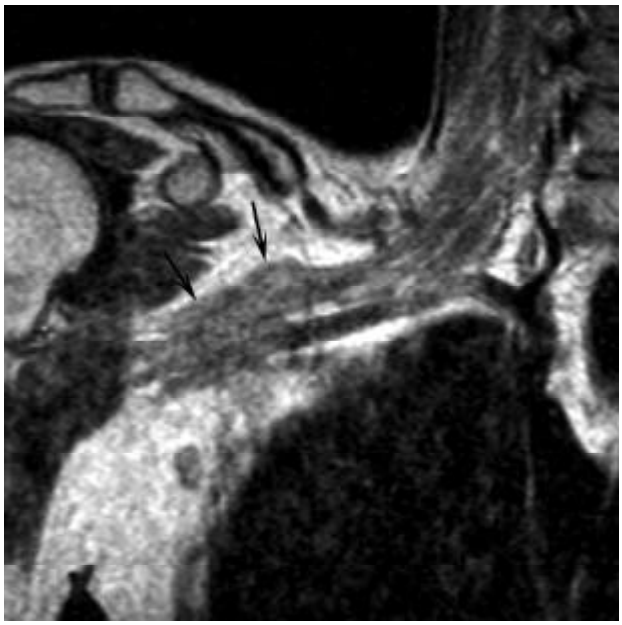

Fig. 26B

Fig. 26. Patient No. 45: synoviosarcoma near the coracoid process which was removed incompletely.

A. Sagittal T1-weighted image with gadolinium-DTPA shows residual tumor infiltrating the cords of the brachial plexus (black arrow), white arrow points to the axillary artery.

B. Coronal T1-weighted image with gadolinium-DTPA shows the enhancing tumor around the cords of the brachial plexus (black arrows). Upon surgery it appeared to be possible to release the lateral and medial cords from the tumor, as well as the axillary artery and vein, the posterior cord had to be removed.

Table 1

Primary tumors of the brachial plexus

pt no	m/f	age	presenting symptoms	diagnosis	location	diagnostic procedure
1	m	46	palpable tumor	malignant schwannoma	upper trunk	surgery
2	f	60	palpable tumor	schwannoma	cord	biopsy
3	f	25	pain and paresthesias in 4th and 5th finger	neurofibroma	C7	surgery
4	m	26	paresthesias ulnar side arm	schwannoma	lower trunk	surgery
5	f	57	palpable tumor and pain in shoulder and upper arm	ancient schwannoma	C8 and lower trunk	biopsy
6	f	24	atrophy intrinsic hand muscles	unknown	Th1 and lower trunk	MR imaging alone
7	m	16	atrophy intrinsic hand muscles	unknown	Th1	MR imaging alone
8	f	51	Horner's syndrome	malignant schwannoma	C7	surgery
9	m	56	palpable tumor and pain in shoulder and upper arm	schwannoma	C6	surgery
10	m	58	pain in arm and 2nd and 3rd finger	schwannoma	C7	surgery

Table 2

Secondary tumors related to the brachial plexus: lung tumors

pt no	m/f	age	presenting symptoms	histology	brachial plexus involvement on MR imaging	therapy
11	f	45	brain metastasis	squamous cell carcinoma	yes	radiation therapy
12	f	36	Horner's syndrome and pain in arm	adenocarcinoma	yes	chemotherapy
13	f	73	pain in shoulder and arm	squamous cell carcinoma	yes	radiation therapy
14	m	47	Horner's syndrome and pain in arm and hand	adenocarcinoma	yes	radiation therapy
15	m	71	tumor on routine chest radiograph	not known	no	radiation therapy
16	m	59	pain in shoulder and arm	adenocarcinoma	yes	surgery
17	m	63	pain at scapula	adenocarcinoma	no	none
18	f	45	Horner's syndrome and pain in arm and hand	not known	yes	radiation therapy
19	m	73	hemoptysis and cough	squamous cell carcinoma	no	surgery
20	m	67	sensory deficit thoracic wall	squamous cell carcinoma	no	radiation therapy
21	m	45	paresthesias 4^{th} and 5^{th} finger	squamous cell carcinoma	yes	radiation therapy
22	m	61	Horner's syndrome and pain in arm	not known	yes	radiation therapy
23	m	55	pneumonia	large cell carcinoma	no	radiation therapy
24	m	74	pain in thoracic wall and shoulder	squamous cell carcinoma	yes	radiation therapy
25	m	39	pain and sensory deficit in lower arm	adenocarcinoma	yes	surgery
26	m	57	Horner's syndrome and pain in shoulder and arm	adenocarcinoma	yes	radiation therapy
27	f	43	tumor on routine chest radiograph	squamous cell carcinoma	yes	surgery
28	m	60	tumor found on CT which was performed for the evaluation of a palpable mass in neck (cervical rib)	squamous cell carcinoma	no	surgery
29	m	72	hemoptysis	not known	no	radiation therapy
30	m	63	pain in axilla	adenocarcinoma	yes	radiation therapy
31	f	64	pain in shoulder, arm and hand	squamous cell carcinoma	yes	radiation therapy
32	m	72	pain in shoulder	not known	no	radiation therapy
33	f	47	tumor on routine chest radiograph	adenocarcinoma	no	surgery
34	f	21	tumor on routine chest radiograph	bronchogenic cyst	no	surgery

Table 3

Secondary tumors related to the brachial plexus: metastases of breast carcinoma

pt no	m/f	age	presenting symptoms	location	brachial plexus involvement on MR imaging	therapy
35	f	27	Horner's syndrome and pain in shoulder and arm	supraclavicular	yes	pain treatment
36	f	42	pain in arm	between major and minor pectoralis muscles	yes	radiation therapy
37	f	76	pain in arm	vertebral body C6 and C7 with epidural extension	yes	not known
38	f	51	pain in arm	vertebral body Th1	yes	radiation therapy
39	f	69	pain in arm	supra- and infraclavicular	no	surgery
40	f	69	pain and paresthesias in fingers	axilla	yes	hormonal therapy
41	f	48	pain in shoulder	interscalene triangle	yes	radiation therapy
42	f	63	pain in arm	axilla	yes	radiation therapy
43	f	56	pain in shoulder, arm and hand	between major and minor pectoralis muscles	yes	surgery

Table 4

Secondary tumors related to the brachial plexus: miscellaneous tumors

pt no	m/f	age	presenting symptoms	histology	brachial plexus involvement on MR imaging	therapy
44	m	42	palpable tumor	aggressive fibromatosis	yes	surgery
45	f	23	pain in shoulder and palpable tumor	synoviosarcoma	yes	surgery
46	f	22	palpable tumor	lipoma	no	surgery
47	m	66	pain in axilla	metastasis 2nd rib from oropharynx carcinoma	no	none
48	f	10	acute swelling in the neck	hematoma in neck cyst	no	surgery
49	m	42	pain in shoulder and arm	metastasis 1st rib from unknown primary (adenocarcinoma)	yes	pain treatment
50	m	70	pain in arm	metastasis larynx carcinoma	yes	radiation therapy
51	m	69	Horner's syndrome and pain in shoulder	B-cell non-Hodgkin's lymphoma	yes	chemotherapy and radiation therapy
52	f	34	pain in arm	chondrosarcoma thoracic wall	yes	radiation therapy
53	m	27	paresthesias in ulnar side hand	metastasis of chondrosarcoma maxillary sinus	yes	surgery
54	m	70	palpable tumor	lipoma	no	surgery
55	m	67	pain in shoulder	metastasis from unknown primary	yes	pain treatment
56	m	41	palpable tumor	lipoma	no	surgery
57	f	71	atrophy muscles shoulder and arm	B-cell non-Hodgkin's lymphoma	yes	chemotherapy
58	m	56	palpable tumor	liposarcoma	yes	surgery
59	m	57	pain in neck	meningocele in von Recklinghausen's disease	yes	surgery
60	f	55	pain in shoulder	chondrosarcoma scapula	yes	surgery
61	m	53	palpable tumor	aggressive fibromatosis	yes	surgery
62	f	39	Horner's syndrome	tumor of unknown origin	yes	not known
63	m	41	pain in arm	metastasis from unknown primary (squamous cell carcinoma)	yes	radiation therapy
64	m	66	pain in shoulder and palpable tumor	metastasis from unknown primary (adenocarcinoma)	yes	none
65	m	43	pain in arm and palpable tumor	leiomyosarcoma	yes	surgery
66	m	47	pain thoracic wall	metastasis renal cell carcinoma	yes	chemotherapy

Table 5

Patients with infection but no tumor

pt no	m/f	age	presenting symptoms	diagnosis	brachial plexus involvement
67	m	50	cough, tumor on chest radiograph	abscess right upper lobe	no
68	f	68	painful ulcer sternum	chronic osteomyelitis sternum after radiation therapy for breast carcinoma	no
69	m	49	edema arm, on CT a tumor supra- and infraclavicular	hemorrhage and infection supra- and infraclavicular with subclavian vein thrombosis	no

Table 6

Patients after radiation therapy without tumor

pt no	m/f	age	presenting symptoms	radiation for	MR imaging	clinical diagnosis
70	f	75	weakness of hand and paresthesias of fingers	breast ca	diffusely thickened brachial plexus	radiation brachial plexopathy
71	f	61	paresthesias 1st and 2nd finger	breast ca	normal	radiation brachial plexopathy
72	m	73	pain shoulder and weakness arm	larynx ca	normal	radiation brachial plexopathy
73	f	49	Horner's syndrome and pain in arm	breast ca	loss of fat planes	radiation brachial plexopathy
74	f	70	weakness hand	breast ca	increased signal intensity in pectoralis muscles	spontaneous improvement
75	f	72	paresthesias 1st-3rd finger	breast ca	increased signal intensity lung apex	carpal tunnel syndrome
76	m	41	atrophy of intrinsic hand muscles	Hodgkin's disease	diffusely swollen and enhancing brachial plexus	radiation brachial plexopathy (extensive fibrosis found with surgery)
77	f	53	pain in arm and hand	breast ca	normal	reflex sympathetic dystrophy
78	f	45	pain in arm	breast ca	normal	radiation brachial plexopathy
79	f	37	pain and sensory deficit in arm	breast ca	increased signal intensity in cords	radiation brachial plexopathy
80	f	41	paresthesias in hand	breast ca	normal	radiation brachial plexopathy
81	f	44	pain in shoulder	breast ca	normal	spontaneous improvement
82	f	45	paresthesias, pain and weakness of hand	breast ca	increased signal intensity in slightly thickened brachial plexus	reversible brachial plexopathy
83	f	62	pain in shoulder	breast ca and malignant schwannoma	focally thickened brachial plexus	no progression of complaints, probably fibrosis
84	f	54	weakness of hand	breast ca	increased signal intensity lung apex	radiation brachial plexopathy
85	f	66	pain in shoulder	breast ca	normal	radiation brachial plexopathy
86	f	62	pain and atrophy intrinsic hand muscles	breast ca	diffusely thickened brachial plexus	radiation brachial plexopathy

Table 7

Symptoms and diagnosis in patients with no abnormalities on MR imaging

pt no	m/f	age	presenting symptoms	clinical diagnosis
87	m	53	atrophy muscles innervated by C5-7	no diagnosis, slight spontaneous improvement
88	f	76	weakness in arm, cecum tumor	paraneoplastic plexopathy
89	m	65	weakness in arm	neuralgic amyotrophy
90	m	29	atrophy deltoideus, supra- and infraspinatus muscles, and pain in shoulder and arm	neuralgic amyotrophy
91	m	58	weakness in hand and pain in arm	neuralgic amyotrophy
92	m	65	weakness and pain in hand	no diagnosis, symptoms have disappeared
93	m	35	pain in shoulder	symptoms disappeared after proximal clavicle resection
94	m	53	pain in shoulder	no diagnosis
95	f	59	pain in arm and hand	carpal tunnel syndrome
96	f	50	neurofibroma in ulnar nerve, extension into brachial plexus?	no neurofibroma in brachial plexus, resection neurofibroma in ulnar nerve
97	f	36	hyperesthesia C8 and Th1 dermatome	reflex sympathetic dystrophy
98	m	61	weakness in arm and pain in shoulder	no diagnosis
99	f	45	pain in axilla, schwannoma 10 years ago	no recurrent schwannoma
100	m	48	anhidrosis	no diagnosis
101	m	63	weakness in arm	stretched brachial plexus during surgery
102	m	78	weakness in arms and legs	Guillain-Barré syndrome
103	m	65	pain arm	disc protrusion C5-6
104	m	48	weakness in upper arm	no diagnosis
105	f	52	pain and weakness in hand	syrinx cervical myelum
106	m	51	pain in shoulder and upper arm	disc protrusion C5-6
107	m	21	pain in shoulder and arm	myalgia
108	m	48	weakness and sensory deficit in hand	neuralgic amyotrophy
109	m	73	paresthesias fingers	carpal tunnel syndrome
110	m	30	pain scapula and paresthesias fingers	no diagnosis
111	f	26	pain in lower arm	no diagnosis
112	m	32	pain in arm	no diagnosis
113	m	57	pain in arm and hand	disc protrusion C7-Th1
114	f	34	pain in arm, schwannoma 8 years ago	no recurrent schwannoma
115	f	43	supraclavicular palpable tumor which caused irradiating pain at palpation	surgery revealed no tumor, but a normal superficially located brachial plexus
116	m	43	weakness in arm and pain in shoulder	neuralgic amyotrophy
117	m	75	pain in arm and hand	no diagnosis
118	m	38	atrophy infraspinous and triceps muscles	disc protrusion C6-7
119	m	51	Horner's syndrome	no diagnosis, Horner's syndrome has disappeared
120	m	44	paresthesias in 1st and 2nd finger after surgery for breast carcinoma	no diagnosis, symptoms have disappeared
121	m	40	paresthesias in 2nd and 3rd finger	no diagnosis
122	f	31	pain in shoulder	no diagnosis
123	f	24	weakness in arm after supraclavicular lymph node dissection	no diagnosis
124	f	30	Horner's syndrome and paresthesias in 4th and 5th finger	no diagnosis
125	m	34	paresthesias in shoulder and arm	narrowing intervertebral foramina C5-6 and C6-7
126	m	35	weakness in arm	hereditary neuralgic amyotrophy
127	f	17	weakness in arm	hereditary neuralgic amyotrophy
128	m	45	weakness in arm	hereditary neuralgic amyotrophy
129	f	55	pain in shoulder	breast reduction
130	m	59	weakness in shoulder and arm after period of pain	neuralgic amyotrophy
131	m	54	sensory deficit hand	no diagnosis
132	f	40	weakness and pain in arm	no diagnosis
133	m	66	weakness in shoulder and arm	no diagnosis
134	f	43	pain in shoulder	disc protrusion C5-6
135	f	40	weakness in arm	hereditary neuralgic amyotrophy
136	f	46	sensory deficit arm	no diagnosis

Chapter 4

Trauma and Thoracic Outlet Syndrome

TRAUMA

Trauma to the brachial plexus can be divided into open injuries and closed injuries.[127] Closed injuries are traction injuries and can be divided into supraclavicular, retroclavicular, infraclavicular and mixed injuries. Supraclavicular lesions are more common than retro- and infraclavicular lesions: in a series of 810 cases 75% of the cases were supraclavicular against 25% retro- and infraclavicular.[6,7] Supraclavicular injuries can be subdivided into supraganglionic (preganglionic) and infraganglionic (postganglionic) lesions. This subdivision has important therapeutic consequences, as a supraganglionic lesion, which is a nerve root avulsion, cannot be repaired directly and neurotization techniques or musculotendinous transpositions may be used,[76,128,129,134,165,166,240,246] while the more distal infraganglionic lesions can be restored by local repair.[150] Neurotization is a technique by which an intact neighboring donor nerve is separated from its end organ and then connected directly or by nerve grafts to the distal portion of a non-functioning nerve. In brachial plexus surgery the spinal accessory nerve, rami of the cervical plexus, or intercostal nerves can be transferred to parts of the brachial plexus. Clinically and electrodiagnostically there are some signs and symptoms which may differentiate between supra- and infraganglionic lesions.[28,133,134] Horner's syndrome is suggestive of a nerve root avulsion of Th1. A positive Tinel's sign, which is distal tingling produced by percussing the injured nerves, indicates an infraganglionic lesion. Paralysis of the serratus anterior and rhomboid muscles suggests a supraganglionic lesion. When there is besides limb muscle denervation, paravertebral muscle denervation, a supraganglionic lesion is suspected. Nerve conduction studies may suggest a supraganglionic lesion if motor conduction is absent and sensory conduction is present, while with infraganglionic lesions they are both absent.

Nerve root avulsions occur when there is simultaneously traction of the arm and throwing of the head to the opposite side. By far the most common cause in adults is a motorcycle accident.[6,7,161,164,226] Another important cause is the birth related brachial

palsy.[81,224,225] Sunderland[237,241] has described two ways by which nerve roots may be avulsed from the spinal cord: the peripheral and central mechanism. With the peripheral mechanism, lateral traction first causes rupture of the ligamentous attachments of the spinal nerve to the transverse processes and tearing of the dural cone, followed by avulsion of the nerve root. The nerve roots of C8 and Th1 lack the ligamentous attachments of the spinal nerve to the transverse processes, so they have a higher incidence of nerve root avulsions than C5, C6 and C7, which do have a strong attachment to the transverse processes.[99,236] The tearing of the dura causes cerebrospinal fluid to escape into the surrounding tissues, so leaving a traumatic meningocele within two or three weeks.[239] With this mechanism it is conceivable that a dural tear coincides with an intact nerve root, which means that the presence of a traumatic meningocele does not always indicate a nerve root avulsion. The central mechanism causes nerve root avulsions by violent displacements of the spinal cord. With this mechanism the nerve roots can avulse without tearing the dural cone, which means that there is no traumatic meningocele. Although not very common, traumatic meningoceles can exist without nerve root avulsions and nerve root avulsions can occur without traumatic meningoceles.[39,95,130,148,169,225,237,239,266]

Retro- and infraclavicular injuries of the brachial plexus can be caused by shoulder dislocation, fractures of the clavicle or shoulder girdle, and by violent movement of the shoulder causing stretching of the brachial plexus. Clavicular fractures can coincide with brachial plexus compression. This can be instantaneous by a piercing bone fragment, or of delayed onset by malunion, nonunion or extensive callus formation, which requires surgery.[13,18,43,80,103,107,146] The space between the clavicle and first rib in particular may be narrowed by a bone fragment or by extensive callus formation. The prognosis for retro- and infraclavicular lesions is better than for supraclavicular ones.[5,131,134,135,163]

Two classifications are in use to determine the severity of the nerve lesion. Seddon[216] used three types: neurotmesis, axonotmesis and neurapraxia. Neurotmesis means literally cutting of a nerve. All essential structures of the nerve have been destroyed, which makes spontaneous healing impossible. In axonotmesis there is damage to the nerve fibers, which causes a complete loss of neurological function distally. Spontaneous recovery is possible, because the Schwann tubes, endoneurium and perineurium are intact. Neurapraxia (apraxia literally means non-action) describes paralysis without an anatomic lesion. There is a spontaneous and complete recovery. Sunderland introduced a more precise classification, consisting of five degrees of injury.[235] First degree injury (= neurapraxia): a reversible conduction block with an intact anatomical continuity. Second degree injury (= axonotmesis): damage to the axons with distally Wallerian degeneration; complete recovery occurs because of the intact endoneurial tubes. Third degree injury: the continuity of the endoneurial tubes is damaged, which causes incorrect reinnervation. Fourth degree injury: there is a complete disorganization of the nerve, which is still continuous; there can be

some recovery, but without a useful degree of function. Fifth degree injury (= neurotmesis): there is a complete interruption of the nerve.
If a nerve is transected, post-traumatic neuromas can develop in infraganglionic, retro- and infraclavicular lesions.[149] A post-traumatic neuroma is a disorganized proliferation of regenerating axons at the proximal stump of a transected nerve. It consists of nerve fascicles with Schwann cells, fibroblasts and axons with myelin.[64] The first published surgical repair of a rupture of the brachial plexus was in 1900 by Thorburn.[206,247] The indication for surgical exploration is absent spontaneous clinical improvement. Surgery within the first six months will give the best prognosis.[15,134] First, an exact intraoperative diagnosis is necessary by exploring the supra- and infraclavicular region of the brachial plexus. Then, depending on the kind of lesion, microsurgical neurolysis, nerve grafting or neurotization can be performed.[15,149] Secondary operations may be necessary and include musculotendinous transfers and arthrodesis.[16]

Imaging

It is important to determine the site of the lesion, as this has significant prognostic and therapeutic consequences. Reliable imaging of the presence or absence of nerve root avulsions is most important. Myelography is very useful to demonstrate traumatic meningoceles in patients with nerve root avulsions.[159,243] It is also possible to see the roots surrounded by contrast.[38,160] CT myelography improved the detection of small traumatic meningoceles.[95,139,154,190,207,264,266,267] If at least 2 mm sections are used, the nerve roots can be well visualized, although the image quality of the lower roots can be less adequate due to artifacts from the shoulders. An important advantage of MR imaging in the detection of nerve root avulsions is its non-invasiveness: no intradural contrast is necessary. There have been several (case) reports about the appearance of nerve root avulsions and traumatic meningoceles on MR imaging.[46,54,74,87,142,144,148,169,177,192,194,200,201,207,254,259,260,266] Traumatic meningoceles are fluid collections extending from the neural foramen which follow the signal intensities of the cerebrospinal fluid in all sequences. MR imaging can depict the traumatic meningoceles very well, even those which do not have a communication with the dural sac, but cannot reliably show all nerve roots.[74,148,169,177,264] Because, as mentioned before, traumatic meningoceles occur without nerve root avulsions and nerve roots can avulse without traumatic meningoceles, it is necessary to image the roots themselves and not only the traumatic meningoceles. CT myelography is considered to be the most reliable investigation for the imaging of the nerve roots.[28,207,266,267] The main advantage of MR imaging in trauma patients is the visualization of the extraforaminal part of the brachial plexus. Thickening of the brachial plexus with and without an increased signal intensity on T2-weighted images can be seen, presumably due to respectively edema[114,200,259,261] and fibrosis.[87,144] Post-traumatic neuromas are seen as well-defined

tumors of the brachial plexus with a low signal intensity on T1-weighted images and a high signal intensity on T2-weighted images.[100,177,200,229] MR imaging can demonstrate other causes of brachial plexopathy after trauma, such as a hematoma[21, 194,229] and a clavicle fracture[21,200,223,229,259,261,262] with brachial plexus compression. The progress of imaging techniques at this time has not been sufficient to preclude diagnostic surgery to define intraoperatively the exact extent of the lesion.[15]

Own material

Patients with trauma and abnormal MR imaging

Table 1 describes 31 patients with a history of trauma and abnormalities with MR imaging, examples are shown in Figs. 1-5. In this group, 10 patients (patients Nos. 139, 140, 142, 144, 146, 148, 151, 153, 155 and 159) are described who presented with a flail arm after a severe trauma, especially motorcycle accidents (seven patients). In five patients a 3D-TSE (Figs. 1 and 2) was performed which was surgically correlated in three patients (patients Nos. 142, 144 and 155). In all three patients there were more avulsions found at surgery than meningoceles demonstrated with MR imaging. Other abnormalities seen with MR imaging were thickening of the brachial plexus in six patients (patients Nos. 139, 140, 142, 144, 148 and 153), hematomas in three patients (patients Nos. 142, 151 and 155), and in two patients compression by a clavicle fracture upon the brachial plexus (patients Nos. 146 and 148). In our experience, MR imaging was not able to demonstrate neurotmesis, as shown in patients Nos. 142 (torn upper trunk found at surgery), 144 (intraforaminal neurotmesis of root C5 found at surgery) and 153 (neuromas of the trunks found at surgery, Fig. 3). No surgery was performed in three patients because of spontaneous improvement (patients Nos. 146, 148 and 151). An explanation for the clinical improvement could be the release of compression of the brachial plexus by a healing clavicle fracture (patients Nos. 146 and 148) and a resolving hematoma (patient No. 151, Fig. 4).

In three patients (patients Nos. 150, 154 and 157) with known nerve root avulsions MR imaging was requested to rule out neuroma formation as an explanation for pain. In this group no neuromas could be demonstrated.

In 14 patients (patients Nos. 138, 141, 145, 147, 149, 152, 156, 158, 160, 161, 162, 164, 165 and 167) MR imaging was performed because of a clavicle fracture with symptoms of brachial plexus compression (Fig. 5). In eight patients (patients Nos. 141, 145, 149, 152, 156, 160, 161 and 165) compression of the brachial plexus was seen, whereas in six patients (patients Nos. 138, 147, 158, 162, 164 and 167) the clavicle fracture or callus did not disturb the brachial plexus. Surgical decompression was done in four patients (patients Nos. 149, 156, 161 and 165) and is planned in one patient (patient No. 145) from the group with brachial plexus involvement on

MR imaging. Clinical improvement was seen in all four patients. Only one patient (patient No. 164) from the group where MR imaging did not show brachial plexus compression was operated and this patient remained symptomatic until surgery for a cervical disc protrusion.
The remaining four patients had various pathology: one patient (patient No. 137) with an old stab wound, one patient (patient No. 143) with a coracoid process fracture, one battered child (patient No. 163) and one patient (patient No. 166) with a shoulder luxation.

Patients with trauma and normal MR imaging

Table 2 describes 18 patients with a possible brachial plexus lesion due to trauma and no abnormalities with MR imaging. In most, spontaneous improvement was seen without a definitive diagnosis. Two patients were operated (patient Nos. 168 and 172). Although no abnormalities with MR imaging were detected, neurotmesis of the axillary, radial, musculocutaneous, median and ulnar nerves in patient No. 168 was found, and neurotmesis of the roots C5 and partially of C6 was found in patient No. 172.

Conclusions

MR imaging of the brachial plexus in a patient who presents with a flail arm after an accident has not been very conclusive diagnostically in our experience. Unfortunately, it is not possible to make a distinction between neurotmesis, axonotmesis and neurapraxia. In two cases (patient Nos. 168 and 172) the brachial plexus appeared to be normal with MR imaging, while at surgery neurotmesis was found. MR imaging can demonstrate compression of the brachial plexus by a hematoma or a clavicle fracture. CT myelography is, up until now, the most sensitive investigation to diagnose traumatic nerve root avulsions.[267] MR imaging can, in our experience demonstrate meningoceles well, but it is not always possible to evaluate the nerve roots themselves. However, the use of a 3D-TSE sequence improves the visualization of the nerve roots and this may replace CT myelography in the future.

THORACIC OUTLET SYNDROME

Thoracic outlet syndrome is a very confusing syndrome with controversial therapeutic options. Although the term thoracic outlet syndrome was introduced by Peet[186] in 1956, this syndrome and its different causes have been extensively described before. Wilbourn[273] has written a nice historical overview with three eras of increased surgical interest. The first was the “invariably symptomatic cervical rib syndrome” era, when

the presence of a cervical rib was consistently associated with any upper extremity symptoms.[14,62,205] The therapy was removal of the cervical ribs. Adson[2] advised performing a tenotomy of the anterior scalene muscle instead of a cervical rib resection, as he found the same relief with this less difficult procedure. The next era was the "scalenus anticus syndrome" era. In 1935 Ochsner reported patients with a cervical rib syndrome without a cervical rib present.[170] The syndrome was thought to be caused by spasm of the anterior scalene muscle. Elevation of the first rib so caused compression of the subclavian artery and lower trunk of the brachial plexus. The therapy was an anterior scalenotomy. The scalenus anticus syndrome lost popularity because of its low surgical success rate, and because cervical radiculopathy and carpal tunnel syndrome were recognized as different causes of upper extremity symptoms.[274] Other described compression sites were the costoclavicular area with the costoclavicular syndrome[66,67] and the subcoracoid region with the hyperabduction syndrome.[277] Peet[186] introduced the term "thoracic outlet syndrome", which includes all described compression syndromes and he described a conservative therapeutic regimen. Surgical interest increased again in the early 1960s in the "disputed neurogenic thoracic outlet syndrome" era. The first rib was then thought to be the main cause of compressing the neurovascular structures and Clagett[37] advised removal of the first rib. He recommended a posterior thoracotomy approach which left a large scar. The first rib resection became popular when Roos[209] introduced the transaxillary approach. Roos[211] also introduced the total anterior scalenectomy for a new type of thoracic outlet syndrome with symptoms around the shoulder, due to compression of the ventral rami of the upper roots of the brachial plexus (C5, C6 and C7). The advantage of excising the anterior scalene muscle instead of only transection is that reattachment and extensive scarring is less likely to occur.[215] The most extensive surgery for thoracic outlet syndrome became a combination of transaxillary first rib resection and excision of the anterior and middle scalene muscles.[199]

In 1988 Wilbourn[274] proposed a new classification of thoracic outlet syndrome, in which there is a separation between the vascular and neurologic types. In this classification there are three vascular types (major arterial, minor arterial, and venous) and two neurologic types (true neurogenic and disputed neurogenic).

The "major arterial vascular thoracic outlet syndrome" is rare and is caused by a cervical rib which compresses the subclavian artery.

The "minor arterial vascular thoracic outlet syndrome" is more common. With hyperabduction and exorotation of the arm positional ischemia occurs. A cervical rib is usually not present.

The "venous vascular thoracic outlet syndrome" causes spontaneous thrombosis of the subclavian vein.

The "true neurogenic thoracic outlet syndrome" is a typical clinical syndrome most often found in young women and is associated with an elongated transverse process of C7 or a cervical rib, from which a fibrous band extends to the first rib. The C8 and

Th1 ventral rami of the roots or the lower trunk are stretched over this fibrous band.[82,90,274] The subclavian artery can also be elevated and compressed by this band.[17] The transverse process of the seventh cervical vertebra is normally not larger than that of the first thoracic vertebra. If the transverse process of C7 extends beyond that of Th1, it can be seen as an abortive attempt to form a cervical rib.[210] The characteristic clinical picture is that of wasting and weakness of especially the lateral thenar muscles, usually combined with the medial forearm muscles. Other symptoms are pain, paresthesias and sensory loss along the medial aspect of the arm, forearm and hand. Nerve conduction studies are often typical and helpful in excluding a carpal tunnel syndrome and ulnar nerve entrapment at the elbow.[83,278] The therapy is surgical division of this fibrous band.[82,90]

The "disputed neurogenic thoracic outlet syndrome" includes all disorders in which there is suspected brachial plexus compression without the typical clinical, and radiologic findings as seen in the true neurogenic thoracic outlet syndrome.[49,274] Many symptoms might be present: pain, numbness and paresthesias in the lower trunk distribution, shoulder pain and back discomfort. The electrophysiologic studies can be normal.[218] Surgical treatment consists of first rib resections or scalenectomies, which can be complicated by serious brachial plexus injuries.[34,271] Because the clinical picture is unclear and there are no reliable diagnostic tests, this type is overdiagnosed and overtreated.[272] Before treatment it is important to exclude other treatable diagnoses, such as carpal tunnel syndrome and cervical radiculopathy.

There has been one report of an athlete with the typical clinical and electrophysiologic findings of a true neurogenic thoracic outlet syndrome but without a cervical rib or an elongated transverse process of C7. At surgery compression of the lower trunk by a hypertrophied anterior scalene muscle was found.[110]

Imaging

Conventional radiographs can show bony abnormalities, which include cervical ribs, elongated transverse processes of C7, and exostoses or old fractures of the first rib and clavicle. Conventional angiography is useful in detecting the major arterial vascular thoracic outlet syndrome, but might be replaced by MR angiography.[172] CT can add only little information regarding osseous abnormalities. Interposition of the transverse process of C7 between the anterior and middle scalene muscles can be shown, as well as the contact between a cervical rib and the brachial plexus. However this is not a very useful sign, as it can occur on both the symptomatic and asymptomatic sides. Fibrous bands cannot be detected on CT scans.[22] With MR imaging distortion of the brachial plexus can be seen. There is only one article which studied the value of MR imaging in thoracic outlet syndromes.[180] This article described that a mid- to low-intensity band, which was called a MRI band, could distort the brachial plexus. A sensitivity of 79% and a specificity of 87.5% was found when the distortion of the

brachial plexus on MR imaging was correlated with the clinical symptoms. However, in the same study a MRI band was also found in three asymptomatic volunteers which was associated with brachial plexus distortion in one, so that the value of these findings remains unclear. These good results have been criticized by Cherington[35], who disagreed with the MR imaging abnormalities. In conclusion thoracic outlet syndrome is a very controversial subject in clinical medicine as well as in diagnostic radiology.

Own material

Table 3 describes 23 patients with a variety of clinical symptoms consistent with thoracic outlet syndrome, examples are shown in Figs. 6-8. Two patients (patients Nos. 189 and 205), with an elongated transverse process of C7, presented with the typical true neurogenic thoracic outlet syndrome. In both patients a fibrous band, which caused neural compression, was found. In patient No. 205 (Fig. 6) a subtle angulation of the ventral ramus of root C8 was found in comparison with the other normal side. MR imaging of patient No. 189 showed no abnormalities. All other patients, except for patient No. 201, had a variety of symptoms consistent with disputed neurogenic thoracic outlet syndrome. From this group surgery was performed in 10 patients. Clinical improvement was seen in seven patients (patients Nos. 186, 192, 196, 198, 199, 203 and 204), while three patients (patients Nos. 191, 207 and 208) remained symptomatic. All of these patients showed no abnormalities with MR imaging.

Three patients with cervical ribs were imaged, two were symptomatic (patients Nos. 190 and 202) and one asymptomatic (patient No. 201, Fig. 7). In patients Nos. 190 and 201 angulation of the brachial plexus was seen, indicating that angulation does not necessarily correlate with symptoms.

Two patients (patients Nos. 196 and 204) were imaged after a resection of a cervical rib and an anterior scalenotomy. In patient No. 204 (Fig. 8) the anterior scalene muscle appeared to be very thick, despite prior surgery. After a new anterior scalenotomy and a first rib resection the symptoms have disappeared.

Conclusions

Thoracic outlet syndrome is clinically very difficult to diagnose. MR imaging does not seem to be very helpful in making this diagnosis. We have not been able to visualize fibrous bands. Angulation of a ventral ramus of nerve root C8 was found in one of the two patients with the true neurogenic thoracic outlet syndrome. However, angulation of the nerves does not necessarily coincide with symptoms, as was demonstrated in a patient with a cervical rib who was asymptomatic.

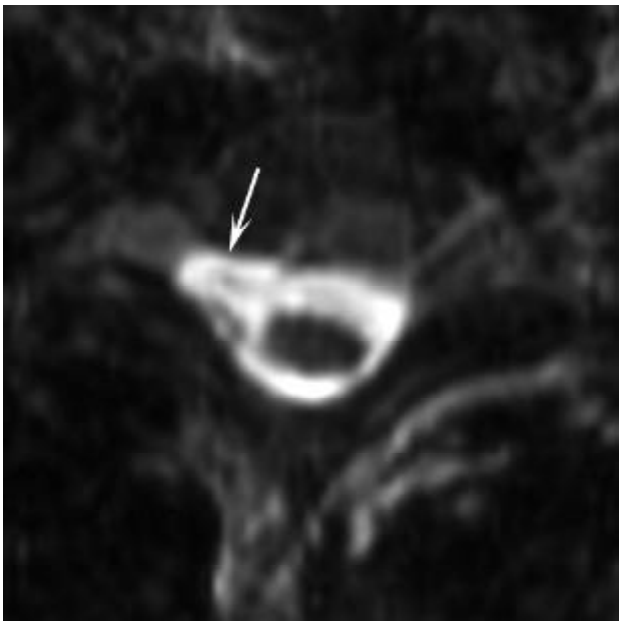

Fig. 1A

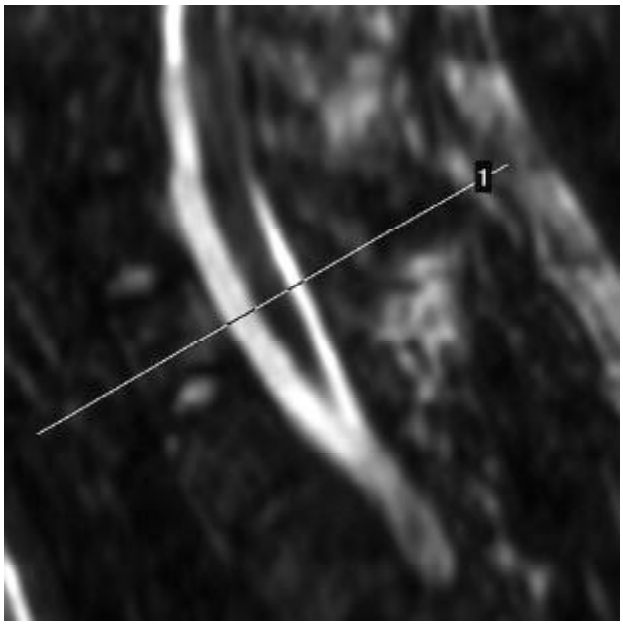

Fig. 1B

Fig. 1. Patient No. 146: traumatic meningocele C6-7 after a motorcycle accident five weeks ago.

A. and **B.** Oblique axial reconstruction of a 3D-TSE volume acquisition (**A**) with the sagittal scanogram (**B**) shows a meningocele (arrow).

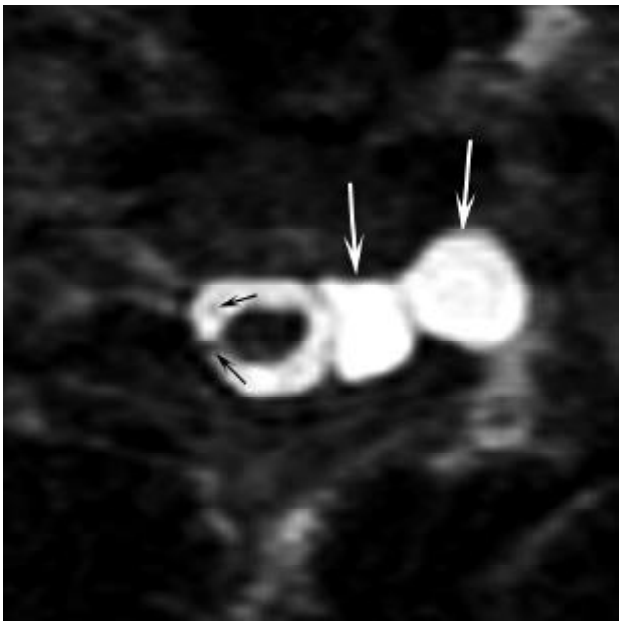

Fig. 2

Fig. 2. Patient No. 154: nerve root avulsion and traumatic meningocele due to a motorcycle accident 20 years ago. Axial TSE image shows a traumatic meningocele (white arrows) on the left with a nerve root avulsion of Th1. Note the intact nerve roots on the right (black arrows).

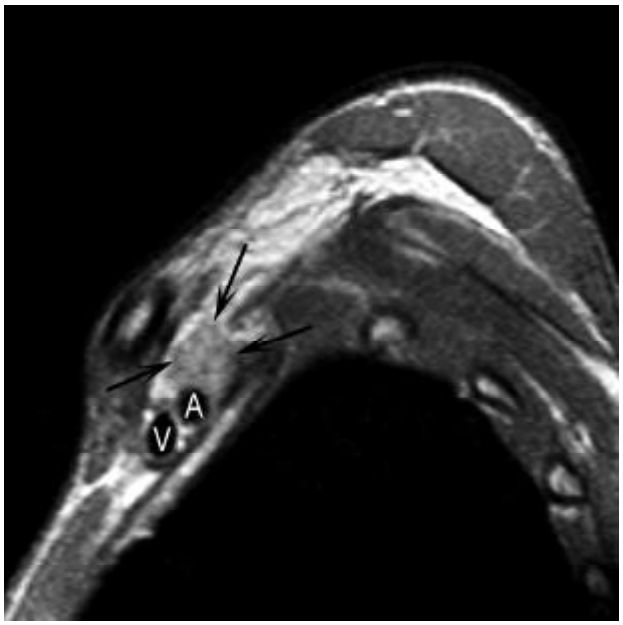

Fig. 3A

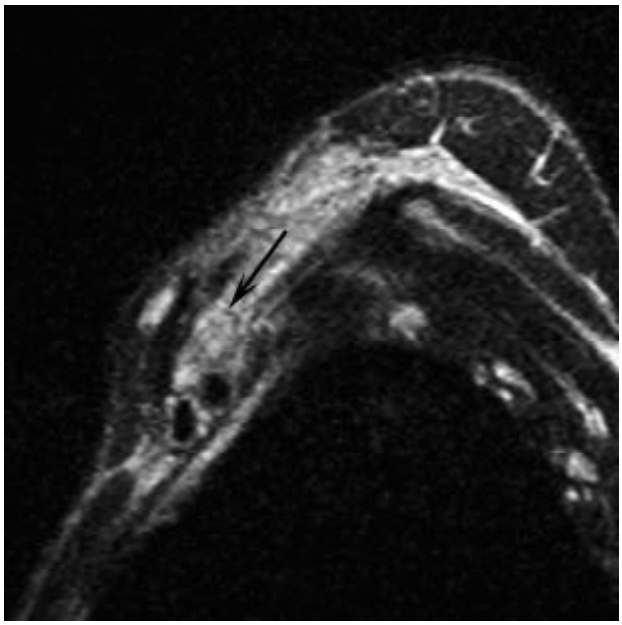

Fig. 3B

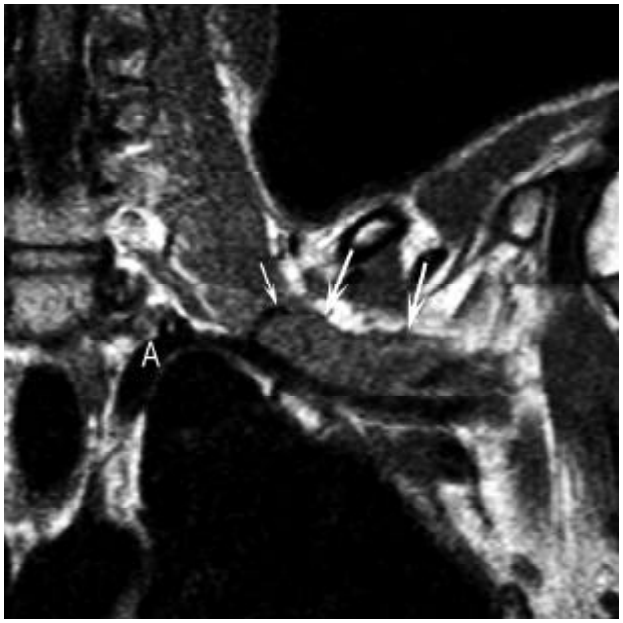

Fig. 3C

Fig. 3. Patient No. 153: swollen brachial plexus in a patient with a paralyzed arm 12 days after a bike accident.

A and **B.** Sagittal proton-density (**A**) and T2-weighted (**B**) image at the level of the divisions show a swollen slightly hyperintense brachial plexus (arrows) consistent with edema. A = subclavian artery, V = subclavian vein.

C. Coronal T1-weighted image shows a diffusely swollen brachial plexus, particularly marked in the trunks and divisions (long arrows). The short arrow points to the dorsal scapular artery, which passes through the brachial plexus. A = subclavian artery.
Surgery performed 12 weeks later showed rupture of the trunks with neuroma formation.

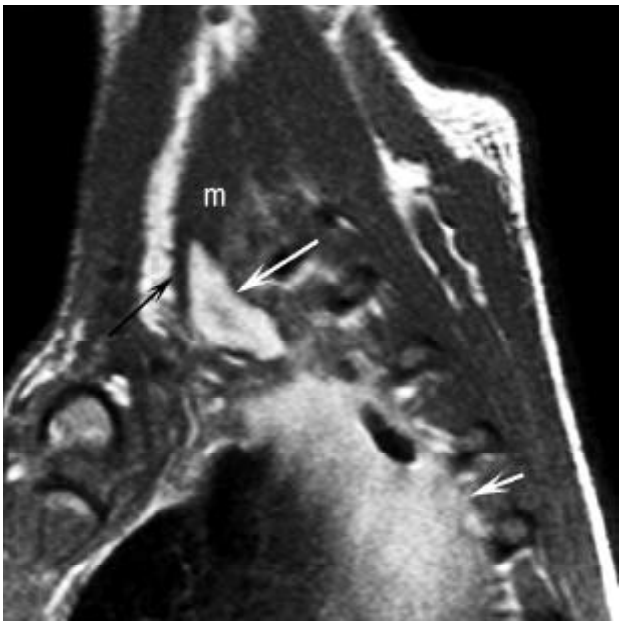

Fig. 4A

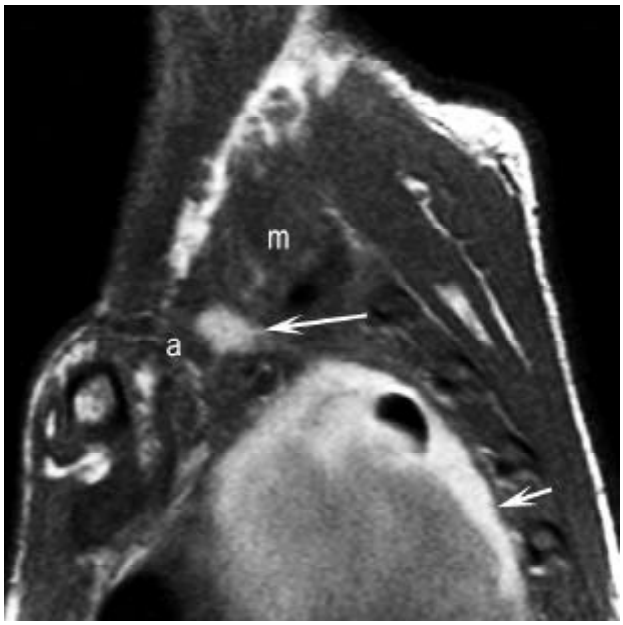

Fig. 4B

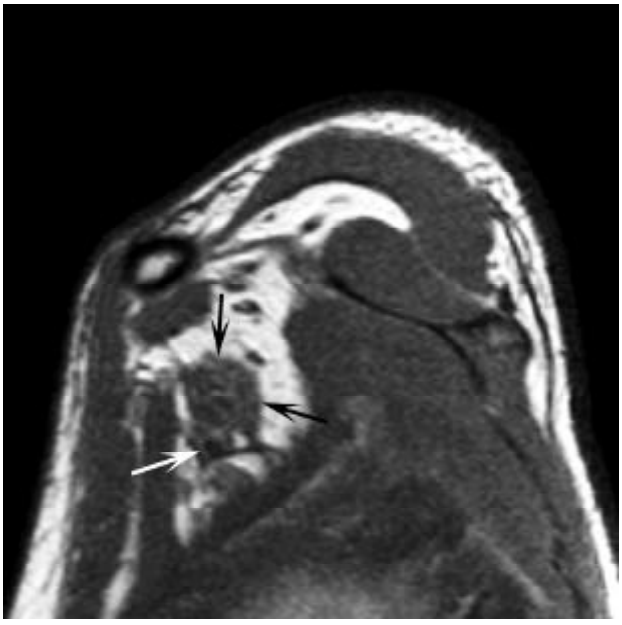

Fig. 4C

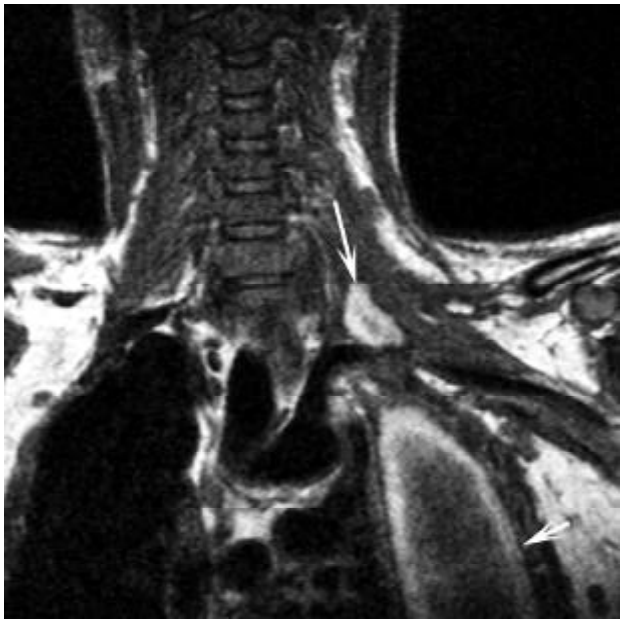

Fig. 4D

Fig. 4. Patient No. 151: hematoma in the interscalene triangle in a patient with a paralyzed arm five weeks after a skiing accident.

A. Sagittal T1-weighted image shows a hematoma in the interscalene triangle (long white arrow). There is also a large hematothorax (short white arrow). The black arrow points to the anterior scalene muscle, m = middle scalene muscle.

B. Sagittal T1-weighted image lateral to **A** shows that the hematoma (long arrow) is located between the anterior (a) and middle (m) scalene muscles. Short arrow points to the hematothorax.

C. Sagittal T1-weighted image at the level of the cords of the brachial plexus shows that the cords (black arrows) are swollen, white arrow points to the axillary artery.

D. Coronal T1-weighted image of the hematoma (long arrow), short arrow points to the hematothorax.

Fig. 5A

Fig. 5B

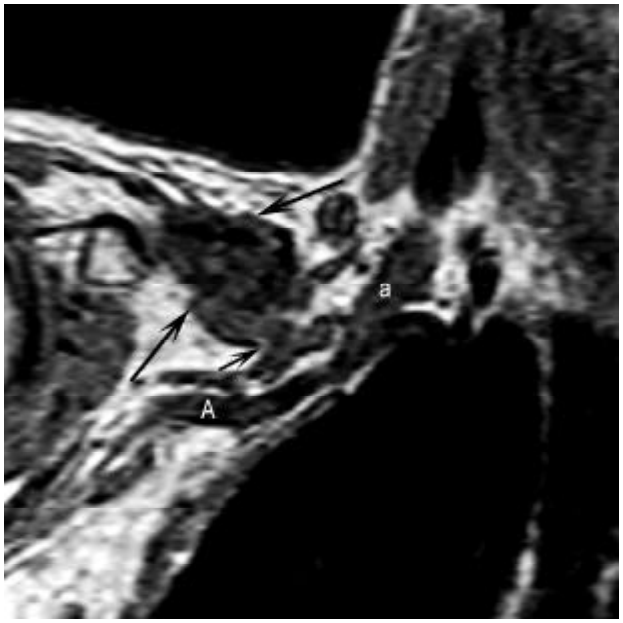

Fig. 5C

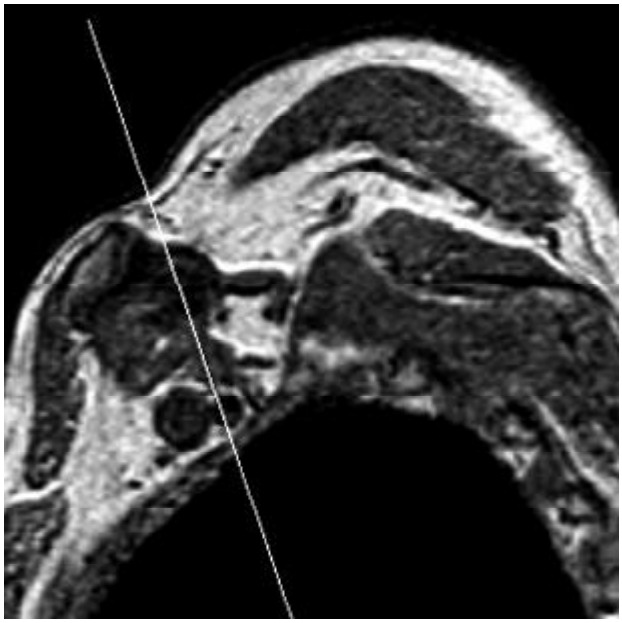

Fig. 5D

Fig. 5. Patient No. 149: clavicle fracture with compression of the brachial plexus.

A. Sagittal image from a T1-weighted 3D volume acquisition shows compression of the brachial plexus (long arrow) by callus (short arrows). A = axillary artery, V = axillary vein.

B. Coronal T1-weighted image demonstrates the relation between the brachial plexus and the callus (arrow).

C. and **D.** Oblique coronal reconstruction of a T1-weighted 3D volume acquisition (**C**) with the sagittal scanogram (**D**) shows the compression of the brachial plexus (short arrow) by the callus (long arrows) better. A = axillary artery, a = anterior scalene muscle.

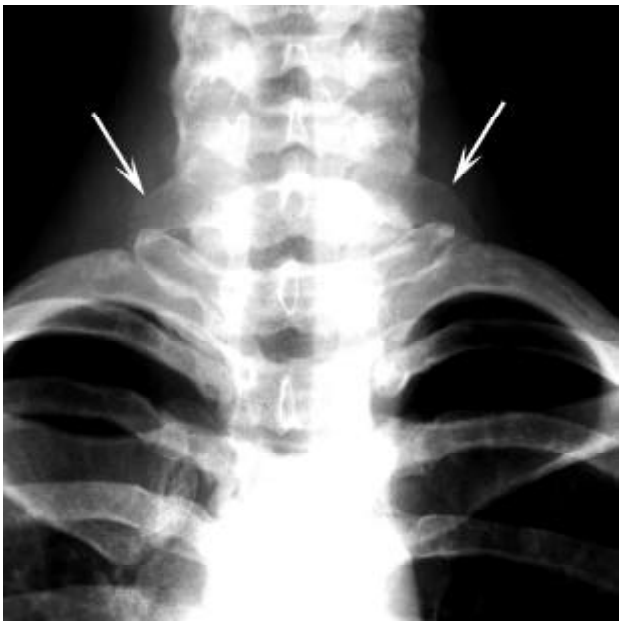

Fig. 6A

Fig. 6. Patient No. 205: left-sided true neurogenic thoracic outlet syndrome in a patient with an elongated transverse process of C7.

A. Conventional radiograph shows the bilateral elongated transverse processes of C7 (arrows).
B. Coronal T1-weighted image demonstrates a normal right ventral ramus of root C8 (arrow). C7, Th1 = vertebral body C7, Th1.
C. Coronal T1-weighted image shows that the left ventral ramus of root C8 is slightly more curved (arrow). Th1 = vertebral body Th1.
D. and **E.** Oblique coronal reconstruction of a T1-weighted 3D volume acquisition (**D**) with the axial scanogram (**E**) shows both ventral rami of root C8 in one plane. Note the angulation on the left side (short arrow) compared to right side (long arrow). C7, Th1 = vertebral body C7, Th1.
At surgery compression of the left ventral ramus of root C8 by a fibrous band was found.

Fig. 6B

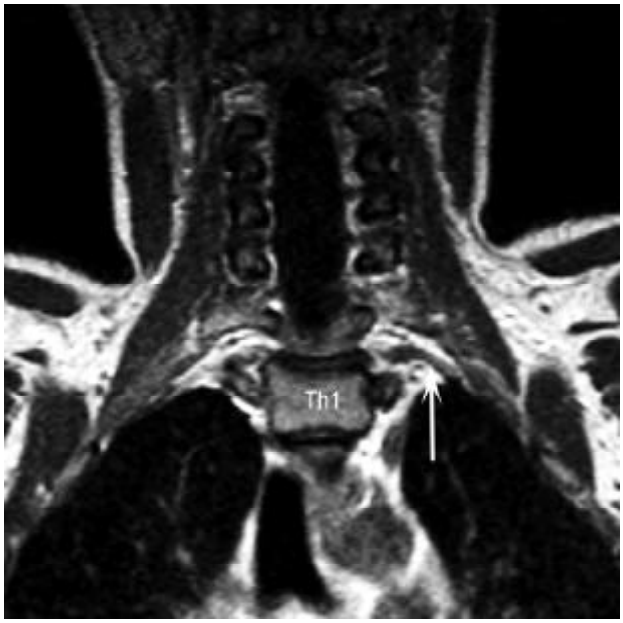

Fig. 6C

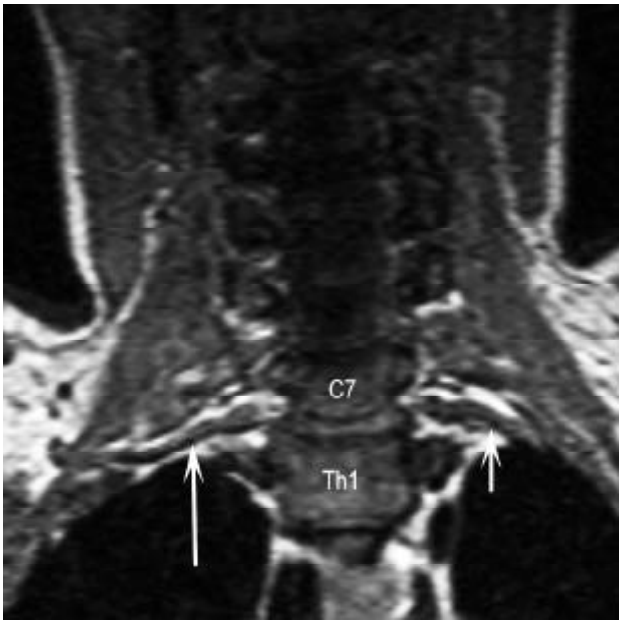

Fig. 6D

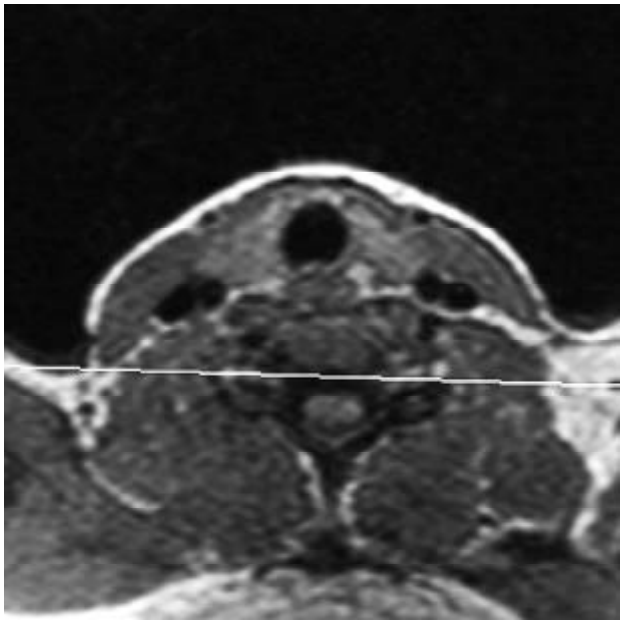

Fig. 6E

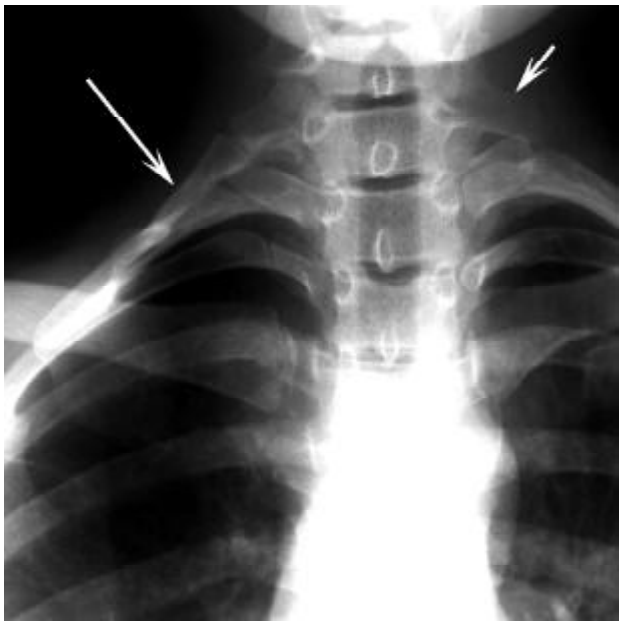

Fig. 7A

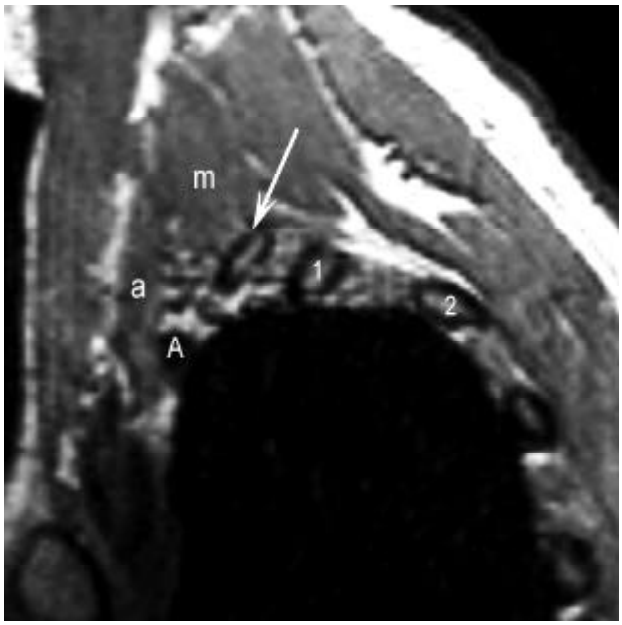

Fig. 7B

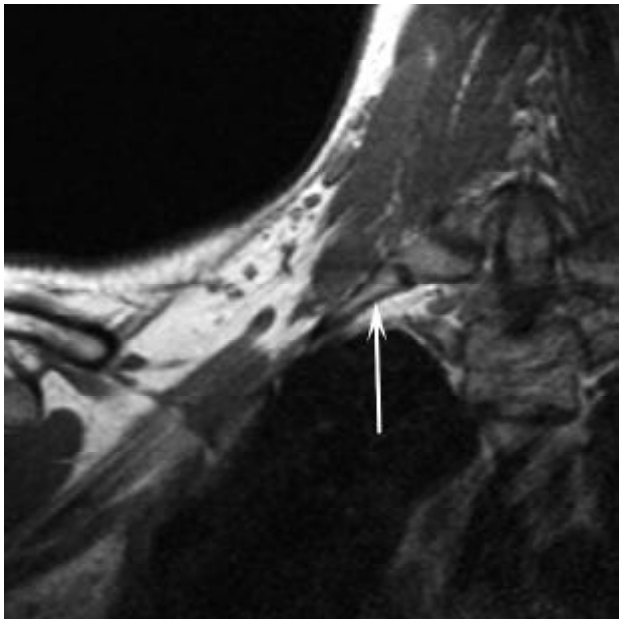

Fig. 7C

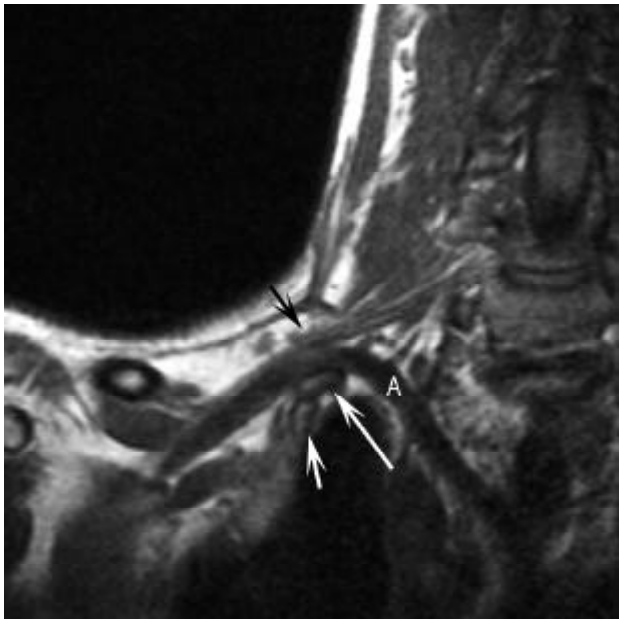

Fig. 7D

Fig. 7. Patient No. 201: asymptomatic cervical rib.

A. Conventional radiograph shows the right cervical rib (long arrow); note the elongated left transverse processes of C7 (short arrow).

B. Sagittal image from a T1-weighted 3D volume acquisition shows the insertion of the middle scalene muscle (m) upon the cervical rib (arrow). A = subclavian artery, a = anterior scalene muscle, 1 = first rib, 2 = second rib.

C. Coronal T1-weighted image shows the articulation of the cervical rib (arrow) with the transverse process of C7.

D. Coronal T1-weighted image more anteriorly than in **C** shows a slight angulation of the brachial plexus (black arrow) and subclavian artery (A) due to the cervical rib (long white arrow) which articulates with the first rib (short white arrow).

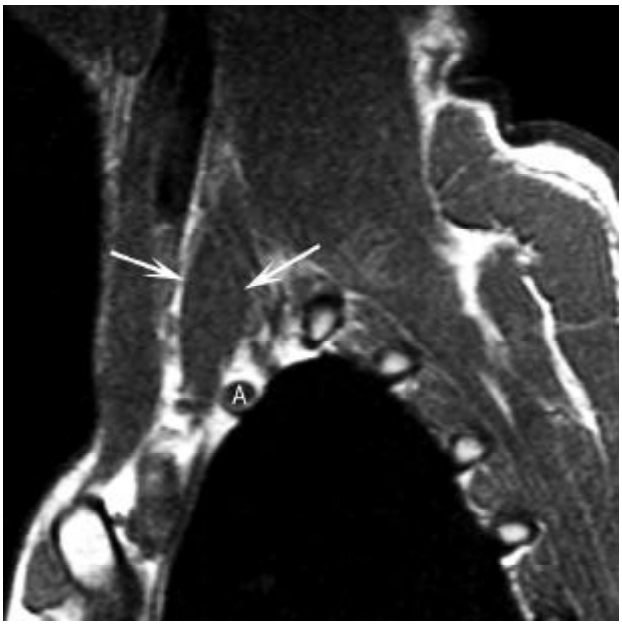

Fig. 8A

Fig. 8B

Fig. 8. Patient No. 204: in this patient a cervical rib was removed and a scalenotomy performed on both sides; the left side remained symptomatic.

A. Sagittal T1-weighted image shows a large anterior scalene muscle (arrows), despite the prior scalenotomy. A = subclavian artery.

B. Coronal T1-weighted image demonstrates the difference in size between the small right anterior scalene muscle (short arrow) after a successful anterior scalenotomy, and the enlarged left anterior scalene muscle (long arrow). After a second anterior scalenotomy and a first rib resection the symptoms of the left side disappeared.

Table 1

Trauma and abnormal MR imaging

pt no	m/f	age	presenting symptoms	MR imaging findings	diagnosis/follow-up
137	m	31	supraclavicular stab wound 4 years ago, pain arm	fibrosis adjacent to the brachial plexus	no therapy, symptoms have disappeared
138	f	39	clavicle fracture 3 years ago, 1st and cervical rib resection 1 year ago, progressive trophy intrinsic hand muscles and paresthesias hand	no brachial plexus compression	hyperabduction trauma during surgery
139	m	20	motorcycle accident 7 months ago, paralysis arm	slightly thickened brachial plexus	surgery 3 months later: avulsion of roots C6 and C7
140	m	20	motorcycle accident 5 weeks ago, paralysis arm, acute surgery 5 weeks ago showed at least avulsions of 3 roots	3D-TSE not assessable due to movement artifacts, thickened trunks, CT myelography: avulsions without meningoceles C5-C7, avulsion with meningocele C8, Th1 not assessable due to streak artifacts of the shoulders	no further surgery
141	m	73	clavicle fracture and partial clavicle resection 6 years ago, pain in neck and shoulder	callus with brachial plexus compression	pain treatment
142	m	29	motorcycle accident 3 weeks ago, paralysis arm	3D-TSE: meningocele C7-Th1, hematoma around the brachial plexus with swollen trunks	surgery 3 months later: avulsions roots C7, C8, Th1, torn upper trunk
143	m	27	coracoid process fracture 7 years ago treated with osteosynthesis which was removed 2 years ago, shoulder remains painful	no brachial plexus compression	cervicothoracic facetsyndrome C3-Th3, pain treatment
144	m	26	motorcycle accident 10 days ago, paralysis arm	3D-TSE: meningoceles C6-7, C7-Th1, thickened brachial plexus	surgery 3 months later: avulsions of C6-Th1, intraforaminal neurotmesis C5 with neuroma formation
145	f	24	clavicle fracture 3 times, last fracture 6 years ago, malunion, paresthesias arm	callus with brachial plexus compression	scheduled for lateral clavicle resection
146	m	19	motorcycle accident 5 weeks ago, clavicle fracture, paralysis arm	3D-TSE: meningoceles C5-6, C6-7, clavicle fracture with compression of brachial plexus	2 months later: spontaneous improvement, except for the triceps muscle; hypesthesia C7, C8 and Th1
147	m	34	clavicle fracture and distal clavicle resection 3 years ago, pain in shoulder and paresthesias hand, normal EMG	no brachial plexus compression	no diagnosis, physiotherapy
148	f	42	hit by car 2 months ago, paralysis arm and clavicle fracture	clavicle fracture with compression of brachial plexus, brachial plexus slightly thickened	no surgery because of spontaneous improvement of C5, C6 and C7 functions
149	m	48	clavicle fracture 2 months ago, severe paresis arm and hand muscles	clavicle fracture with compression of brachial plexus	surgery: decompression of the brachial plexus, weakness disappeared postoperatively
150	m	34	motorcycle accident 16 years ago, paralyzed arm, pain in hand	3D-TSE: meningoceles C6-7, C7- Th1, Th1-Th2, no neuroma	reflex sympathetic dystrophy
151	m	31	skiing accident 5 weeks ago, clavicle and 1st rib fracture, paresis arm	hematoma in interscalene triangle	spontaneous improvement

Table 1 *Continued.*

Trauma and abnormal MR imaging

pt no	m/f	age	presenting symptoms	MR imaging findings	diagnosis/follow-up
152	f	51	clavicle fracture followed by resection 1st rib and part clavicle 2 years ago, pain arm and hand	callus and fibrosis with brachial plexus compression	no surgery
153	m	20	bike accident 12 days ago, paralyzed arm	diffusely swollen brachial plexus	surgery 3 months later: neuromas of the trunks
154	f	39	motorcycle accident 20 years ago, paralyzed arm, pain in arm and hand	3D-TSE: meningoceles C6-7, C7- Th1, Th1-Th2, no neuroma	reflex sympathetic dystrophy
155	m	28	motorcycle accident 3 weeks ago, paralyzed arm, acute surgery: rupture brachial plexus and subclavian artery reconstruction	3D-TSE: meningoceles C5-6, C6-7, C7-Th1 and Th1-2, multiple hematomas around the brachial plexus	surgery: avulsions of all roots
156	m	49	clavicle fracture 16 months ago, paresthesias in hand, after 1st rib resection still paresthesias and pain in hand	callus with brachial plexus compression	surgery: brachial plexus decompression, post-operatively the pain has disappeared, paresthesias still present
157	m	40	old trauma, neuroma formation?	meningoceles C5-6, C6-7, C7-Th1, no neuroma	no surgery
158	m	23	clavicle fracture 2 years ago, malunion, pain in shoulder	no brachial plexus compression	pain treatment
159	m	23	motorcycle accident 10 months ago, paresis arm with partially functioning hand musculature	3D-TSE: meningoceles C5-6, C6-7, C7-Th1, old clavicle and 1st rib fracture without brachial plexus compression	no surgery
160	f	58	clavicle fracture 2 months ago, pain in shoulder, arm and hand	clavicle fracture with compression of brachial plexus	no surgery, spontaneous improvement
161	f	56	clavicle fracture 24 years ago, non-union, pain in hand	callus with brachial plexus compression	surgery: decompression brachial plexus, post-operatively the pain has disappeared
162	m	53	old clavicle fracture, thoracic pain	no brachial plexus compression	no therapy
163	f	2	battered child, paralysis proximal arm muscles	normal brachial plexus, myelum contusion	not known
164	m	37	clavicle fracture 3½ months ago, paresthesias arm	no brachial plexus compression	surgery: repositioning fractured parts clavicle, symptoms remained, 8 months later anterior and medius scalenectomy, symptoms remained, 3 months later surgery for protrusion C5-6, post-operatively asymptomatic
165	m	46	clavicle fracture 10 months ago, non-union, pain in shoulder and arm	clavicle fracture with compression of brachial plexus	surgery, postoperatively asymptomatic
166	m	62	shoulder luxation and lesser tubercle fracture, weakness arm	normal brachial plexus, fluid around humeral head	spontaneous improvement
167	m	28	car accident 2 years ago followed by osteotomy clavicle, pain in shoulder and arm	no brachial plexus compression	spontaneous improvement

Table 2

Trauma and normal MR imaging

pt no	m/f	age	presenting symptoms	3D-TSE performed	diagnosis/follow-up
168	m	29	motorcycle accident 2 months ago, paralysis arm	yes	surgery 9 months later: neurotmesis axillary, radial, musculocutaneous, median and ulnar nerves
169	m	25	motorcycle accident 4 months ago, paralysis arm	yes	spontaneous but not complete recovery
170	m	32	neck trauma 6 months ago, weakness shoulder muscles	no	entrapment suprascapular nerve
171	m	33	trauma 1 year ago, sensory deficit Th2	no	no diagnosis
172	m	29	trauma 2 weeks ago, paralysis shoulder and upper arm	yes	surgery 9 months later: neurotmesis of C5 and partially of C6
173	m	39	arthroscopy shoulder 4 months ago, weakness and paresthesias 4th and 5th finger, EMG: lesion C6, C7 and C8	no	traction lesion medial cord, spontaneous improvement
174	m	14	contusion shoulder	no	physiotherapy
175	f	22	motorcycle accident 1 year ago, paralysis arm, normal EMG	yes	psychotherapy
176	m	36	motorcycle accident 10 days ago, weakness abductors and exorotators shoulder	yes	no surgery, revalidation
177	m	68	polytrauma 5 months ago, weakness supraspinous muscle and small hand muscles	no	spontaneous improvement
178	f	85	fall on shoulder, paresis arm	no	spontaneous improvement
179	f	27	trauma 4 weeks ago, paralysis arm, EMG: possible neuropraxia	no	spontaneous improvement
180	m	73	trauma in the past, pain and paresthesias 3rd, 4th and 5th finger	no	spontaneous improvement
181	m	32	fall of rock 4 weeks ago, surgery of the skull, 5 days later paresthesias arm and hand, EMG: C5-6 lesion	no	neuropraxia, revalidation
182	m	52	car accident 4 months ago, paresthesias arm	no	whiplash
183	m	57	after fall 10 months ago weakness in shoulder and upper arm	no	cervical spinal canal stenosis
184	m	30	after trauma 1 year ago pain and weakness in shoulder and arm	no	no diagnosis, no therapy
185	m	36	motorcycle accident 2 months ago, weakness in shoulder and upper arm	no	spontaneous improvement

Table 3

Thoracic outlet syndrome and cervical ribs

pt no	m/f	age	presenting symptoms	MR imaging findings	diagnosis/follow-up
186	m	28	thoracic outlet syndrome	normal	anterior and medius scalenectomy, clinical improvement
187	m	48	pain in neck and arm	normal	thoracic outlet syndrome, no surgery
188	m	48	atrophy intrinsic hand muscles for 3 years, EMG suggests lower brachial plexus lesion	elongated transverse process of C7 on radiograph, no brachial plexus compression	not known
189	f	22	paresthesias in hand and weakness in 1st 2nd and 3rd fingers, EMG suggests C8 and Th1 lesion	elongated transverse process of C7 on radiograph, no brachial plexus compression	surgery: fibrous band with compression C8 and Th1
190	f	41	cervical rib and paresthesias in hand	cervical rib with slight angulation C8	not known
191	m	41	pain in neck and shoulder	normal	anterior and medius scalenectomy, no clinical improvement
192	f	37	thoracic outlet syndrome on both sides	elongated left transverse process of C7 on radiograph, no brachial plexus compression	anterior and medius scalenectomy on both sides and removal left transverse process of C7, left side asymptomatic, right side pain in shoulder
193	m	38	paresthesias in hand	normal	thoracic outlet syndrome, no surgery
194	f	32	costoclavicular syndrome	normal	carpal tunnel syndrome or thoracic outlet syndrome
195	f	39	pain in arm and paresthesias in hand	normal	thoracic outlet syndrome, no surgery
196	f	39	removal cervical rib and scalenotomy on both sides 2 years ago, left arm and hand remain painful	small remnant anterior scalene muscle, no brachial plexus compression	1st rib resection on the left side, pain has disappeared
197	f	47	surgery for thoracic outlet syndrome 2 years ago, surgical diagnosis was a neurofibroma, 1 year later tenotomy of pectoralis minor muscle, still paresthesias in arm and hand	elongated transverse process of C7 on radiograph, pectoralis minor and anterior scalene muscle atrophic, no brachial plexus compression	spontaneous improvement
198	f	31	thoracic outlet syndrome	normal	anterior and medius scalenectomy, clinical improvement
199	f	41	pain in shoulder and paresthesias hand	normal	anterior and medius scalenectomy, pain in shoulder remains, hand asymptomatic
200	f	39	paresthesias in arm and hand	small cervical ribs on radiograph, no brachial plexus compression	no surgery
201	f	19	asymptomatic supraclavicular palpable mass	cervical rib with slight compression subclavian artery and slight angulation brachial plexus	no therapy
202	f	32	cervical ribs on both sides, paresthesias and weakness left arm	cervical ribs, relation brachial plexus and cervical ribs not well seen due to little fat	no surgery
203	m	45	thoracic outlet syndrome	normal	anterior and medius scalenectomy, clinical improvement
204	m	38	removal cervical rib and scalenotomy on both sides (right side 3 years ago, left side 1 year ago), paresthesias unchanged on the left side	normal left anterior scalene muscle, atrophic right anterior scalene muscle	1st rib resection and anterior scalenotomy on left side, symptoms have disappeared
205	f	16	atrophy intrinsic hand muscles, EMG: C8 lesion	elongated transverse process of C7 on radiograph, angulation of C8	surgery: fibrous band with compression of C8
206	m	50	costoclavicular compression	normal	not known
207	f	48	paresthesias hand	normal	anterior and medius scalenectomy, clinical improvement, 9 months later recurrence of symptoms
208	f	41	thoracic outlet syndrome	normal	anterior and medius scalenectomy, no clinical improvement, 4 months later after transposition ulnar nerve asymptomatic

Chapter 5

Radiation-induced Brachial Plexopathy: MR Imaging

Neurological symptoms and signs of brachial plexopathy may develop in patients who have had radiation therapy to the axilla, infraclavicular and supraclavicular regions. Symptoms consist of paresthesias, hypesthesias, weakness, decreased muscle stretch reflexes and pain. The most common causes are neoplastic, due to recurrent or metastatic tumor, or radiation-induced brachial plexopathy. Radiation-induced brachial plexopathy is a well recognized clinical entity,[10,92,116,126,140,162,174,175,191,214,227,230,245] but there have been only a few reports about the MR imaging findings.[21,25,152,194,200,248] In this chapter we describe three patients with three different MR imaging appearances of radiation-induced brachial plexopathy.

Case Reports

All MR studies were performed on a 0.5 Tesla system (Gyroscan T5-II, Philips, Philips Medical Systems, Best, The Netherlands), except for the second investigation of case 1, which was done on a 1.5 Tesla system (Gyroscan ACS-NT, Philips, Philips Medical Systems, Best, The Netherlands).

Case 1 (patient No. 70, see Table 6, Chapter 3)

A 75-year-old woman presented with weakness of the left hand and paresthesias in the fingers, radiating to the upper arm. Physical examination revealed absent reflexes of the left arm, sensory loss in the C6, C7 and C8 dermatomes and atrophy of the small hand muscles, especially the thenar muscles and the first interosseus muscle. The patient had undergone a mastectomy and axillary lymph node dissection on the left side 17 years earlier for breast carcinoma, followed by radiation therapy. Nine years later the symptoms, which were slowly progressive, started. The total given dose was 4000 centiGray (cGy) in 20 fractions with a cobalt unit, delivered to the thoracic wall and regional lymph nodes. EMG confirmed an extensive brachial plexus lesion. MR imaging of the brachial plexus showed that the perineural fat was replaced by structures with a low signal intensity on both T1- and T2-weighted images (Fig. 1A and B), consistent with perineural fibrosis. Three-year clinical follow-up revealed no signs of metastatic tumor. Repeated MR imaging results (Fig. 1C) were unchanged. The normal right side was studied for comparison (Fig. 1D).

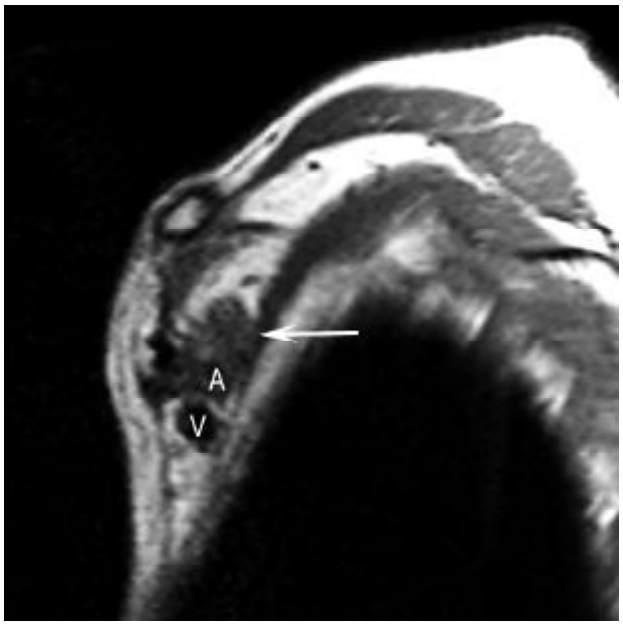

Fig. 1A

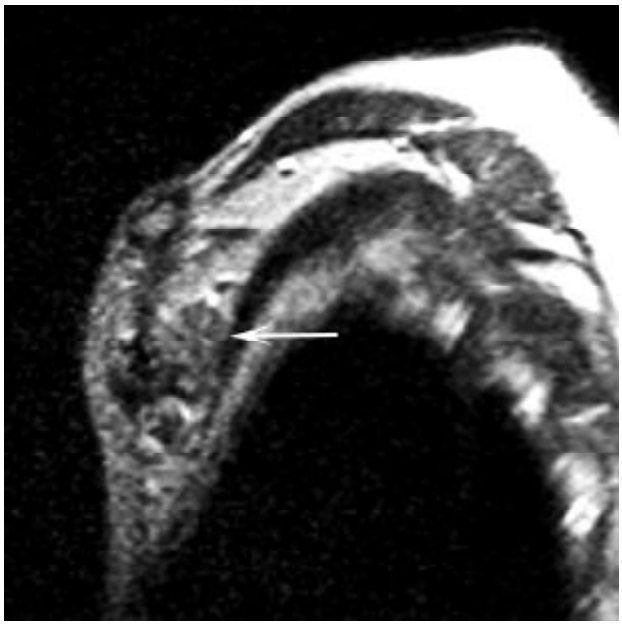

Fig. 1B

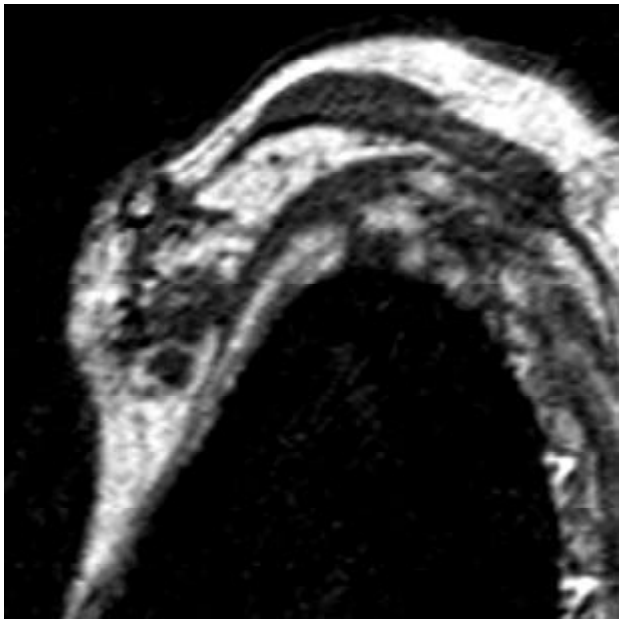

Fig. 1C

Fig. 1D

Fig. 1. Case 1.

A. Sagittal T1-weighted image shows the low signal intensity of the perineural fibrosis, which causes indistinctness of the cords of the left brachial plexus (arrow). A = axillary artery, V = axillary vein.

B. Sagittal T2-weighted image at the same level as in **A** demonstrates the low signal intensity of the perineural fibrosis (arrow).

C. Sagittal image from a 3D-TFE sequence three years later shows no change.

D. Sagittal image from a 3D-TFE sequence of the right side demonstrates the normal aspect of the cords (black arrow). Note the pectoralis muscles (white arrows), which are resected on the left side.

Case 2 (patient No. 82, see Table 6, Chapter 3)

A 45-year-old woman with a left-sided breast carcinoma underwent mastectomy and axillary lymph node dissection. Postoperative radiation therapy (total dose 4700 cGy in 20 fractions with a linear accelerator) was given to the thoracic wall and

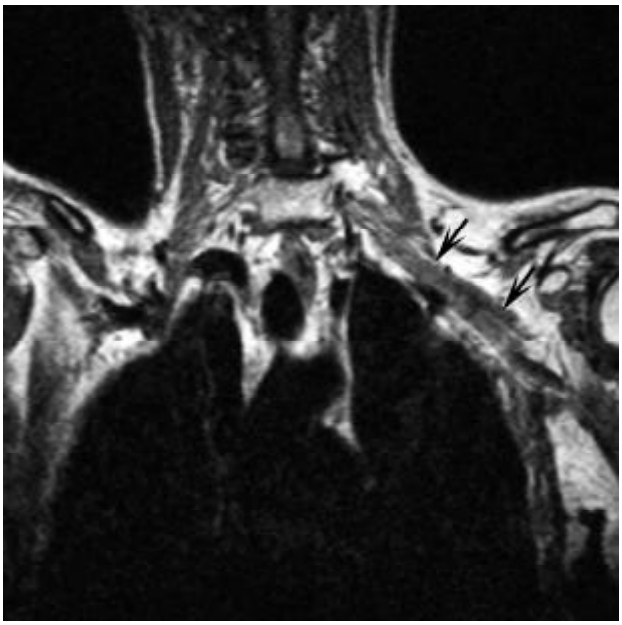

Fig. 2A

Fig. 2B

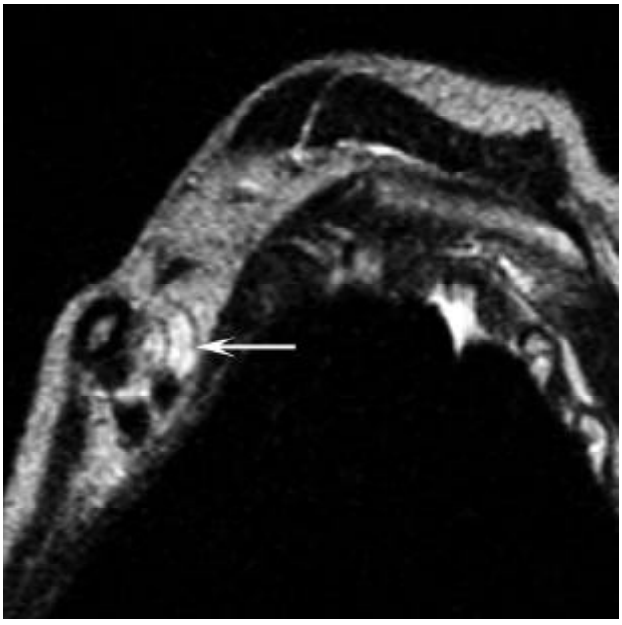

Fig. 2C

Fig. 2. Case 2.

A. Coronal T1-weighted image shows a straight course of the slightly swollen left brachial plexus (arrows).

B. For comparison the normal right brachial plexus (arrows).

C. Sagittal T2-weighted image at the level of the cords of the left brachial plexus clearly shows the increased signal intensity (arrow).

regional lymph nodes. Adjuvant chemotherapy in six cycles (cyclophosphamide, methotrexate and 5-fluorouracil) followed radiation therapy. One month after the radiation therapy the patient noticed paresthesias, with pain and weakness of the left hand. EMG located the lesion proximally in the brachial plexus. The pain and weakness were progressive. Nine months after radiation therapy MR imaging showed a slightly swollen brachial plexus with an increased signal intensity on T2-weighted images within the trunks through to the cords (Fig. 2). Seven months later the symptoms had improved, with less weakness and only a slight disturbance of the coordination of the small hand muscles. Three and a half years after surgery, there were no signs of metastatic tumor, although the left arm was still painful and a slight weakness of the hand remained.

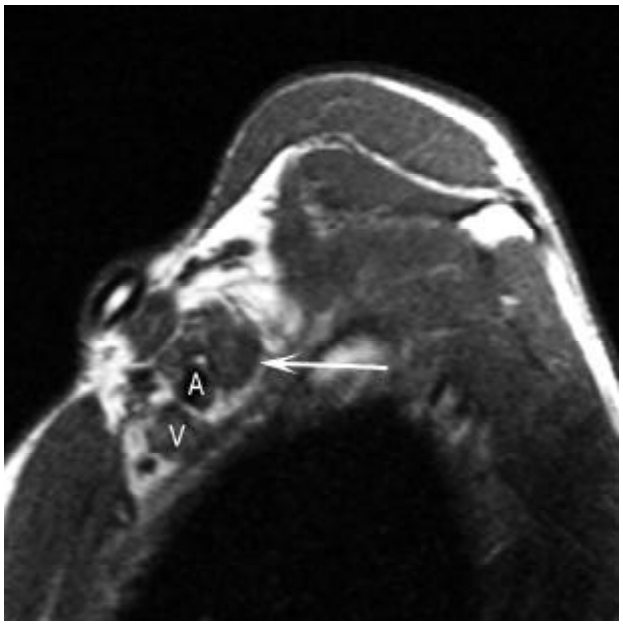

Fig. 3A

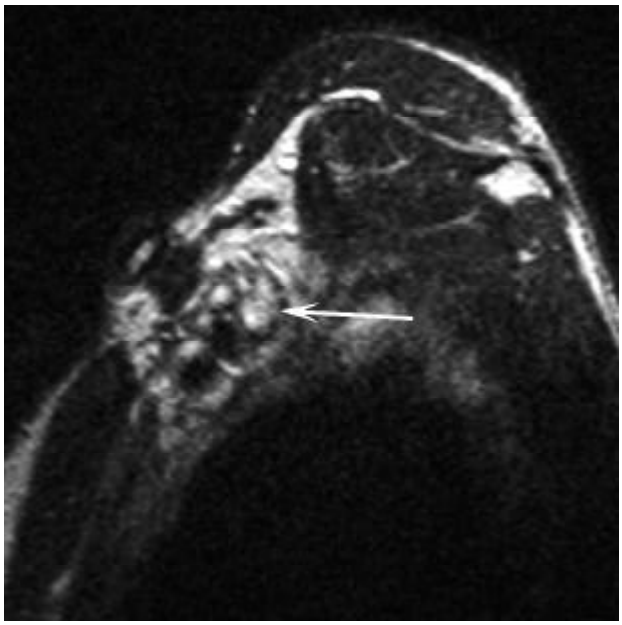

Fig. 3B

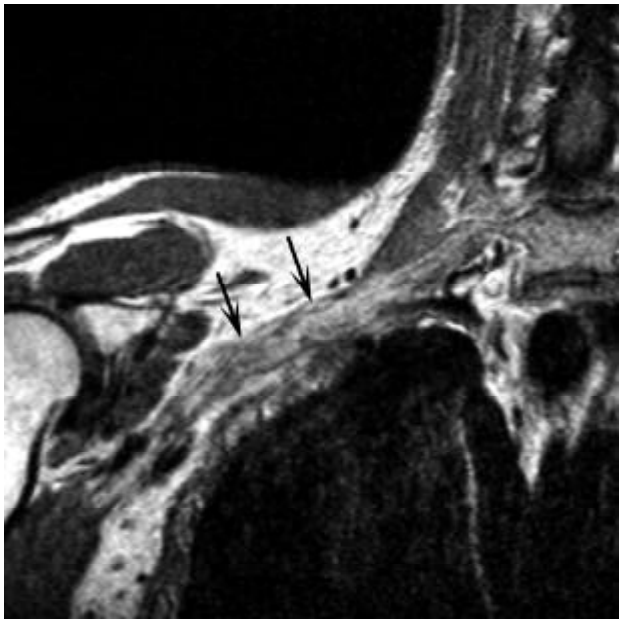

Fig. 3C

Fig. 3. Case 3.

A. Sagittal T1-weighted image shows the low signal tissue which cannot be separated from the cords of the brachial plexus (arrow). A = axillary artery, V = axillary vein. At surgery this appeared to be perineural fibrosis.

B. Sagittal T2-weighted image at the same level as in **A** shows a high signal intensity (arrow).

C. Postcontrast coronal T1-weighted image shows a diffuse enhancement of the perineural fibrosis (arrows).

Case 3 (patient No. 76, see Table 6, Chapter 3)

A 41-year-old man with Hodgkin's lymphoma was irradiated on the following four irradiation fields: (1) mediastinum, (2) neck, supraclavicular and submandibular regions on both sides, (3) right and (4) left axilla with a cobalt unit. The estimated total dose given for each area was 4000 cGy; the gap between different fields was 0.5 cm. The patient had no symptoms until 19 years later, when he presented with weakness of the right hand. At physical examination a decreased sensibility of the ulnar side of the hand and atrophy of the thenar, hypothenar and interosseus muscles was found. One year later a surgical deviation of the ulnar nerve was performed, without any relief of the complaints. MR imaging (Fig. 3), 21 years after the radiation therapy, showed indistinctness of the whole brachial plexus due to the replacement

of the perineural fat by low signal intensity tissue on T1-weighted images. A markedly increased signal intensity was seen on the T2-weighted images, and after administration of gadolinium-DTPA diffuse enhancement was noted. To establish the diagnosis and to rule out recurrence of Hodgkin's disease surgical exploration and biopsy were performed. At surgery extensive fibrosis was seen around the brachial plexus; the biopsy revealed sclerotic scar tissue around the brachial plexus and thick-walled vessels without signs of malignancy. The symptoms have changed little up to now, two years after surgery.

Discussion

Because of its location, radiation-induced damage to the brachial plexus can occur in patients who have had radiation therapy for neoplasms of the mediastinum, breast, lung or lymph nodes. This was recognized in 1966 by Stoll,[230] who found delayed damage to the brachial plexus in patients treated with radiation therapy after surgery for breast carcinoma. Besides this progressive radiation-induced brachial plexopathy, reversible brachial plexopathy has also been reported.[191,214] Salner[214] reported eight of 565 patients with paresthesias, less commonly with weakness and pain at a median time of four and a half months after radiation therapy. Complete resolution of all complaints was found in five patients, in three patients mild paresthesias persisted. A relationship to chemotherapy has been noted by several authors,[174,175,191,214] however the etiology is not known.

The main problem in diagnosing radiation-induced brachial plexopathy is its differentiation from neoplastic brachial plexopathy. Clinical signs and symptoms may be useful. Kori[116] studied 100 patients and found useful clinical criteria. Horner's syndrome, lower brachial plexus (C7, C8, Th1) involvement, early and severe pain, hand weakness, a radiation dose less than 6000 cGy and a latency period more than a year are suggestive of tumor infiltration. On the other hand, upper brachial plexus (C5, C6) involvement, doses more than 6000 cGy, a latency period of less than a year, no pain and lymphedema favor radiation-induced brachial plexopathy.

CT was the first useful radiographic study.[12,30,44,45,71,72] CT is able to show axillary masses consistent with metastatic or recurrent tumor. In patients with radiation-induced brachial plexopathy distortion of the tissue planes and increased density of the axillary fat can be present. MR imaging has several advantages above CT, the most important being the inherent contrast differences between the brachial plexus, the vessels and the surrounding fat, and the multiplanar imaging possibilities.

MR imaging has proven to be useful in diagnosing masses in or near the brachial plexus.[3,21,31,54,114,194,200,201,223,260,261] Early reports about radiation fibrosis in general suggested that radiation fibrosis can be differentiated from recurrent tumor using T2-weighted sequences. Radiation fibrosis usually has a low signal intensity, while

tumor shows a higher signal intensity on T2-weighted images.[61,85] There have been some reports about the appearance of radiation-induced brachial plexopathy on MR imaging.[21,25,152,194,200,248] Three studies reported low signal intensity tissue on T2-weighted images around the brachial plexus;[21,152,200] another author[194] reported a case with slightly hyperintense tissue on T2-weighted images. One study[248] found high signal intensity on T2-weighted images in or around the brachial plexus in patients with neoplastic brachial plexopathy as well as in patients with radiation-induced brachial plexopathy, but the presence of a mass was the most reliable sign in differentiating between the two. Another study[25] confirmed these findings in a patient who was treated for a supraglottic carcinoma.

In this paper we describe three appearances of radiation-induced brachial plexopathy on MR imaging: one case with low signal intensity fibrosis, another case with high signal intensity fibrosis, and a third case with more extensive high signal intensity fibrosis with gadolinium-DTPA enhancement 21 years after radiation therapy. Cases 1 and 2 were confirmed by strong clinical evidence with a follow-up of respectively three and three and a half years; case 3 was diagnosed by surgical biopsy. In case 3 the possibility exists that the dose exceeded 5000 cGy due to overlap of fields and the use of the cobalt unit; however it is remarkable that this patient was irradiated on both sides and did not have any symptoms on the left side. In cases 1 and 2 the given doses were within the normal limits. The histories of cases 1 and 3 are both consistent with radiation-induced brachial plexopathy; the progressive symptoms started nine and 19 years respectively after the radiation therapy. The history and clinical course of case 2 are consistent with the reported reversible brachial plexopathy.[214] This patient also had chemotherapy, which is said to be related to the induction of brachial plexopathy. In this case, where there was an improvement of the symptoms, the perineural fibrosis seemed to be less extensive on the MR images than in cases 1 and 3.

We conclude that radiation-induced brachial plexopathy can be of low and high signal intensity on T2-weighted sequences, and that fibrosis can enhance even 21 years after radiation therapy. High signal on T2-weighted images and contrast enhancement do not preclude the diagnosis of fibrosis.

Chapter 6

MR Imaging of the Brachial Plexus in Patients with Multifocal Motor Neuropathy

Multifocal motor neuropathy (MMN) is a disorder that clinically simulates lower motor neuron disease (LMND) as both may be characterized by progressive asymmetric weakness of the limbs and muscular atrophy without sensory symptoms.[33,117,122,167,181-183,188,189,213,256,257] However, in MMN electrodiagnostic studies reveal the multifocal motor conduction block that also occurs in chronic inflammatory demyelinating polyradiculoneuropathy (CIDP). This has led to the hypothesis that, like CIDP, MMN is an immune-mediated neuropathy. Improvement of muscle strength following treatment with cyclophosphamide or high-dose intravenous immunoglobulins (IvIg) and the presence of elevated serum anti-GM1 antibodies in many patients with MMN support this hypothesis.[33,117,122,167,181-183,188,189,213,256,257]
MR imaging is useful in examining the normal anatomy and pathology of the brachial plexus.[24,194,200,261,262] MR imaging delineates the brachial plexus due to the inherent contrast differences among the peripheral nerves, the surrounding fat, the related vessels, and the muscles; this makes it suitable for studying peripheral nerve disease of the upper extremities. As symptoms of MMN, LMND and CIDP usually involve the upper extremities, we studied whether MR imaging of the brachial plexus can distinguish MMN from LMND and whether abnormalities resemble those of CIDP. We performed MR imaging scans in patients with MMN and compared them with LMND and CIDP, as well as with normal and a variety of other abnormal controls.

Patients and methods

Patients

Included in the study were nine patients with MMN, five patients with CIDP, and eight patients with LMND. The clinical and MR imaging features of the patients with MMN and CIDP are described in Table 1. The patients with MMN and LMND had a progressive asymmetrical weakness, atrophy, areflexia or hyporeflexia in affected limbs, absence of upper motor neuron features, and no or only minor sensory loss. The patients with MMN had electrophysiologic evidence of motor nerve conduction block (see electrophysiologic studies). All nine patients with MMN

responded to treatment with IvIg as was previously published for patients Nos. 1, 6 and 8.[256,257] All patients with CIDP fulfilled the established research criteria for CIDP[1] of which the definitions for conduction block and temporal dispersion were modified.[125,256]

In the patients with MMN, 12 MR imaging scans were performed of the brachial plexus of the affected sides. The non-affected brachial plexus of patients Nos. 2 and 3 was also scanned. MR imaging scans of patients Nos. 2, 4, 5, 6, 7 and 9 were performed before IvIg treatment was started, while patients Nos. 3 and 8 were scanned after one year, and patient No. 1 after two years of IvIg maintenance treatment. In patient No. 2 the MR imaging scan was repeated after one year of IvIg maintenance treatment. In the patients with CIDP the brachial plexus of both sides was scanned, while in the patients with LMND only the clinically affected sides were scanned. Other controls were 174 patients with clinically suspected brachial plexus pathology of which MR imaging scans were performed between 1992 and 1996.[258,260-262]

Electrophysiologic studies

To detect conduction block or demyelination, the following investigations were done. Motor nerve conduction was measured, on both sides, in the median, ulnar, and deep peroneal nerves using surface electrodes. When no conduction block could be detected the musculocutaneous and tibial nerves were investigated. The compound muscle action potential (CMAP) was recorded from the abductor pollicis brevis, flexor carpi radialis, abductor digiti minimi, biceps brachii, extensor digitorum brevis and abductor hallucis brevis muscles. Stimulation sites were wrist, 5 cm below the elbow, 5 cm above the elbow, axilla, Erb's point, ankle, below the fibular head and popliteal fossa. When stimulation at Erb's point revealed abnormalities, the stimulator was set at maximal output. F waves were recorded after 20 stimuli delivered to the median, ulnar, deep peroneal and tibial nerves at the wrist or ankle. Prior to conduction studies the arms and legs were warmed in water of 37ºC for 30 minutes.[75] For each nerve segment the negative part of the CMAP on proximal stimulation was compared with that on distal stimulation in order to detect definitive conduction block (reduction in CMAP area of at least 50%, irrespective of the amplitude reduction),[203] possible conduction block (reduction in CMAP amplitude of at least 30% for arm nerves or 40% for leg nerves),[4] and increased temporal dispersion (increase in CMAP duration of at least 30%).[125] Evidence of demyelination included: (1) conduction block, (2) increased temporal dispersion, (3) reduction of motor nerve conduction velocity, or increased distal motor latency (DML), or increased minimal F wave latency according to previously described criteria for demyelination,[1] (4) absent F waves. Conduction block was only considered when the CMAP amplitude on distal stimulation exceeded 1 mV. F waves were included only if the DML and motor conduction velocity in the same nerve were not compatible with demyelination. Evidence of demyelination at

common entrapment sites did not count.
Of the nine patients with MMN, all had conduction block (definite in 15 nerve segments of eight patients; possible in 14 nerve segments of six patients). Other evidence of demyelination (i.e., increased temporal dispersion or motor conduction velocity, DML or minimal F wave latency compatible with demyelination) was found in 25 nerves of nine patients.
Of the five patients with CIDP, all had conduction block (definite in seven nerve segments of three patients; possible in 14 nerve segments of five patients). Other evidence of demyelination was found in 19 nerves of five patients.
None of the eight patients with LMND had conduction block. Other evidence of demyelination was found in three nerves of two patients.
Abnormal sensory conduction was found only in the patients with CIDP. Evidence of axonal loss (reduced CMAP amplitude on distal stimulation or abnormalities on concentric needle electromyography) was found in MMN, CIDP and LMND.

MR Imaging

The patients were scanned on a 0.5 Tesla system (Gyroscan T5-II, Philips, Philips Medical Systems, Best, The Netherlands) with the use of a body-wrap-around surface coil or on a 1.5 Tesla system (Gyroscan ACS-NT, Philips, Philips Medical Systems, Best, The Netherlands) with the body coil.
The standard protocol included sagittal T1-weighted spin echo images or a T1-weighted 3D volume acquisition, sagittal proton-density and T2-weighted spin echo images of one side from the spinal cord to the medial side of the humeral head. In the coronal plane thin T1-weighted spin echo images were performed of both sides. An additional coronal fat-suppressed T2-weighted turbo spin echo sequence (TSE STIR) was done in patients Nos. 1, 3, 6, 7, 9, 10, 11, 12, 13 and 14. Gadolinium-DTPA was administered in patients Nos. 1, 2, 5, 11 and 12, and in four patients with LMND.

Results

The MR imaging findings in the patients with MMN were abnormal in four patients (in one patient on both sides, in three patients on one side). MR imaging of patient No. 1 showed pronounced abnormalities of both brachial plexuses (Fig. 1): the right brachial plexus was diffusely swollen and there was an increased signal intensity on the T2-weighted images. No enhancement of the swollen nerves was noted after the intravenous administration of gadolinium-DTPA. The brachial plexus of the less symptomatic left side showed an increased signal intensity of the ventral rami of roots C7 and C8, the trunks, divisions and cords. In patient No. 2 the ventral rami of the roots of the left brachial plexus were slightly swollen, and an increased signal intensity on the T2-weighted images from the ventral rami of the roots through the

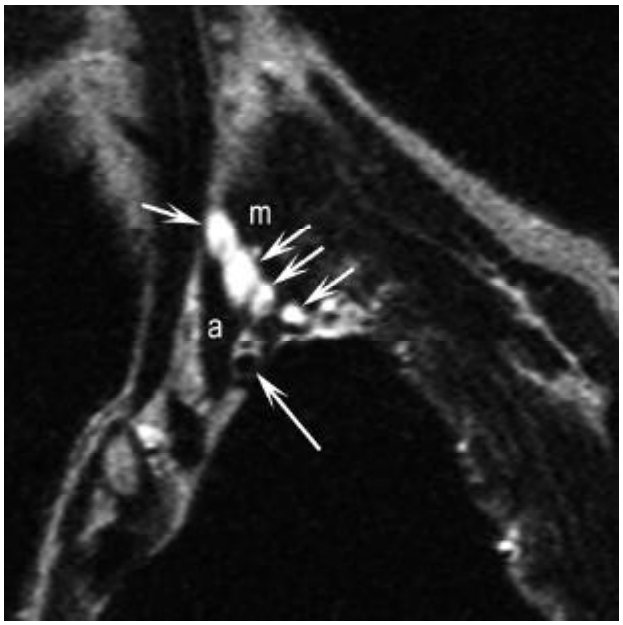

Fig. 1A

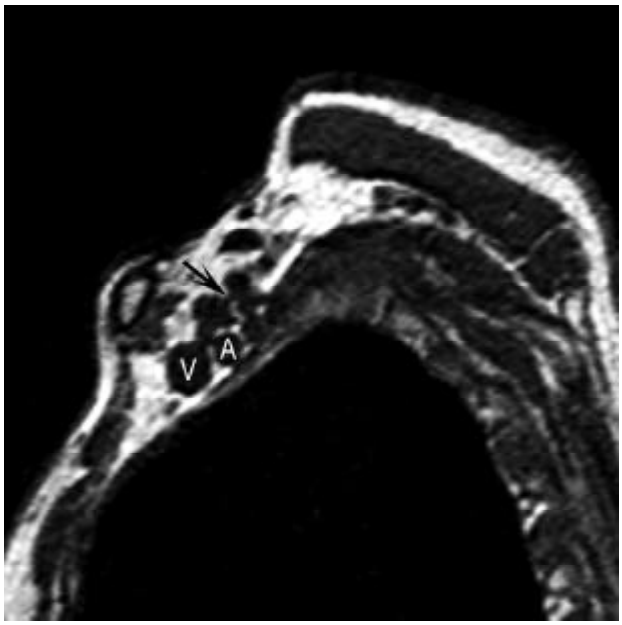

Fig. 1B

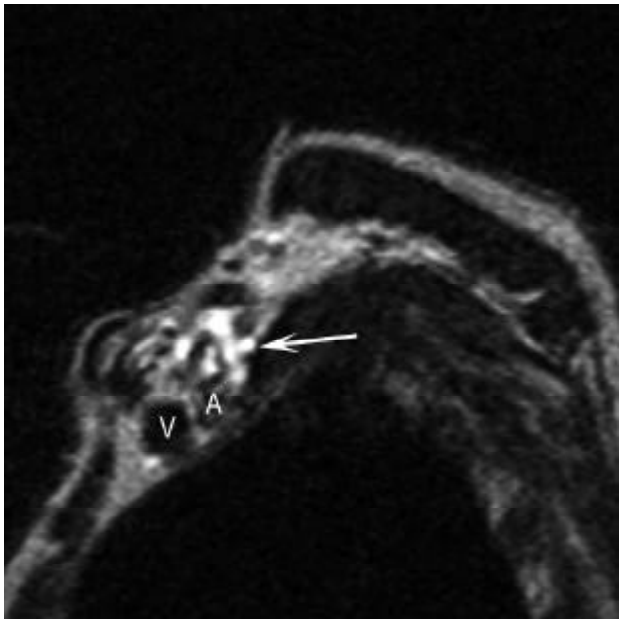

Fig. 1C

Fig. 1. Patient No. 1: MMN.

A. Sagittal T2-weighted image at the level of the right interscalene triangle. The thickened ventral rami of the roots (short arrows) with an increased signal intensity are seen between the anterior (a) and middle (m) scalene muscles. The long arrow points to the subclavian artery.

B. Sagittal T1-weighted image at the level of the divisions shows the thickened right brachial plexus (arrow). A = subclavian artery, V = subclavian vein.

C. Sagittal T2-weighted image at the same level as in **B** demonstrates the increased signal intensity in the thickened brachial plexus. A = subclavian artery, V = subclavian vein.

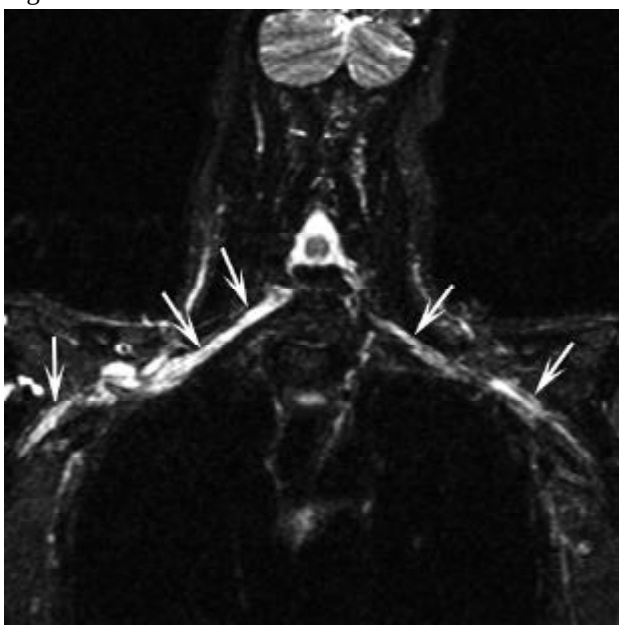

Fig. 1D

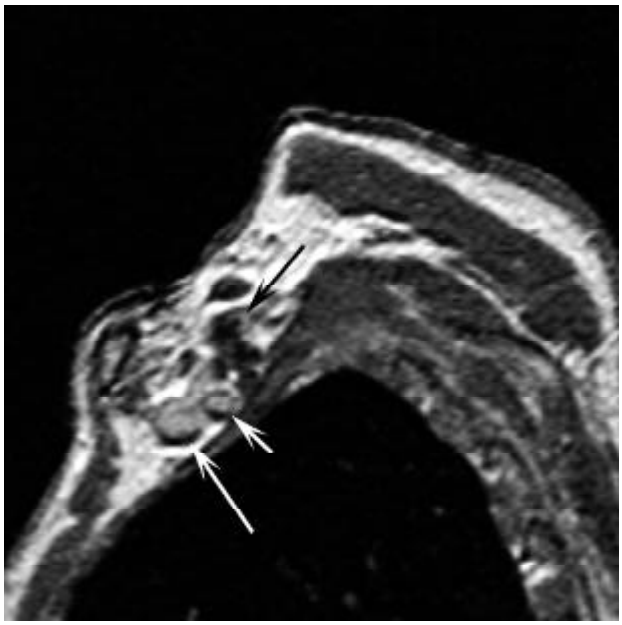

Fig. 1E

origin of the peripheral nerves in the axilla was seen (Fig. 2). There was no enhancement after the administration of gadolinium-DTPA. The right non-symptomatic brachial plexus was scanned for comparison and was unremarkable. After the patient was diagnosed as having MMN, he received IvIg maintenance therapy, which resulted in a nearly complete recovery of muscle strength. Fourteen months after onset of treatment MR imaging was repeated and, despite the beneficial effect of therapy, the MR imaging abnormalities did not show any improvement. Patient No. 3 showed an increased signal intensity on the T2-weighted images in the nerves in the right axilla (Fig. 3). The non-symptomatic left side was normal. Patient No. 4 demonstrated a focal increased signal intensity on the T2-weighted images at the level of the left interscalene triangle where the ventral rami of the roots C5 through Th1 join to form the trunks, and in the peripheral nerves in the left axilla (Fig. 4). In patients Nos. 5, 6, 7, 8 and 9 no abnormalities were detected by MR imaging. Gadolinium-DTPA was given in patient No. 5 and no enhancement was seen.

MR imaging of the patients with CIDP was abnormal in three of the five patients. Patients Nos. 10, 11 and 12 showed an increased signal intensity of both the right and left brachial plexus (Fig. 5). Gadolinium-DTPA was given in patient Nos. 11 and 12 and no enhancement was noted. In contrast with our findings in MMN, the abnormalities on both sides were similar in the CIDP patients.

None of the MR imaging scans of the patients with LMND showed any of the abnormalities found in MMN or CIDP.

In the last four years we have performed MR imaging of the brachial plexus in 174 patients with clinically suspected brachial plexus pathology. No abnormalities were seen in 82 patients. Pathology was found in 92 patients and included trauma (n=30), primary tumors of the brachial plexus (n=6), primary or metastatic tumors near the brachial plexus with or without brachial plexus involvement (n=49), radiation fibrosis (n=4), infection (n=2) and thoracic outlet syndrome (n=1). In this group we found an increased signal intensity of the brachial plexus in two patients with radiation fibrosis and in four patients after trauma.[258,260] The six patients with primary tumors showed an increased signal intensity within the brachial plexus, but this coincided with a well defined mass which enhanced after administration of gadolinium-DTPA.[260-262]

Fig. 1. *Continued.*

D. Coronal TSE STIR image shows the increased signal intensity in both the right and left brachial plexus (arrows). Note that the right brachial plexus is thicker than the left.

E. Sagittal T1-weighted image with gadolinium-DTPA at the level of the divisions shows the thickened brachial plexus (black arrow) which does not enhance (compare to **B**). Note the enhancing subclavian artery (short white arrow) and subclavian vein (long white arrow).

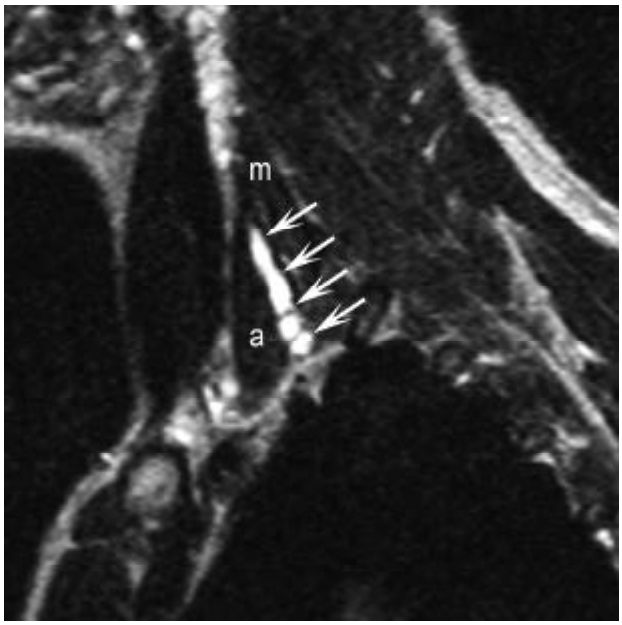

Fig. 2A

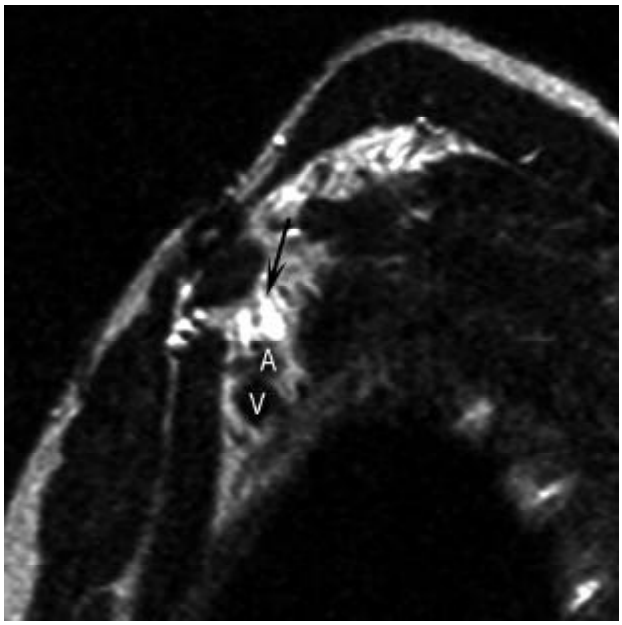

Fig. 2B

Fig. 2C

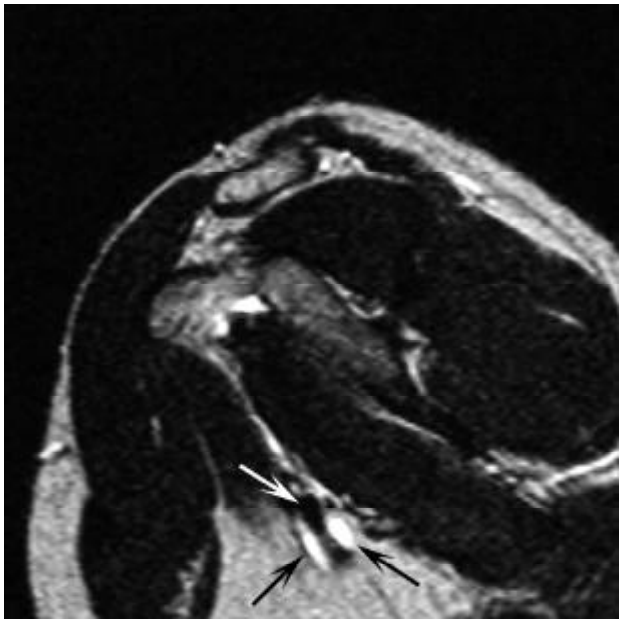

Fig. 2D

Fig. 2. Patient No. 2: MMN.

A. Sagittal T2-weighted image at the level of the left interscalene triangle. The swollen ventral rami of the roots (arrows) with an increased signal intensity are seen between the anterior (a) and middle (m) scalene muscles.

B. Sagittal T2-weighted image shows the increased signal intensity in the cords (arrow) of the left brachial plexus. A = axillary artery, V = axillary vein.

C. Sagittal T2-weighted image of the normal right brachial plexus at the same level as **B** demonstrates the low signal intensity of the cords (arrow).

D. Sagittal T2-weighted image at the level of the left axilla shows the increased signal intensity of the proximal peripheral nerves (black arrows) surrounding the axillary artery (white arrow).

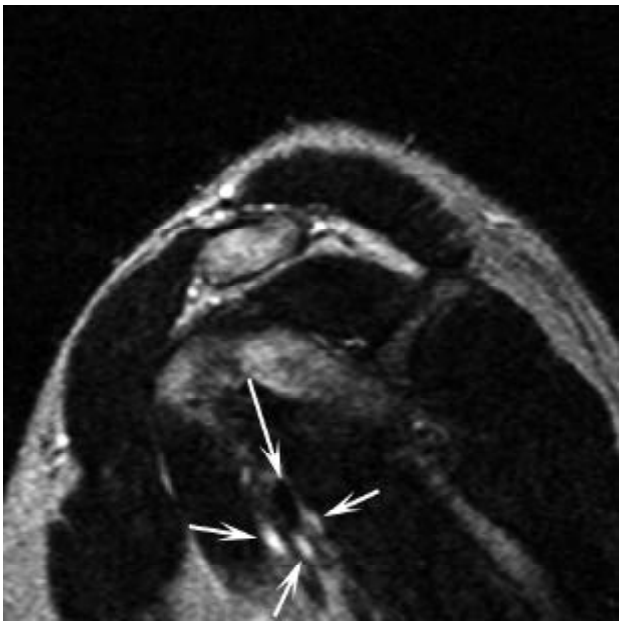

Fig. 3

Fig. 3. Patient No. 3: MMN.
Sagittal T2-weighted image of the right axilla shows the increased signal intensity of the proximal peripheral nerves (short arrows), which was the only abnormality found in this patient. Long arrow points to the axillary artery.

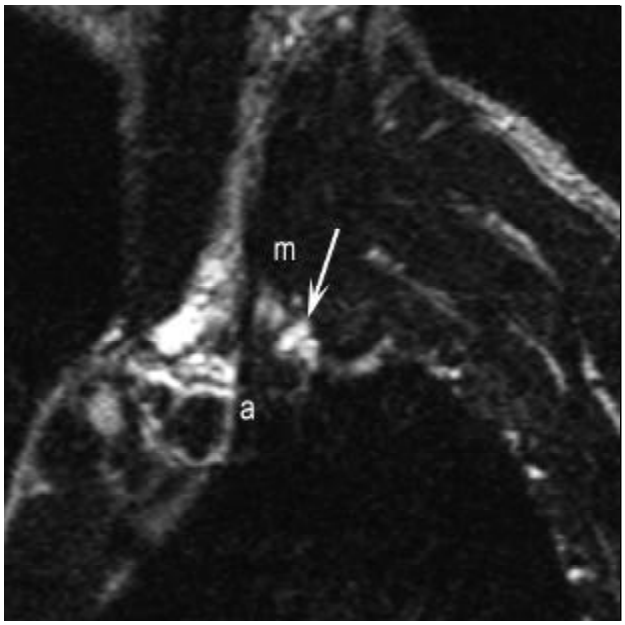

Fig. 4

Fig. 4. Patient No. 4: MMN.
Sagittal T2-weighted image of the left interscalene triangle shows the increased signal intensity of the ventral rami of the roots (arrow), a = anterior scalene muscle, m = middle scalene muscle.

Fig. 5. Patient No. 10: CIDP.

A. Sagittal T2-weighted image of the right interscalene triangle shows an increased signal intensity of the ventral rami of the roots (arrows).

B. Coronal TSE STIR image shows the increased signal intensity of the brachial plexus of both sides (arrows).

Fig. 5A

Fig. 5B

Discussion

In the present study we found abnormalities of the brachial plexus in patients with MMN and CIDP by MR imaging. The abnormalities included increased signal intensities of the affected nerves on the T2-weighted images that can be associated with a diffuse nerve swelling. In contrast, MR imaging scans of the clinically non-affected brachial plexus of patients with MMN and of the brachial plexus of patients with LMND were normal. The abnormalities in patients with MMN were similar to those in CIDP. The distribution of the MR imaging abnormalities corresponded with the distribution of symptoms of the patients: asymmetrical in MMN and symmetrical in CIDP.

In MMN and CIDP more than only the brachial plexus is affected, but the brachial plexus is the portion of the peripheral nervous system that can be easily studied with MR imaging, as the brachial plexus can be easily delineated from the surrounding fat, vessels and muscles. The peripheral nerves have the same signal intensity as muscle, which is low to intermediate on both T1- and T2-weighted images.[24,194] As we and other authors have demonstrated, the brachial plexus can have a pathologically increased signal intensity on T2-weighted images in cases of tumor,[194,200,260-262] trauma[114,200,260] or after radiation therapy.[248,258] MR imaging of tumor involvement of the brachial plexus usually demonstrates a more focal increased signal intensity and contrast enhancement. The MR imaging features of brachial plexopathy after radiation therapy, and after trauma, can resemble the abnormalities found with MMN.

The pathological substrate of the swelling of nerves and the increased signal intensity demonstrated by MR imaging of the brachial plexus in our patients with MMN and CIDP is not known. The cause of the MR imaging lesions cannot only be a result of axonal degeneration, as we have not found abnormalities in patients with LMND. The increased signal intensity on T2-weighted images may be due to demyelination, while inflammation and edema might lead to swelling in nerves. In CIDP, neurophysiologic and pathologic studies provide substantial evidence for inflammatory demyelination of peripheral nerves.[1,60]

In MMN, the pathological substrate is less clear than in CIDP, but several studies indicate demyelination of motor nerves. Neuropathologic findings at autopsy in one patient with MMN showed inflammatory demyelination in the motor cranial nerves and motor roots of peripheral nerves.[171] Kaji et al.[108] performed a biopsy a few millimeters distally of a nerve enlargement of the brachial plexus that revealed demyelination, although the pathology of the enlargement itself remained unknown. In another patient with palpable nerves in the supraclavicular region and proximal conduction block, a biopsy from the brachial plexus revealed onion bulb type hypertrophic changes associated with inflammatory cell infiltrates.[26] Another

indication for demyelination in MMN is a study showing mild demyelinating features in sural nerve biopsies of patients with MMN, suggesting that the demyelinating pathophysiology also affects sensory fibers, but to a lesser degree than motor fibers.[47] MR imaging of sciatic nerves of rabbits with experimental demyelination shows an increased signal intensity on T2-weighted images, without signal changes on T1-weighted images.[244] Moreover, MR imaging of the sciatic nerve in a patient with Déjérine-Sottas disease also showed a high signal intensity on T2-weighted images, thought to be due to demyelination and onion bulb formation.[242]

Two case reports by Kaji et al.[108] and Parry[181] described MR imaging of nerves in patients with MMN. Kaji et al.[108] reported MR imaging findings in two patients with MMN. They found a focal enlargement of the median nerve at the site of conduction block with enhancement after the administration of gadolinium-DTPA in one patient. In another patient, a MR imaging scan showed a mass lesion of the brachial plexus. Parry[181] described a high signal intensity on the T2-weighted images and gadolinium-DTPA enhancement of an enlarged upper trunk of the brachial plexus in a patient with MMN. Six reports have described contrast enhancement of swollen lumbosacral roots in patients with CIDP.[20,32,48,53,84,153] One report mentioned that the contrast enhancement disappeared during clinical improvement and reappeared during a relapse.[20] In addition to these studies, we report the MR imaging scans of the brachial plexus in a larger group of nine patients with MMN, of five patients with CIDP, as well as of eight patients with LMND and other controls.

It is important to differentiate MMN from LMND because MMN is a potentially treatable disease. As we found no abnormalities with MR imaging in patients with LMND, MR imaging of the brachial plexus may be useful to distinguish MMN from LMND. In this study we demonstrate that MMN can involve the brachial plexus and that this can be demonstrated with MR imaging, which is important to recognize, regardless of the pathological substrate of the swelling of the nerves and the increased signal intensity.

Table 1

The clinical and MR imaging features of the patients with MMN and CIDP

pt no	m/f	age	duration	distribution weakness	MR imaging
MMN					
1.	m	55	9 y	RA>LA; D>P asymmetric	right brachial plexus diffusely swollen with increased signal intensity, left brachial plexus slightly swollen with increased signal intensity
2.	m	35	3 y	LA; D>P asymmetric	left brachial plexus slightly swollen with increased signal intensity
3.	m	50	7 y	RA,RL; D>P asymmetric	increased signal intensity in the nerves in the right axilla
4.	m	26	4 y	LA,LL,RL; D>P asymmetric	increased signal intensity in the left interscalene triangle and in the nerves in the axilla
5.	m	50	2 y	RA; D>P asymmetric	normal
6.	m	41	11 y	RA,LA,RL,LL; D>P asymmetric	normal
7.	m	34	5 y	RA,LA,LL; D>P asymmetric	normal
8.	f	34	4 y	RA,LL; D>P asymmetric	normal
9.	m	60	2 y	RA,LA,LL; D>P asymmetric	normal
CIDP					
10.	m	26	5 m	RA,LA,RL,LL; D=P symmetric	increased signal intensity of both the right and left brachial plexus
11.	m	48	8 m	RA,LA,RL,LL; P>D symmetric	increased signal intensity of both the right and left brachial plexus
12.	m	66	5 m	RA, LA, RL, LL; D=P symmetric	increased signal intensity of both the right and left brachial plexus
13.	m	22	6 m	RA,LA,RL,LL; D=P symmetric	normal
14.	f	61	8 m	RA,LA,RL,LL; D>P symmetric	normal

pt no = patient number; m = male; f = female; y = years, m = months, LA = left arm; RA = right arm; LL = left leg; RL = right leg; D = distal; P = proximal

Chapter 7
Summary and Conclusions

In this retrospective study we describe the MR imaging findings in 230 consecutive patients with suspected pathology in or near the brachial plexus. These patients were studied from 1991 through to 1996.

Chapter 2 describes the anatomy and the MR imaging techniques. As the anatomy of the brachial plexus and the related structures is quite complicated, we eventually use as protocol of choice a 3D volume acquisition for the best understanding of this complex anatomy. The advantages of this 3D volume acquisition are, besides the use of thin overlapping slices, the MPR and cine-display viewing mode possibilities. The use of thin slices (2 mm) provides excellent anatomical detail. The following anatomic details can be discerned: the individual ventral rami of the nerve roots, the three trunks, the three cords and the stellate ganglion. The overlapped images can be reconstructed in any plane with the same image quality, and the use of the cine-display viewing mode affords a better insight into the continuity of the nerves and vessels. In our experience, the use of a 3D volume acquisition markedly improves the understanding of the normal anatomy of the brachial plexus on MR imaging and can possibly better delineate the pathology involving the brachial plexus.

Chapter 3 mainly deals with the tumors we have found in or near the brachial plexus. In this chapter we also describe a group of patients alleged to have a tumor, but where no tumor was found.
The first group consists of 66 patients where a tumor in or near the brachial plexus was found with MR imaging. We found 10 neurogenic tumors (five schwannomas, one neurofibroma, two malignant schwannomas and two without a histological diagnosis). These tumors show characteristic MR imaging findings: a low signal intensity on the T1-weighted images, an increased signal intensity on the proton-density images, a high signal intensity on the T2-weighted images, enhancement after administration of gadolinium-DTPA, a fusiform growth, a sharply defined edge, and the involved nerve can often be found entering and leaving the tumor. These specific imaging characteristics applied to nine of these 10 tumors. Besides these 10

neurogenic tumors, we describe 56 non-neurogenic tumors: lung tumor (n=24), metastasis of breast carcinoma (n=9), metastasis of other tumors (n=8), B-cell non-Hodgkin's lymphoma (n=2), leiomyosarcoma (n=1), liposarcoma (n=1), chondrosarcoma (n=2), synoviosarcoma (n=1), aggressive fibromatosis (n=2), meningocele (n=1), lipoma (n=3), a hematoma in a neck cyst (n=1), and one tumor of unknown origin. In the preoperative evaluation of tumors near the brachial plexus, the 3D volume acquisition provides the radiologists and the surgeons with better insight into the precise extension of the tumor. MR imaging could delineate the extension of these tumors well, and determine whether or not there was brachial plexus involvement.
The second group consists of 70 patients where no tumor was detected with MR imaging. Three patients had an infection, 17 patients were imaged after radiation therapy and had no signs of tumor recurrence, and 50 patients had normal MR imaging findings.

Chapter 4 discusses the value of MR imaging in patients with brachial plexopathy after trauma and in patients with thoracic outlet syndromes.
We found 31 abnormal MR imaging investigations in patients with a history of trauma. Ten of these patients presented with a flail arm after a severe accident, in most cases a motorcycle accident. In five of these patients an additional 3D-TSE sequence of the C-spine was done in order to visualize traumatic nerve root avulsions and traumatic meningoceles. Abnormalities we found in this group were thickening of the brachial plexus, hematoma, and a clavicle fracture with compression of the brachial plexus. We were not able to visualize a rupture of the brachial plexus, nor visualize all the nerve root avulsions. Abnormalities we found in the remaining 21 patients included clavicle fractures with suspected brachial plexus compression (n=14), traumatic meningoceles in patients with known nerve root avulsions to exclude neuroma formation (n=3), a stab wound (n=1), a coracoid process fracture (n=1), a battered child (n=1) and a shoulder luxation (n=1).
In 18 patients with a history of trauma MR imaging was normal. Two of these patients were operated upon and appeared to have a rupture of a part of the brachial plexus. We conclude that MR imaging is not very good at predicting the surgical findings in cases of brachial plexus rupture or nerve root avulsions. MR imaging can be helpful in demonstrating brachial plexus compression by a hematoma or a clavicle fracture with callus formation.
In this chapter we also describe a group of 23 patients with a wide variety of symptoms, which could be due to a thoracic outlet syndrome. In three patients a cervical rib was present, two patients had had a cervical rib removal previously. In one patient, who had the typical true neurogenic thoracic outlet syndrome, a slight angulation of the ventral ramus of root C8 was seen, which appeared to be due to a fibrous band at surgery. Most patients did not show any abnormalities with MR imaging. We were

not able to demonstrate a fibrous band with MR imaging. We conclude that MR imaging in patients with a thoracic outlet syndrome is not very useful, except for serving to exclude other structural abnormalities.

Chapter 5 describes the MR imaging appearance of radiation-induced brachial plexopathy. MR imaging was performed in two patients with the clinical diagnosis of radiation-induced brachial plexopathy and in one with surgically proven radiation fibrosis of the brachial plexus. Three patients who had had radiation therapy to the axilla and supraclavicular region (two with breast carcinoma and one with Hodgkin's lymphoma) presented with symptoms of the arm and hand. To exclude metastases or tumor recurrence MR imaging was performed. In one patient, fibrosis showing low signal intensity was found, while in two patients high signal intensity fibrosis surrounding the brachial plexus was found on the T2-weighted images. In one case gadolinium-DTPA enhancement of the fibrosis 21 years after radiation therapy was seen. We conclude that radiation-induced brachial plexopathy can have different MR imaging appearances. We found that radiation fibrosis can have both low and high signal intensities on T2-weighted images, and that fibrosis can enhance even decades after radiation therapy.

In *Chapter 6* we studied whether MR imaging of the brachial plexus is useful to distinguish multifocal motor neuropathy (MMN) from lower motor neuron disease (LMND) and whether abnormalities resemble those of chronic inflammatory demyelinating polyradiculoneuropathy (CIDP). MMN is a potentially treatable pure motor neuropathy which clinically resembles LMND. Both diseases are characterized by progressive asymmetric weakness of the limbs and muscular atrophy without sensory symptoms. CIDP is a symmetric polyneuropathy which affects both motor and sensory fibers. Both CIDP and MMN are probably immune-mediated neuropathies, as autoantibodies to peripheral nerve myelin have been found.
We compared MR imaging scans of the brachial plexus from nine patients with MMN with scans from five patients with CIDP, eight patients with LMND, and 174 controls. In two patients with MMN, and in three patients with CIDP, the MR imaging scans showed an increased signal intensity on the T2-weighted images of the brachial plexus. Two other patients with MMN demonstrated a more focal increased signal intensity on the T2-weighted images, in one patient only in the axilla, and in one patient in the axilla and in the ventral rami of the roots. MR imaging of the brachial plexus of eight patients with LMND was normal. The distribution of the MR imaging abnormalities corresponded with the distribution of symptoms of the patients: asymmetrical in MMN and symmetrical in CIDP. These findings demonstrate that MR imaging abnormalities of the brachial plexus in patients with MMN resemble those seen in CIDP and may be useful to distinguish MMN from LMND.

SAMENVATTING EN CONCLUSIES

Dit retrospectief onderzoek beschrijft de MRI bevindingen bij 230 patiënten die onderzocht werden vanwege verdenking op pathologie van of in de omgeving van de plexus brachialis. Deze patiënten werden onderzocht in de periode van 1991 tot en met 1996.

Hoofdstuk 2 beschrijft de anatomie van de plexus brachialis en de MRI technieken die gebruikt zijn gedurende dit onderzoek. Aangezien de anatomie van de plexus brachialis en de omliggende structuren complex is, gebruiken wij routinematig een 3D volume acquisitie om de anatomie beter te kunnen afbeelden. De voordelen van deze 3D volume acquisitie zijn: de mogelijkheden om in elke gewenste richting reconstructies te vervaardigen, het kunnen bekijken van het volume als een film en het gebruik van dunne overlappende coupes. Het gebruik van dunne coupes (2 mm) zorgt ervoor dat gedetailleerde anatomische details zichtbaar worden. De overlappende coupes kunnen worden gereconstrueerd in elk vlak met behoud van beeldkwaliteit. Het bekijken van de 3D volume acquisitie als een film verschaft een beter inzicht in de continuïteit van de zenuwen en vaten. Met name bij de pre-operatieve evaluatie van tumoren in de nabijheid van de plexus brachialis kan een 3D volume acquisitie de chirurg en radioloog helpen om de juiste uitbreiding van de tumor te bepalen. In onze ervaring vergroot het gebruik van een 3D volume acquisitie het begrip van de normale anatomie van de plexus brachialis en kan de uitbreiding van de pathologie beter in beeld gebracht worden.

Hoofdstuk 3 behandelt tumoren die wij hebben gevonden van of in de omgeving van de plexus brachialis. In dit hoofdstuk wordt naast de groep patiënten met tumoren tevens een tweede groep patiënten beschreven waarbij geen tumoren gevonden zijn.
De eerste groep bestaat uit 66 patiënten, waarbij met IM een tumor in of in de omgeving van de plexus brachialis gevonden is. Wij hebben 10 neurogene tumoren gevonden (vijf schwannomen, één neuroflbroom, twee maligne schwannomen en twee tumoren zonder histologische diagnose). Deze tumoren hebben karakteristieke MRI eigenschappen: een lage signaal intensiteit op de TI -gewogen opnames, een verhoogde signaal intensiteit op de protondensity opnames, een hoge signaal intensiteit op de T2-gewogen opnames, aankleuring na toediening van gadolinium-DTPA, de tumor is scherp afgrensbaar met een fusiforme groei en vaak kan de relatie tussen de betrokken zenuw en de tumor worden gezien. Deze specifieke eigenschappen vonden wij bij negen van de 10 tumoren. Naast deze 10 neurogene tumoren beschrijven wij 56 tumoren van niet neurogene origine: long tumor (n=24), metastase vanmammacarcinoom (n=9), metastase van andere tumoren (n=8), B-cel non-Hodgkin's lymfoom (n=2), leiomyosarcoom (n=1), liposarcoom (n=l), chondrosarcoom (n=2), synoviosarcoom (n=l), agressieve fibromatosis (n7=2), meningocele (n=l), lipoom (n=3), een hematoom in een halscyste (n=l) en één tumor van onbekende origine. MRI kon de uitbreiding van deze tumoren goed visualiseren en bepalen of de plexus brachialis wel of niet bij het proces betrokken was.

De tweede groep bestaat uit 70 patiënten bij wie met MRI geen tumoren gevonden zijn. Drie patiënten hadden een infectie, 17 patiënten zijn onderzocht na bestraling en hadden geen tekenen van rest of recidief tumor en 50 patiënten hadden een normale MRI.

Hoofdstuk 4 bespreekt de waarde van MRI bij patiënten na een trauma en bij patiënten met een thoracic outlet syndroom.

Wij vonden 31 abnormale MRI onderzoeken bij patiënten met in de voorgeschiedenis een trauma. Tien van deze patiënten presenteerden zich met een paralytische arm na een ernstig ongeval, in de meeste gevallen was er sprake van een motorfiets ongeval. Bij vijf van deze patiënten is er een aanvullende 3D-TSE sequentie van de cervicale wervelkolom gemaakt om traumatische wortel avulsies en traumatische meningoceles af te beelden. Afwijkingen die we in deze groep zijn tegengekomen zijn een verdikking van de plexus brachialis, een hematoom en een clavicula fractuur met compressie van de plexus brachialis. Een ruptuur van de plexus brachialis kon niet gevisualiseerd worden, noch konden alle wortel avulsies afgebeeld worden. De afwijkingen die wij vonden in de resterende 21 patiënten bestonden uit clavicula fracturen met verdenking op plexus brachialis compressie (n= 14), traumatische meningoceles bij patiënten met bekende traumatische wortel avulsies die onderzocht werden om neuroom vorming uit te sluiten (n=3), een steekwond (n=l), een processus coracoideus fractuur (n=l), afwijkingen bij een patiënt met kindermishandeling (n=l) en een schouderluxatie (n=1).
Bij 18 patiënten met trauma in de voorgeschiedenis was de MRI normaal. Twee van deze patiënten zijn geopereerd en bleken een ruptuur van de plexus brachialis te hebben. Wij concluderen dat MRI de bevindingen bij operatie niet goed kan voorspellen in gevallen met een plexus brachialis ruptuur of bij wortel avulsies. MRI heeft wel waarde bij het aantonen van plexus brachialis compressie door een hematoom of een clavicula fractuur.

In dit hoofdstuk wordt tevens een groep van 23 patiënten met een breed scala aan symptomen beschreven, die kunnen passen bij een thoracic outlet syndroom. Bij drie patiënten was er een halsrib aanwezig, twee patiënten werden onderzocht nadat er een halsrib verwijderd was. Bij één patiënt, die klachten had passend bij een zogenaamd "true neurogenic thoracic outlet syndrome", werd er een lichte uitbochting gezien van wortel C8, die bij operatie bleek te worden veroorzaakt door een flbreuze band. De meeste patiënten hadden geen afwijkingen met MRI. In onze ervaring kon een fibreuze band niet worden afgebeeld met MRI. Wij concluderen dat MRI bij patiënten met een thoracic outlet syndroom niet erg zinvol is, behalve ter uitsluiting van andere afwijkingen.

Hoofdstuk 5 beschrijft de MRI afwijkingen die gevonden werden bij drie patiënten met bestralingsfibrose van de plexus brachialis. MRI werd uitgevoerd bij twee patiënten met de klinische diagnose bestralingsfibrose van de plexus brachialis en bij één patiënt waarbij de diagnose bevestigd werd met operatie. De drie patiënten presenteerden zich met klachten van de arm en hand na bestraling ter plaatse van de axilla en supraclaviculair (bij twee patiënten met mammacarcinoorn en bij één patiënt met Hodgkin's lymfoom). Om metastasen of tumor uit te sluiten werd er een MRI gedaan. Bij één patiënt toonde de fibrose een lage signaal intensiteit, bij de twee andere patiënten werd er een verhoogde signaal intensiteit gezien op de T2-gewogen opnames. Bij één patiënt was er gadolinium-DTPA gegeven en werd er aankleuring van de flbrose gezien, 21 jaar na de bestraling. Wij concluderen dat het XM beeld van bestralingsfibrose van de plexus brachialis verschillende verschijningsvormen kan hebben. Bestralingsfibrose kan zowel een lage als hoge signaal intensiteit hebben op T2-gewogen opnames en fibrose kan aankleuren, zelfs 21 jaar na bestraling.

In *Hoofdstuk 6* wordt beschreven of MRI van de plexus brachialis zinvol is om multifocale motore neuropathie (MMN) van progressieve spinale spieratrofie (PSS)

te onderscheiden en of de gevonden afwijkingen lijken op die bij chronische inflammatoire demyeliniserende polyradiculoneuropathie (CIDP). MMN is een behandelbare zuivere motore neuropathie die klinisch lijkt op PSS. Beide ziekten worden gekarakteriseerd door een progressieve asymmetrische zwakte van de ledematen en spieratrofie zonder sensibele stoornissen. CIDP is een symmetrische polyneuropathie die zowel de motore als sensibele zenuwvezels aantast. Zowel CIDP als MMN zijn mogelijk het gevolg van een auto-immuun proces, aangezien auto antilichamen tegen myeline van perifere zenuwen gevonden zijn.
Wij hebben de MRI onderzoeken van de plexus brachialis van negen patiënten met NIMN vergeleken met die van vijf patiënten met CIDP, acht patiënten met PSS en 174 andere controle patiënten. Bij twee patiënten met MMN en bij drie patiënten met CIDP toonden de MRI onderzoeken een verhoogde signaal intensiteit van de plexus brachialis op de T2-gewogen opnames. Twee andere patiënten met MMN hadden alleen een focaal verhoogde signaal intensiteit van de plexus brachialis, bij één patiënt in de axilla en bij de andere in de axilla en bij de wortels. NM van de plexus brachialis bij acht patiënten met PSS was normaal. De verdeling van de gevonden afwijkingen kwam overeen met de distributie van symptomen bij de patiënten met MMN en CIDP: asymmetrisch bij MMN en symmetrisch bij CIDP. Deze bevindingen tonen aan dat de bij MRI gevonden afwijkingen van de plexus brachialis bij patiënten met MMN lijken op die bij patiënten met CIDP en dat MRI gebruikt kan worden om MMN van PSS te onderscheiden.

List of References

1. Ad Hoc Subcommittee of the American Academy of Neurology AIDS Task Force. Research criteria for diagnosis of chronic inflammatory demyelinating polyneuropathy (CIDP). Neurology 1991; 41:617-618.
2. Adson AW, Coffey JR. Cervical rib; a method of anterior approach for relief of symptoms by division of the scalenus anticus. Ann Surg 1927; 85:839-857.
3. Ahern V, Soo YS, Langlands AD. MRI scanning in brachial plexus neuropathy. Australas Radiol 1991; 35:379-381.
4. Albers JW, Donofrio PD, McGonagle TK. Sequential electrodiagnostic abnormalities in acute inflammatory demyelinating polyradiculoneuropathy. Muscle Nerve 1985; 8:528-539.
5. Alnot JY. Traumatic brachial plexus palsy in the adult. Retro- and infraclavicular lesions. Clin Orthop 1988; 237:9-16.
6. Alnot JY. Traumatic brachial plexus lesions in the adult: indications and results. Microsurgery 1995; 16:22-29.
7. Alnot JY. Traumatic brachial plexus lesions in the adult. Indications and results. Hand Clin 1995; 11:623-631.
8. Armington WG, Harnsberger HR, Osborn AG, Seay AR. Radiographic evaluation of brachial plexopathy. AJNR 1987; 8:361-367.
9. Attar S, Miller JE, Satterfield J, et al. Pancoast's tumor: irradiation or surgery? Ann Thorac Surg 1979; 28:578-586.
10. Bagley FH, Walsh JW, Cady B, Salzman FA, Oberfield RA, Pazianos AG. Carcinomatous versus radiation-induced brachial plexus neuropathy in breast cancer. Cancer 1978; 41:2154-2157.
11. Barentsz JO, Jager G, Mugler JP III, et al. Staging urinary bladder cancer: value of T1-weighted three-dimensional magnetization prepared-rapid gradient-echo and two-dimensional spin-echo sequences. AJR 1995; 164:109-115.
12. Barr LC, Kissin MW. Radiation-induced brachial plexus neuropathy following breast conservation and radical radiotherapy. Br J Surg 1987; 74:855-856.

13. Bateman JE. Neurovascular syndromes related to the clavicle. Clin Orthop 1968; 58:75-82.
14. Beck C. The surgical importance of the cervical rib. JAMA 1905; 44:1913-1915.
15. Berger A, Becker MHJ. Brachial plexus surgery: our concept of the last twelve years. Microsurgery 1994; 15:760-767.
16. Berger A, Brenner P. Secondary surgery following brachial plexus injuries. Microsurgery 1995; 16:43-47.
17. Bergquist E, Hugosson R, Westerberg CE. A wasted hand; case with uncommon neurological and radiological features caused by a cervical band. J Neurol Neurosurg Psychiatry 1975; 38:100-102.
18. Berkheiser EJ. Old ununited clavicular fractures in the adult. Surg Gynecol Obstet 1937; 64:1064-1072.
19. Berlin O, Stener B, Lindahl S, Irstam L, Lodding P. Vascularization of peripheral neurilemomas: angiographic, computed tomographic, and histologic studies. Skeletal Radiol 1986; 15:275-283.
20. Bertorini T, Halford H, Lawrence J, Vo D, Wassef M. Contrast-enhanced magnetic resonance imaging of the lumbosacral roots in the dysimmune inflammatory polyneuropathies. J Neuroimag 1995; 5:9-15.
21. Bilbey JH, Lamond RG, Mattrey RF. MR imaging of disorders of the brachial plexus. J Magn Reson Imaging 1994; 4:13-18.
22. Bilbey JH, Muller NL, Connell DG, Luoma AA, Nelems B. Thoracic outlet syndrome: evaluation with CT. Radiology 1989; 171:381-384.
23. Birch R. Peripheral nerve tumors. In: Dyck PJ, Thomas PK, eds. Peripheral neuropathy. 3rd ed. Philadelphia: Saunders, 1993; 1623-1640.
24. Blair DN, Rapoport S, Sostman HD, Blair OC. Normal brachial plexus: MR imaging. Radiology 1987; 165:763-767.
25. Bowen BC, Verma A, Brandon AH, Fiedler JA. Radiation-induced brachial plexopathy: MR and clinical findings. AJNR 1996; 17:1932-1936.
26. Bradley WG, Bennett RK, Good P, Little B. Proximal chronic inflammatory polyneuropathy with multifocal conduction block. Arch Neurol 1988; 45:451-455.
27. Brant-Zawadzki M, Gillan GD, Nitz WR. MP RAGE: a three-dimensional, T1-weighted, gradient-echo sequence. Initial experience in the brain. Radiology 1992; 182:769-775.
28. Brunelli GA, Brunelli GR. Preoperative assessment of the adult plexus patient. Microsurgery 1995; 16:17-21.
29. Bush CH, Spanier SS, Gillespy T III. Imaging of atypical lipomas of the extremities: report of three cases. Skeletal Radiol 1988; 17:472-475.

30. Cascino TL, Kori S, Krol G, Foley KM. CT of the brachial plexus in patients with cancer. Neurology 1983; 33:1553-1557.
31. Castagno AA, Shuman WP. MR imaging in clinically suspected brachial plexus tumor. AJR 1987; 149:1219-1222.
32. Castillo M, Mukherji SK. MRI of enlarged dorsal ganglia, lumbar roots, and cranial nerves in polyradiculoneuropathies. Neuroradiology 1996; 38:516-520.
33. Chaudry V, Corse AM, Cornblath DR, et al. Multifocal motor neuropathy: response to human immune globulin. Ann Neurol 1993; 33:237-242.
34. Cherington M, Happer I, Machanic B, Parry L. Surgery for thoracic outlet syndrome may be hazardous to your health. Muscle Nerve 1986; 9:632-634.
35. Cherington M, Wilbourn AJ, Schils J, Whitaker J. Thoracic outlet syndromes and MRI (letter). Brain 1995; 118:819-821.
36. Chui MC, Bird BL, Rogers J. Extracranial and extraspinal nerve sheath tumors: computed tomographic evaluation. Neuroradiology 1988; 30:47-53.
37. Clagett OT. Research and prosearch. J Thorac Cardiovasc Surg 1962; 44:153-166.
38. Cobby MJD, Leslie IJ, Watt I. Cervical myelography of nerve root avulsion injuries using water-soluble contrast media. Br J Radiol 1988; 61:673-678.
39. Coene LNJEM. Mechanisms of brachial plexus lesions. Clin Neurol Neurosurg 1993; 95 (Suppl.):S24-S29.
40. Cohen LM, Schwartz AM, Rockoff SD. Benign schwannomas: pathologic basis for CT inhomogeneities. AJR 1986; 147:141-143.
41. Collins JD, Disher AC, Miller TQ. The anatomy of the brachial plexus as displayed by magnetic resonance imaging: technique and application. J Natl Med Assoc 1995; 87:489-498.
42. Collins JD, Shaver ML, Disher AC, Miller TQ. Compromising abnormalities of the brachial plexus as displayed by magnetic resonance imaging. Clin Anat 1995; 8:1-16.
43. Connolly JF, Dehne R. Nonunion of the clavicle and thoracic outlet syndrome. J Trauma 1989; 29:1127-1133.
44. Cooke J, Cooke D, Parsons C. The anatomy and pathology of the brachial plexus as demonstrated by computed tomography. Clin Radiol 1988; 39:595-601.
45. Cooke J, Powell S, Parsons C. The diagnosis by computed tomography of brachial plexus lesions following radiotherapy for carcinoma of the breast. Clin Radiol 1988; 39:602-606.
46. Cornelius RS, Leach JL. Imaging evaluation of cervical spine trauma. Neuroimag Clin North Am 1995; 5:451-463.

47. Corse AM, Chaudry V, Crawford TO, Cornblath DR, Kuncl RW, Griffin JW. Sensory nerve pathology in multifocal motor neuropathy. Ann Neurol 1996; 39:319-325.
48. Crino PB, Grossman RI, Rostami A. Magnetic resonance imaging of the cauda equina in chronic inflammatory demyelinating polyneuropathy. Ann Neurol 1993; 33:311-313.
49. Cuetter AC, Bartoszek DM. The thoracic outlet syndrome: controversies, overdiagnosis, overtreatment, and recommendations for management. Muscle Nerve 1989; 12:410-419.
50. Cunningham DJ. Cunningham's textbook of anatomy. Romanes GJ, ed. 12th ed. Oxford: Oxford University Press, 1981.
51. Cusimano MD, Bilbao JM, Cohen SM. Hypertrophic brachial plexus neuritis: a pathological study of two cases. Ann Neurol 1988; 24:615-622.
52. Dart LH Jr, MacCarty CS, Love JG, Dockerty MB. Neoplasms of the brachial plexus. Minn Med 1970; 53:959-964.
53. de Silva RN, Willison HJ, Doyle D, Weir AI, Hadley DM, Thomas AM. Nerve root hypertrophy in chronic inflammatory demyelinating polyneuropathy. Muscle Nerve 1994; 17:168-170.
54. de Verdier HJ, Colletti PM, Terk MR. MRI of the brachial plexus: a review of 51 cases. Comput Med Imag Graph 1993; 17:45-50.
55. Does MD, Snyder RE. T2 relaxation of peripheral nerve measured in vivo. Magn Reson Imaging 1995; 13:575-580.
56. Dooms GC, Hricak H, Sollitto RA, Higgins CB. Lipomatous tumors and tumors with fatty component: MR imaging potential and comparison of MR and CT results. Radiology 1985; 157:479-483.
57. Dow DR. The anatomy of rudimentary first thoracic ribs with special reference to the arrangement of the brachial plexus. J Anat 1925; 59:166-179.
58. Ducatman BS, Scheithauer BW. Postirradiation neurofibrosarcoma. Cancer 1983; 51:1028-1033.
59. Ducatman BS, Scheithauer BW, Piepgras DG, Reiman HM, Ilstrup DM. Malignant peripheral nerve sheath tumors. A clincopathologic study of 120 cases. Cancer 1986; 57:2006-2021.
60. Dyck PJ, Prineas J, Pollard J. Chronic inflammatory demyelinating polyradiculoneuropathy. In: Dyck PJ, Thomas PK, eds. Peripheral neuropathy. 3rd ed. Philadelphia: Saunders, 1993; 1498-1517.
61. Ebner F, Kressel HY, Mintz MC, et al. Tumor recurrence versus fibrosis in the female pelvis: differentiation with MR imaging at 1.5 T. Radiology 1988; 166:333-340.
62. Editorial. Cervical ribs. JAMA 1907; 48:878.

63. Enzinger FM, Weiss SW. Fibromatoses. In: Soft tissue tumors. 2nd ed. St. Louis: Mosby, 1988; 136-163.
64. Enzinger FM, Weiss SW. Benign tumors of peripheral nerves. In: Soft tissue tumors. 2nd ed. St. Louis: Mosby, 1988; 719-780.
65. Enzinger FM, Weiss SW. Malignant tumors of peripheral nerves. In: Soft tissue tumors. 2nd ed. St. Louis: Mosby, 1988; 781-815.
66. Falconer MA, Franklin WP. Resection of the first rib in costoclavicular compression of the brachial plexus. Lancet 1962; 1:59-63.
67. Falconer MA, Weddel G. Costoclavicular compression of the subclavian artery and vein. Lancet 1943; 2:539-543.
68. Feld R, Burk DL Jr, McCue P, Mitchell DG, Lackman R, Rifkin MD. MRI of aggressive fibromatosis: frequent appearance of high signal intensity on T2-weighted images. Magn Reson Imaging 1990; 8:583-588.
69. Filler AG, Howe FA, Hayes CE, et al. Magnetic resonance neurography. Lancet 1993; 341:659-661.
70. Filler AG, Kliot M, Howe FA, et al. Application of magnetic resonance neurography in the evaluation of patients with peripheral nerve pathology. J Neurosurg 1996; 85:299-309.
71. Fishman EK, Campbell JN, Kuhlman JE, Kawashima A, Ney DR, Friedman NB. Multiplanar CT evaluation of brachial plexopathy in breast cancer. J Comput Assist Tomogr 1991; 15:790-795.
72. Fishman EK, Zinreich ES, Jacobs CG, Rostock RA, Siegelman SS. CT of the axilla: normal anatomy and pathology. Radiographics 1986; 6:475-502.
73. Foley KM, Woodruff JM, Ellis FT, Possner JB. Radiation-induced malignant and atypical peripheral nerve sheath tumors. Ann Neurol 1980; 7:311-318.
74. Francel PC, Koby M, Park TS, et al. Fast spin-echo magnetic resonance imaging for radiological assessment of neonatal brachial plexus injury. J Neurosurg 1995; 83:461-466.
75. Franssen H, Wieneke GH. Nerve conduction and temperature: necessary warming time. Muscle Nerve 1994; 17:336-344.
76. Friedman AH, Nunley JA II, Goldner RD, Oakes WJ, Goldner JL, Urbaniak JR. Nerve transposition for the restoration of elbow flexion following brachial plexus avulsion injuries. J Neurosurg 1990; 72:59-64.
77. Gage M, Parnell H. Scalenus anticus syndrome. Am J Surg 1947; 73:252-268.
78. Gardner G, Gray DJ, O'Rahilly R. Anatomy. A regional study of human structure. O'Rahilly R, ed. 5th ed. Philadelphia: Saunders, 1986.
79. Gebarski KS, Glazer GM, Gebarski SS. Brachial plexus: anatomic, radiologic, and pathologic correlation using computed tomography. J Comput Assist Tomogr 1982; 6:1058-1063.

80. Ghormley RK, Black JR, Cherry JH. Ununited fractures of the clavicle. Am J Surg 1941; 51:343-349.
81. Gilbert A, Brockman R, Carlioz H. Surgical treatment of brachial plexus birth palsy. Clin Orthop 1991; 264:39-49.
82. Gilliatt RW, Le Quesne PM, Logue V, Sumner AJ. Wasting of the hand associated with a cervical rib or band. J Neurol Neurosurg Psychiatry 1970; 33:615-624.
83. Gilliatt RW, Willison RG, Dietz V, Williams IR. Peripheral nerve conduction in patients with a cervical rib and band. Ann Neurol 1978; 4:124-129.
84. Ginsberg L, Platts AD, Thomas PK. Chronic inflammatory demyelinating polyneuropathy mimicking a lumbar spinal stenosis syndrome. J Neurol Neurosurg Psychiatry 1995; 59:189-191.
85. Glazer HS, Lee JKT, Levitt RG, et al. Radiation fibrosis: differentiation from recurrent tumor by MR imaging. Radiology 1985; 156:721-726.
86. Gray H. Gray's Anatomy. Williams PL, Bannister LH, Berry MM et al, eds. 38th ed. Edinburgh: Churchill Livingstone, 1995.
87. Gupta RK, Mehta VS, Banerji AK, Jain RK. MR evaluation of brachial plexus injuries. Neuroradiology 1989; 31:377-381.
88. Gyhra A, Israel J, Santander C, Acuna D. Schwannoma of the brachial plexus with intrathoracic extension. Thorax 1980; 35:703-704.
89. Haggar AM, Pearlberg JL, Froelich JW, et al. Chest-wall invasion by carcinoma of the lung: detection by MR imaging. AJR 1987; 148:1075-1078.
90. Hardy RW Jr, Wilbourn AJ, Hanson M. Surgical treatment of compressive cervical band. Neurosurgery 1980; 7:10-13.
91. Harnsberger HR. Handbook of head and neck imaging. 2nd ed. St. Louis: Mosby, 1995.
92. Harper CM Jr, Thomas JE, Cascino TL, Litchy WJ. Distinction between neoplastic and radiation-induced brachial plexopathy, with emphasis on the role of EMG. Neurology 1989; 39:502-506.
93. Harris W. Prefixed and postfixed types of brachial plexus. Brain 1903; 26:613-615.
94. Harris W. The true form of the brachial plexus, and its motor distribution. J Anat Physiol 1904; 38:399-442.
95. Hashimoto T, Mitomo M, Hirabuki N, et al. Nerve root avulsion of birth palsy: comparison of myelography with CT myelography and somatosensory evoked potential. Radiology 1991; 178:841-845.
96. Heelan RT, Demas BE, Caravelli JF, et al. Superior sulcus tumors: CT and MR imaging. Radiology 1989; 170:637-641.
97. Hepper NGG, Herskovic T, Witten DM, Mulder DW, Woolner LB. Thoracic inlet tumors. Ann Intern Med 1966; 64:979-989.

98. Herringham WP. The minute anatomy of the brachial plexus. Proc Roy Soc London 1887; 41:423-441.
99. Herzberg G, Narakas AO, Comtet JJ, Bouchet A, Carret JP. Microsurgical relations of the roots of the brachial plexus. Practical applications. Ann Hand Surg 1985; 4:120-133.
100. Higgins CB, Steinbach LS. The Brachial Plexus. In: Higgins CB, Hricak H, Helms CA, eds. Magnetic Resonance Imaging of the Body. 2nd ed. New York: Raven Press, 1992; 443-460.
101. Hogan QH, Erickson SJ. MR imaging of the stellate ganglion: normal appearance. AJR 1992; 158:655-659.
102. Hovelacque A. Anatomie des nerfs craniens et rachidiens et du systeme grand sympathique chez l'homme. Gaston Doin, ed. Paris: Librairie Octave Doin, 1927.
103. Howard FM, Shafer SJ. Injuries to the clavicle with neurovascular complications. J Bone Joint Surg 1965; 47A:1335-1346.
104. Howe FA, Filler AG, Bell BA, Griffiths JR. Magnetic resonance neurography. Magn Reson Med 1992; 328-338.
105. Hudson TM, Vandergriend RA, Springfield DS, et al. Aggressive fibromatosis: evaluation of computed tomography and angiography. Radiology 1984; 150:495-501.
106. Iyer RB, Fenstermacher MJ, Libshitz HI. MR imaging of the treated brachial plexus. AJR 1996; 167:225-229.
107. Jupiter JB, Leffert RD. Non-union of the clavicle. Associated complications and surgical management. J Bone Joint Surg 1987; 69A:753-760.
108. Kaji R, Oka N, Tsuji T, et al. Pathological findings at the site of conduction block in multifocal motor neuropathy. Ann Neurol 1993; 33:152-158.
109. Kaplan EB, Spinner M. Normal and anomalous innervation patterns in the upper extremity. In: Omer GE Jr, Spinner M, eds. Management of peripheral nerve problems. Philadelphia: Saunders, 1980; 75-99.
110. Katirji B, Hardy RW Jr. Classic neurogenic thoracic outlet syndrome in a competitive swimmer: a true scalenus anticus syndrome. Muscle Nerve 1995; 18:229-233.
111. Kauer JM. The brachial plexus: basic anatomical and functional considerations. Microsurgery 1995; 16:9-12.
112. Kellman GM, Kneeland JB, Middleton WD, et al. MR imaging of the supraclavicular region: normal anatomy. AJR 1987; 148:77-82.
113. Kerr AT. The brachial plexus of nerves in man, the variations in its formation and branches. Am J Anat 1918; 23:285-395.
114. Kneeland JB, Kellman GM, Middleton WD, et al. Diagnosis of diseases of the supraclavicular region by use of MR imaging. AJR 1987; 148:1149-1151.

115. Komaki R, Roh J, Cox JD, Lopes da Conceicao A. Superior sulcus tumors: results of irradiation of 36 patients. Cancer 1981; 48:1563-1568.
116. Kori SH, Foley KM, Posner JB. Brachial plexus lesions in patients with cancer: 100 cases. Neurology 1981; 31:45-50.
117. Kornberg AJ, Pestronk A. Chronic motor neuropathies: diagnosis, therapy, and pathogenesis. Ann Neurol 1995; 37(S1):S43-S50.
118. Kransdorf MJ. Malignant soft-tissue tumors in a large referral population: distribution by age, sex, and location. AJR 1995; 164:129-134.
119. Kransdorf MJ. Benign soft-tissue tumors in a large referral population: distribution of specific diagnoses by age, sex, and location. AJR 1995; 164: 395-402.
120. Kransdorf MJ, Jelinek JS, Moser RP Jr, et al. Soft tissue masses: diagnosis using MR imaging. AJR 1989; 153:541-547.
121. Kransdorf MJ, Jelinek JS, Moser RP Jr, et al. Magnetic resonance appearance of fibromatosis. A report of 14 cases and review of the literature. Skeletal Radiol 1990; 19:495-499.
122. Krarup C, Stewart JD, Sumner AJ, Pestronk A, Lipton SA. A syndrome of asymmetric limb weakness with motor conduction block. Neurology 1990; 40:118-127.
123. Kuhlman JE, Bouchardy L, Fishman EK, Zerhouni EA. CT and MR imaging evaluation of chest wall disorders. Radiographics 1994; 14:571-595.
124. Kumar AJ, Kuhajda FP, Martinez CR, Fishman EK, Jezic DV, Siegelman SS. Computed tomography of extracranial nerve sheath tumors with pathological correlation. J Comput Assist Tomogr 1983; 7:857-865.
125. Lange DJ, Trojaborg W, Latov N, et al. Multifocal motor neuropathy with conduction block: is it a distinct entity? Neurology 1992; 42:497-505.
126. Lederman RJ, Wilbourn AJ. Brachial plexopathy: recurrent cancer or radiation? Neurology 1984; 34:1331-1335.
127. Leffert RD. Brachial plexus injuries. N Engl J Med 1974; 291:1059-1067.
128. Leffert RD. Surgical treatment of closed traction injuries of the brachial plexus. In: Brachial plexus injuries. New York: Churchill Livingstone, 1985; 161-188.
129. Leffert RD. Peripheral reconstruction of the upper limb following brachial plexus injury. In: Brachial plexus injuries. New York: Churchill Livingstone, 1985; 189-235.
130. Leffert RD. Clinical assessment of closed traction injury to the brachial plexus. In: Brachial plexus injuries. New York: Churchill Livingstone, 1985; 75-90.
131. Leffert RD. Infraclavicular brachial plexus injuries. In: Brachial plexus injuries. New York: Churchill Livingstone, 1985; 57-73.
132. Leffert RD. The anatomy of the brachial plexus. In: Brachial plexus injuries. New York: Churchill Livingstone, 1985; 1-38.

133. Leffert RD. Clinical diagnosis, testing, and electromyographic study in brachial plexus traction injuries. Clin Orthop 1988; 237:24-31.
134. Leffert RD. Brachial plexus. In: Green DP, ed. Operative hand surgery. 3rd ed. New York: Churchill Livingstone, 1993; 1483-1516.
135. Leffert RD, Seddon HJ. Infraclavicular brachial plexus injuries. J Bone Joint Surg 1965; 47B:9-22.
136. Levine E, Huntrakoon M, Wetzel LH. Malignant nerve-sheath neoplasms in neurofibromatosis: distinction from benign tumors by using imaging techniques. AJR 1987; 149:1059-1064.
137. Lusk MD, Kline DG, Garcia CA. Tumors of the brachial plexus. Neurosurgery 1987; 21:439-453.
138. Maggi G, Casadio C, Pischedda F, et al. Combined radiosurgical treatment of pancoast tumor. Ann Thorac Surg 1994; 57:198-202.
139. Marshall RW, de Silva RDD. Computerised axial tomography in traction injuries of the brachial plexus. J Bone Joint Surg 1986; 68B:734-738.
140. Match RM. Radiation-induced brachial plexus paralysis. Arch Surg 1975; 110:384-386.
141. Mayo JR. Magnetic Resonance Imaging of the chest: where we stand. Radiol Clin North Am 1994; 32:795-809.
142. McKillop G, Beggs I. Case report: apical pleural cap mimicked by post-traumatic pseudomeningocele. Clin Radiol 1995; 50:870-872.
143. McLoud TC, Filion RB, Edelman RR, Shepard JA. MR imaging of superior sulcus carcinoma. J Comput Assist Tomogr 1989; 13:233-239.
144. Mehta VS, Banerji AK, Tripathi RP. Surgical treatment of brachial plexus injuries. Br J Neurosurg 1993; 7:491-500.
145. Meller I, Alkalay D, Mozes M, Geffen DB, Ferit T. Isolated metastases to peripheral nerves. Report of five cases involving the brachial plexus. Cancer 1995; 76:1829-1832.
146. Miller DS, Boswick JA Jr. Lesions of the brachial plexus associated with fractures of the clavicle. Clin Orthop 1969; 64:144-149.
147. Miller JI, Mansour KA, Hatcher CR Jr. Carcinoma of the superior pulmonary sulcus. Ann Thorac Surg 1979; 28:44-47.
148. Miller SF, Glasier CM, Griebel ML, Boop FA. Brachial plexopathy in infants after traumatic delivery: evaluation with MR imaging. Radiology 1993; 189: 481-484.
149. Millesi H. Surgical management of brachial plexus injuries. J Hand Surg 1977; 2:367-379.
150. Millesi H. Brachial plexus injuries. Nerve grafting. Clin Orthop 1988; 237: 36-42.
151. Moore KL. Clinical Anatomy. 3rd ed. Baltimore: Williams&Wilkins, 1992.

152. Moore NR, Dixon AK, Wheeler TK, Freer CEL, Hall LD, Sims C. Axillary fibrosis or recurrent tumour. An MRI study in breast cancer. Clin Radiol 1990; 42:42-46.
153. Morgan GW, Barohn RJ, Bazan C III, King RB, Klucznik RP. Nerve root enhancement with MRI in inflammatory demyelinating polyradiculo-neuropathy. Neurology 1993; 43:618-619.
154. Morris RE, Hasso AN, Thompson JR, Hinshaw DB Jr, Vu LH. Traumatic dural tears: CT diagnosis using metrizamide. Radiology 1984; 152:443-446.
155. Mountain CF. A new international staging system for lung cancer. Chest 1986; 89 (Suppl.):225S-233S.
156. Mountain CF. Prognostic implications of the international staging system for lung cancer. Semin Oncol 1988; 15:236-245.
157. Mugler JP III, Brookeman JR. Three-dimensional magnetization-prepared rapid gradient-echo imaging (3D MP RAGE). Magn Reson Med 1990; 15:152-157.
158. Mumenthaler M, Schliack H. Lesions of the cervicobrachial plexus. In: Peripheral nerve lesions; diagnosis and therapy. Stuttgart: Georg Thieme Verlag, 1991; 155-202.
159. Murphey F, Hartung W, Kirklin JW. Myelographic demonstration of avulsing injury of the brachial plexus. AJR 1947; 58:102-105.
160. Nagano A, Ochiai N, Sugioka H, Tsuyama N. Usefulness of myelography in brachial plexus injuries. J Hand Surg 1989; 14B:59-64.
161. Narakas AO. Surgical treatment of traction injuries of the brachial plexus. Clin Orthop 1978; 133:71-90.
162. Narakas AO. Operative treatment for radiation-induced and metastatic brachial plexopathy in 45 cases, 15 having an omentoplasty. Bull Hosp Jt Dis 1984; 44:354-375.
163. Narakas AO.The treatment of brachial plexus injuries. Int Orthop 1985; 9:29-36.
164. Narakas AO. Lesions found when operating traction injuries of the brachial plexus. Clin Neurol Neurosurg 1993; 95 (Suppl.):S56-S64.
165. Narakas AO. Muscle transpositions in the shoulder and upper arm for sequelae of brachial plexus palsy. Clin Neurol Neurosurg 1993; 95 (Suppl.):S89-S91.
166. Narakas AO, Hentz VR. Neurotization in brachial plexus injuries. Indications and results. Clin Orthop 1988; 237:43-56.
167. Nobile-Orazio E, Meucci N, Barbieri S, Carpo M, Scarlato G. High-dose intravenous immunoglobulin therapy in multifocal motor neuropathy. Neurology 1993; 43:537-544.
168. O'Connell RS, McLoud TC, Wilkins EW. Superior sulcus tumor: radiographic diagnosis and workup. AJR 1983; 140:25-30.

169. Ochi M, Ikuta Y, Watanabe M, Kimori K, Itoh K. The diagnostic value of MRI in traumatic brachial plexus injury. J Hand Surg 1994; 19B:55-59.
170. Ochsner A, Gage M, DeBakey M. Scalenus anticus (Naffziger) syndrome. Am J Surg 1935; 28:669-695.
171. Oh SJ, Claussen GC, Odabasi Z, Palmer CP. Multifocal demyelinating motor neuropathy: pathologic evidence of 'inflammatory demyelinating polyradiculoneuropathy'. Neurology 1995; 45:1828-1832.
172. Ohkawa Y, Isoda H, Hasegawa S, Furuya Y, Takahashi M, Kaneko M. MR angiography of thoracic outlet syndrome. J Comput Assist Tomogr 1992; 16:475-477.
173. Okubo K, Wada H, Fukuse T, et al. Treatment of Pancoast tumors. Thorac Cardiovasc Surgeon 1995; 43:284-286.
174. Olsen NK, Pfeiffer P, Johannsen L, Schroder H, Rose C. Radiation-induced brachial plexopathy: neurological follow-up in 161 recurrence-free breast cancer patients. Int J Radiat Oncol Biol Phys 1993; 26:43-49.
175. Olsen NK, Pfeiffer P, Mondrup K, Rose C. Radiation-induced brachial plexus neuropathy in breast cancer patients. Acta Oncol 1990; 29:885-890.
176. Padovani B, Mouroux J, Seksik L, et al. Chest wall invasion by bronchogenic carcinoma: evaluation with MR imaging. Radiology 1993; 187:33-38.
177. Panasci DJ, Holliday RA, Shpizner B. Advanced imaging techniques of the brachial plexus. Hand Clin 1995; 11:545-553.
178. Pancoast HK. Importance of careful roentgen-ray investigation of apical chest tumors. JAMA 1924; 83:1407-1411.
179. Pancoast HK. Superior pulmonary sulcus tumor: tumor characterized by pain, Horner's syndrome, destruction of bone and atrophy of hand muscles. JAMA 1932; 99:1391-1396.
180. Panegyres PK, Moore N, Gibson R, Rushworth G, Donaghy M. Thoracic outlet syndromes and magnetic resonance imaging. Brain 1993; 116:823-841.
181. Parry GJ. AAEM case report #30: multifocal motor neuropathy. Muscle Nerve 1996; 19:269-276.
182. Parry GJ, Clarke S. Multifocal acquired demyelinating neuropathy masquerading as motor neuron disease. Muscle Nerve 1988; 11:103-107.
183. Parry GJ, Sumner AJ. Multifocal motor neuropathy. Neurol Clin 1992; 10: 671-684.
184. Parsonage MJ, Aldren Turner JW. Neuralgic amyotrophy: the shoulder-girdle syndrome. Lancet 1948; 254:973-978.
185. Paulson DL. Carcinomas in the superior pulmonary sulcus. J Thorac Cardiovasc Surg 1975; 70:1095-1104.
186. Peet RM, Henriksen JD, Anderson TP, Martin GM. Thoracic-outlet syndrome:

evaluation of a therapeutic exercise program. Mayo Clin Proc 1956; 31:281-287.
187. Perlow S, Vehe KL. Variations in the gross anatomy of the stellate and lumbar sympathetic ganglia. Am J Surg 1935; 30:454-458.
188. Pestronk A, Chaudry V, Feldman EL, et al. Lower motor neuron syndromes defined by patterns of weakness, nerve conduction abnormalities, and high titers of antiglycolid antibodies. Ann Neurol 1990; 27:316-326.
189. Pestronk A, Cornblath DR, Ilyas AA, et al. A treatable multifocal motor neuropathy with antibodies to GM1 ganglioside. Ann Neurol 1988; 24:73-78.
190. Petras AF, Sobel DF, Mani JR, Lucas PR. CT myelography in cervical nerve root avulsion. J Comput Assist Tomogr 1985; 9:275-279.
191. Pierce SM, Recht A, Lingos TI, et al. Long-term radiation complications following conservative surgery (cs) and radiation therapy (rt) in patients with early stage breast cancer. Int J Radiat Oncol Biol Phys 1992; 23:915-923.
192. Popovich MJ. MR imaging of birth-related brachial plexus avulsion. AJNR 1989; 10 (Suppl.):S98.
193. Posniak HV, Olson MC. Questions and answers. AJR 1995; 165:224-225.
194. Posniak HV, Olson MC, Dudiak CM, Wisniewski R, O'Malley CO. MR imaging of the brachial plexus. AJR 1993; 161:373-379.
195. Powers SK, Norman D, Edwards MSB. Computerized tomography of peripheral nerve lesions. J Neurosurg 1983; 59:131-136.
196. Price AJ, Compson JP, Calonje E. Fibrolipomatous hamartoma of nerve arising in the brachial plexus. J Hand Surg 1995; 20B:16-18.
197. Pugatch RD. Radiologic evaluation in chest malignancies. Chest 1995; 107:294S-297S.
198. Quinn SF, Erickson SJ, Dee PM, et al. MR imaging in fibromatosis: results in 26 patients with pathologic correlation. AJR 1991; 156:539-542.
199. Qvarfordt PG, Ehrenfeldt WK, Stoney RJ. Supraclavicular radical scalenectomy and transaxillary first rib resection for the thoracic outlet syndrome. A combined approach. Am J Surg 1984; 148:111-116.
200. Rapoport S, Blair DN, McCarthy SM, Desser TS, Hammers LW, Sostman HD. Brachial plexus: correlation of MR imaging with CT and pathologic findings. Radiology 1988; 167:161-165.
201. Reede DL. Magnetic resonance imaging of the brachial plexus. MRI Clin North Am 1993; 1:185-195.
202. Reede DL. Brachial plexus. In: Som PM, Curtin HD, eds. Head and neck imaging. 3rd ed. St. Louis: Mosby, 1996; 976-991.
203. Rhee EK, England JD, Sumner AJ. A computer simulation of conduction block: effects produced by actual block versus interphase cancellation. Ann Neurol 1990; 28:146-156.
204. Richardson RR, Siqueira EB, Oi S, Nunez C. Neurogenic tumors of the brachial

plexus: report of two cases. Neurosurgery 1979; 4:66-70.
205. Roberts JB. The surgical importance of cervical ribs to the general practitioner. JAMA 1908; 51:1126-1130.
206. Robotti E, Longhi P, Verna G, Bocchiotti G. Brachial plexus surgery. An historical perspective. Hand Clin 1995; 11:517-533.
207. Roger B, Travers V, Laval-Jeantet M. Imaging of posttraumatic brachial plexus injury. Clin Orthop 1988; 237:57-61.
208. Roger DJ, Richli WR. A CT table attachment for parasagittal scanning of the axilla. AJR 1987; 149:555-556.
209. Roos DB. Transaxillary approach for first rib resection to relieve thoracic outlet syndrome. Ann Surg 1966; 163:354-358.
210. Roos DB. Congenital anomalies associated with thoracic outlet syndrome: anatomy, symptoms, diagnosis, and treatment. Am J Surg 1976; 132:771-778.
211. Roos DB. The place for scalenectomy and first-rib resection in thoracic outlet syndrome. Surgery 1982; 92:1077-1085.
212. Russell DS, Rubinstein LJ. Tumours of the cranial, spinal and peripheral nerve sheaths. In: Pathology of tumours of the nervous system. 5th ed. London: Edward Arnold, 1989; 533-589.
213. Sadiq SA, Thomas FP, Kilidireas K, et al. The spectrum of neurologic disease associated with anti-GM1 antibodies. Neurology 1990; 40:1067-1072.
214. Salner AL, Botnick LE, Herzog AG, et al. Reversible brachial plexopathy following primary radiation therapy for breast cancer. Cancer Treat Rep 1981; 65:797-802.
215. Sanders RJ, Monsour JW, Gerber WF, Adams WR, Thompson N. Scalenectomy versus first rib resection for treatment of the thoracic outlet syndrome. Surgery 1979; 109:109-121.
216. Seddon HJ. Three types of nerve injury. Brain 1943; 66:237-288.
217. Sell PJ, Semple JC. Primary nerve tumours of the brachial plexus. Br J Surg 1987; 74:73-74.
218. Sellke FW, Kelly TR. Thoracic outlet syndrome. Am J Surg 1988; 156:54-57.
219. Shahian DM, Neptune WB, Ellis FH Jr. Pancoast tumors: improved survival with preoperative and postoperative radiotherapy. Ann Thorac Surg 1987; 43:32-38.
220. Shaw RR, Paulson DL, Kee JL Jr. Treatment of the superior sulcus tumor by irradiation followed by resection. Ann Surg 1961; 154:229-240.
221. Shea WJ Jr, de Geer G, Webb WR. Chest wall after mastectomy. Part I. CT appearance of normal postoperative anatomy, postirradiation changes, and optimal scanning techniques. Radiology 1987; 162:157-161.
222. Shea WJ Jr, de Geer G, Webb WR. Chest wall after mastectomy. Part II. CT

appearance of tumor recurrence. Radiology 1987; 162:162-164.
223. Sherrier RH, Sostman HD. Magnetic resonance imaging of the brachial plexus. J Thorac Imag 1993; 8:27-33.
224. Slooff ACJ. Obstetric brachial plexus lesions and their neurosurgical treatment. Clin Neurol Neurosurg 1993; 95 (Suppl.):S73-S77.
225. Slooff ACJ. Obstetric brachial plexus lesions and their neurosurgical treatment. Microsurgery 1995; 16:30-34.
226. Songcharoen P. Brachial plexus injury in Thailand: a report of 520 cases. Microsurgery 1995; 16:35-39.
227. Spittle MF. Brachial plexus neuropathy after radiotherapy for breast cancer; lower doses and surgical management of the axilla may be the answer. Br Med J 1995; 311:1516-1517.
228. Stanford W, Barnes RP, Tucker AR. Influence of staging in superior sulcus (Pancoast) tumors of the lung. Ann Thorac Surg 1980; 29:406-409.
229. Steinbach LS, Higgins CB. Magnetic resonance imaging of the brachial plexus. In: Higgins CB, Petterson H, eds. Chest and cardiac radiology. Vol 1. Nycomed Intercontinental Continuing Education in Radiology Series on Diagnostic Imaging. London: Merit Communications, 1991; 186-207.
230. Stoll BA, Andrews JT. Radiation-induced peripheral neuropathy. Br Med J 1966; 1966(1):834-837.
231. Stull MA, Moser RP Jr, Kransdorf MJ, Bogumill GP, Nelson MC. Magnetic resonance appearance of peripheral nerve sheath tumors. Skeletal Radiol 1991; 20:9-14.
232. Suarez GA, Giannini C, Bosch EP, et al. Immune brachial plexus neuropathy: suggestive evidence for an inflammatory-immune pathogenesis. Neurology 1996; 46:559-561.
233. Subramony SH. AAEE case report #14: neuralgic amyotrophy (acute brachial neuropathy). Muscle Nerve 1988; 11:39-44.
234. Suh J, Abenoza P, Galloway HR, Everson LI, Griffiths HJ. Peripheral (extracranial) nerve tumors: correlation of MR imaging and histologic findings. Radiology 1992; 183:341-346.
235. Sunderland S. A classification of peripheral nerve injuries producing loss of function. Brain 1951; 74:491-516.
236. Sunderland S. Meningeal-neural relations in the intervertebral foramen. J Neurosurg 1974; 756-763.
237. Sunderland S. Mechanisms of cervical nerve root avulsion in injuries of the neck and shoulder. J Neurosurg 1974; 41:705-714.
238. Sunderland S. The brachial plexus. Normal anatomy. In: Nerves and nerve injuries. 2nd ed. Edinburgh: Churchill Livingstone, 1978; 854-869.
239. Sunderland S. Brachial plexus lesions due to compression, stretch and penetrating injuries. In: Nerves and nerve injuries. 2nd ed. Edinburgh: Churchill

Livingstone, 1978; 870-900.
240. Sunderland S. Repair of the brachial plexus directed to restoring elbow flexion. In: Nerve injuries and their repair. A critical appraisal. Edinburgh: Churchill Livingstone, 1991; 509-517.
241. Sunderland S. Traction nerve injury. In: Nerve injuries and their repair. A critical appraisal. Edinburgh: Churchill Livingstone, 1991; 147-158.
242. Tachi N, Kozuka N, Ohya K, Chiba S, Naganuma M. MRI of peripheral nerves and pathology of sural nerves in hereditary motor and sensory neuropathy type III. Neuroradiology 1995; 37:496-499.
243. Tarlov IM, Day R. Myelography to help localize traction lesions of the brachial plexus. Am J Surg 1954; 88:266-271.
244. Teresi LM, Hovda D, Seeley AB, Nitta K, Lufkin RB. MR imaging of experimental demyelination. AJNR 1989; 10:307-314.
245. Thomas JE, Colby MY Jr. Radiation-induced or metastatic brachial plexopathy? A diagnostic dilemma. JAMA 1972; 222:1392-1395.
246. Thomeer RTWM, Malessy MJA. Surgical repair of brachial plexus injury. Clin Neurol Neurosurg 1993; 95 (Suppl.):S65-S72.
247. Thorburn W. A clinical lecture on secondary suture of the brachial plexus. Br Med J 1900; 1:1073-1075.
248. Thyagarajan D, Cascino T, Harms G. Magnetic resonance imaging in brachial plexopathy of cancer. Neurology 1995; 45:421-427.
249. Tobias JW. Syndrome apico-costo-vertebral doloroso por tumor, apexiano: su valor diagnostico en el cancer primitivo pulmonar. Rev Med Lat Am 1932; 17:1522-1666.
250. Totty WG, Murphy WA, Lee JKT. Soft-tissue tumors: MR imaging. Radiology 1986; 160:135-141.
251. Tsairis P, Dyck PJ, Mulder DW. Natural history of brachial plexus neuropathy. Report on 99 patients. Arch Neurol 1972; 27:109-117.
252. Tukkie R, Willems CRB, Dautzenberg HAA, Beijersbergen RSH. Amyotrofische neuritis; de patiënt ‘vleugellam’. Ned Tijdschr Geneeskd 1994; 138: 1201-1204.
253. Tung GA, Davis LM. The role of magnetic resonance imaging in the evaluation of the soft tissue mass. Crit Rev Diagn Imaging 1993; 34:239-308.
254. Urabe F, Matsuishi T, Kojima K, Abe T, Utsunomiya H, Okudera T. MR imaging of birth brachial palsy in a two-month-old infant. Brain Dev 1991; 13:130-131.
255. Usselman JA, Vint VC, Waltz TA. CT demonstration of a brachial plexus neuroma. AJNR 1980; 1:346-347.
256. van den Berg LH, Franssen H, Wokke JH. Improvement of multifocal motor neuropathy during long-term weekly treatment with human immunoglobulin.

Neurology 1995; 45:987-988.
257. van den Berg LH, Kerkhoff H, Oey PL, et al. Treatment of multifocal motor neuropathy with high dose intravenous immunoglobulins: a double blind, placebo controlled study. J Neurol Neurosurg Psychiatry 1995; 59:248-252.
258. van Es HW, Engelen AM, Witkamp TD, Ramos LMP, Feldberg MAM. Radiation-induced brachial plexopathy: MR imaging. Skeletal Radiol 1997; 26:284-288.
259. van Es HW, Feldberg MAM, Ramos LMP, Witkamp TD. MRI of the brachial plexus. MedicaMundi 1995; 40:84-90.
260. van Es HW, Witkamp TD, Feldberg MAM. MRI of the brachial plexus and its region: anatomy and pathology. Eur Radiol 1995; 5:145-151.
261. van Es HW, Witkamp TD, Feldberg MAM. MR imaging of the brachial plexus: anatomy and pathology. In: Selected neuroradiology scientific exhibits: RSNA 1994. Radiographics 1995; 15 (compact disc):1266 (abstract).
262. van Es HW, Witkamp TD, Ramos LMP, Feldberg MAM, Nowicki BH, Haughton VM. MR imaging of the brachial plexus using a T1-weighted three-dimensional volume acquisition. Int J Neuroradiol 1996; 2:264-273.
263. van Houtte P, MacLennan I, Poulter C, Rubin P. External radiation in the management of superior sulcus tumor. Cancer 1984; 54:223-227.
264. Vielvoye GJ, Hoffmann CFE. Neuroradiological investigations in cervical root avulsion. Clin Neurol Neurosurg 1993; 95 (Suppl.):S36-S38.
265. Vock P, Owens A. Computed tomography of the normal and pathological thoracic inlet. Eur J Radiol 1982; 2:187-193.
266. Volle E, Assheuer J, Hedde JP, Gustorf-Aeckerle R. Radicular avulsion resulting from spinal injury: assessment of diagnostic modalities. Neuroradiology 1992; 34:235-240.
267. Walker AT, Chaloupka JC, de Lotbiniere ACJ, Wolfe SW, Goldman R, Kier EL. Detection of nerve rootlet avulsion on CT myelography in patients with birth palsy and brachial plexus injury after trauma. AJR 1996; 167: 1283-1287.
268. Walsh JF. The anatomy of the brachial plexus. Am J Med Sci 1877; 74: 387-399.
269. Webb WR. MR imaging of thoracic disease: clinical uses. Radiology 1992; 182:621-630.
270. Webb WR, Jeffrey RB, Godwin JD. Thoracic computed tomography in superior sulcus tumors. J Comput Assist Tomogr 1981; 5:361-365.
271. Wilbourn AJ. Thoracic outlet syndrome surgery causing severe brachial plexopathy. Muscle Nerve 1988; 11:66-74.
272. Wilbourn AJ. The thoracic outlet syndrome is overdiagnosed. Arch Neurol

1990; 47:328-330.
273. Wilbourn AJ. Brachial plexus disorders. In: Dyck PJ, Thomas PK, eds. Peripheral neuropathy. 3rd ed. Philadelphia: Saunders, 1993; 911-950.
274. Wilbourn AJ, Porter JM. Thoracic outlet syndromes. Spine: State of the Art Rev 1988; 2:597-626.
275. Windebank AJ. Inherited recurrent focal neuropathies. In: Dyck PJ, Thomas PK, eds. Peripheral neuropathy. 3rd ed. Philadelphia: Saunders, 1993; 1137-1148.
276. Wright CD, Moncure AC, Shepard JO, Wilkins EW Jr, Mathisen DJ, Grillo HC. Superior sulcus lung tumors. Results of combined treatment (irradiation and radical resection). J Thorac Cardiovasc Surg 1987; 94:69-74.
277. Wright IS. The neurovascular syndrome produced by hyperabduction of the arms. Am Heart J 1945; 29:1-19.
278. Wulff CH, Gilliatt RW. F waves in patients with hand wasting caused by a cervical rib and band. Muscle Nerve 1979; 2:452-457.
279. Zbaren P, Becker M. Schwannoma of the brachial plexus. Ann Otol Rhinol Laryngol 1996; 105:748-750.

Subject Index

(bold numbers refer to figures)